SOLAR POWERED ELECTRIC PROPULSION SPACECRAFT

Bi-Monthly Report

JUL 1968
RECEIVED
NASA STI FACILITY
INPUT BRANCH

HUGHES AIRCRAFT COMPANY
Space Systems Division

Robert H Stivers
Robert H. Stivers, Manager
Electric Propulsion Programs

Prepared for JPL under
Contract No. 951144

May 1965

N68-87593
(ACCESSION NUMBER)
153
(PAGES)
CR-96168
(NASA CR OR TMX OR AD NUMBER)
(THRU)
None
(CODE)
(CATEGORY)
FACILITY FORM 602

TABLE OF CONTENTS

I. INTRODUCTION

II. TECHNICAL DISCUSSION

- A. Mission Analysis
  - 1. Solar-Electric Spacecraft Performance Analysis
  - 2. All-Chemical Spacecraft Performance
  - 3. Performance Comparison
- B. Propulsion System Studies
  - 1. Component Evaluation and Parametric Study
  - 2. Reliability Analysis
  - 3. Conceptual Design
- C. Spacecraft System Design
  - 1. General Arrangement
  - 2. Scientific Payload
  - 3. Retro Propulsion
  - 4. Thermal Control
  - 5. Spacecraft Attitude Control
  - 6. Telecommunication
  - 7. System Analysis
- D. Feasibility Hardware

JUL 1968
RECEIVED
NASA STI FACILITY
INPUT BRANCH

I. INTRODUCTION

This report is the first of bi-monthly reports due under JPL contract No. 951144. A briefing was made at JPL on 7 April. That briefing is essentially presented here in report form.

The program is a comparison between a chemical-electric propulsion system and an all-chemical propulsion system for a Mars orbiting mission. The ultimate objective is a cost comparison per pound of payload in orbit.

The first phase is an initial iteration. It is to achieve a design point to be used for the spacecraft and propulsion system design. This design point is based on a mission analysis limited to a 1971 Mars rendezvous mission utilizing a Saturn IB/Centaur boost vehicle with zero excess hyperbolic velocity and zero coast during the electric propulsion stage. This mission analysis will be expanded extensively during the remainder of the program.

A primary objective of the program is to prove feasibility of packaging an entire payload in the spacecraft including the solar array, the propulsion system, the telecommunication system, the guidance and control, and the scientific payload. As is apparent in the body of the report, there exists many trade-offs in a study of this kind, the choice of alternatives of which are extremely important to a proper evaluation. These trade-offs will be extensively studied during the remainder of the program.

It is logical to present the report in the following order:

1. Mission Analysis
2. Propulsion System Design
3. Spacecraft Design
4. Feasibility Hardware

The general approach to low-thrust mission analysis is presented. It should be noted that the approach is quite general, with the advantages that parameters may be easily varied to determine their effects. The analysis can be readily applied to any low-thrust system, and the mission can be optimized for varying requirements. The influence of various effects, such as launch window, and flight times are demonstrated.

An important feature of comparison with a chemical mission is the use of proper constraints. In addition to launch constraints, it is necessary to examine carefully the purposes of the mission, and be certain that desired scientific experiments may be accomplished. These constraints and their effects are discussed herein.

The propulsion system design relating to the mission point is discussed. This includes a selection of the number of modules, the choice of components, and a layout of the system. A reliability analysis is an important part of the selection and is included.

Extensive discussion of spacecraft configurations appears. Possible configurations are included which integrate the propulsion system and solar array with the remainder of the system. Also there are definitions of subsystems and discussions of the relationships of the constraints to various design possibilities.

A discussion of the planned feasibility test hardware concludes the report. The state-of-the-art of components is included to show the realism of parameters used. These parameters were used to develop the mission design point and the propulsion system design. In turn, the feasibility hardware test must be extrapolable to the system design. Obviously, it is not reasonable to have an exact duplication of the system for test due to cost, schedule and the fact that the system may be different at the end of the program, and would necessarily be different for different missions. A planned test program is presented which is believed to best take all compromises and constraints into account and which should clearly demonstrate feasibility for a wide range of mission possibilities.

Most of the items discussed herein will be expanded in considerably more detail in the remainder of the program. Other mission profiles will be investigated and the role that electric propulsion should play in these missions remains to be determined. The propulsion system presently is a conceptual design. There remains the detailed mechanical, electrical, and thermal integration of the system. The spacecraft design will be affected by several areas in which extensive trade-off studies remain to be conducted. These include the design mission profile, solar array concept, variable thrust direction, type of attitude control, and lander capsule shape and size.

II. TECHNICAL DISCUSSION

A. MISSION ANALYSIS

The main objective of the mission is to deliver a scientific payload and a reliable telecommunications system into an orbit around the planet Mars. Such a delivery can be accomplished by either an all chemical system or by use of a solar electric powered final stage spacecraft. The purpose then to be fulfilled in this study is a comparison of the chemical and the solar electric mission within the constraints stipulated by the contracting agency.

1. Solar Electric Spacecraft Performance Analysis

The low thrust mission analysis and propulsion system design which is being performed during this program is somewhat different from that which has been done previously. In the past many constant power interplanetary missions have been studied but in this case the power availability decreases monotonically as the spacecraft proceeds towards Mars. This one single difference has posed many new and unique problems. For some of these problems the solutions have already been found during this first reporting period; for others only a definition of possible solutions can be provided at this time.

Although the total mission objective is a Mars Orbiter, the specific role which the ion propulsion system will play in accomplishing this objective must still be decided. There are various possible mission profiles for the ion propulsion stage, for example:

1) Optimum Coast Rendezvous

The hyperbolic velocity for heliocentric transfer plus the velocity increment for capture. In this case, a coast period is employed midway in the heliocentric flight such that the final-to initial vehicle mass ratio is maximized for a given total flight time.

2) Zero Coast Rendezvous

The hyperbolic velocity for heliocentric transfer plus the velocity increment for capture. For this mission profile, thrust is applied throughout flight such that the initial acceleration is minimized for a given transfer time.

3) Minimum Time Flyby

The hyperbolic velocity for heliocentric transfer plus a velocity increment to minimize the approach velocity to the target planet.

4) Flyby

The hyperbolic velocity for heliocentric transfer.

The mission profiles above are listed in such a way that, for a given flight time, the initial acceleration and, therefore, power requirement decrease in the same order. However, it is also possible that the payload capacity will also decrease in that order. Obviously the total effect on mission performance and system design must be evaluated before a final choice is made.

Furthermore,in evaluating each individual mission profile there are several options which must be considered, namely

1) Departure Date
2) Launch Year
3) Hyperbolic Excess
4) Flight Time
5) Specific Impulse
6) Thrust Orientation

During the first months a first iteration of the overall program was completed. In order to accomplish this, two ground rules were established: First, that the propulsion system and vehicle design be based on a 350 day, 1971, zero coast rendezvous mission and second, that the low thrust mission analysis be extended to include the effects of departure date, launch year, flight time, and specific impulse. These data were generated for zero excess hyperbolic velocity and optimum variable thrust orientation. The results to be presented are, therefore, related to a specific type of mission and any conclusions drawn can not necessarily be generalized to all missions.

Two of the main objectives of the low thrust mission studies which have been performed are (1) to determine the payload capability of an electrically propelled spacecraft and subsequently compare it to an all chemical vehicle and (2) to establish the optimum design points for the propulsion system. Since there are, at least, several thrust devices under consideration and since the exact characteristics of flight type electric propulsion systems are still somewhat uncertain, a general approach to the mission analyses was chosen. That is, the trajectory analysis was separated from all propulsion system constraints. The results of the

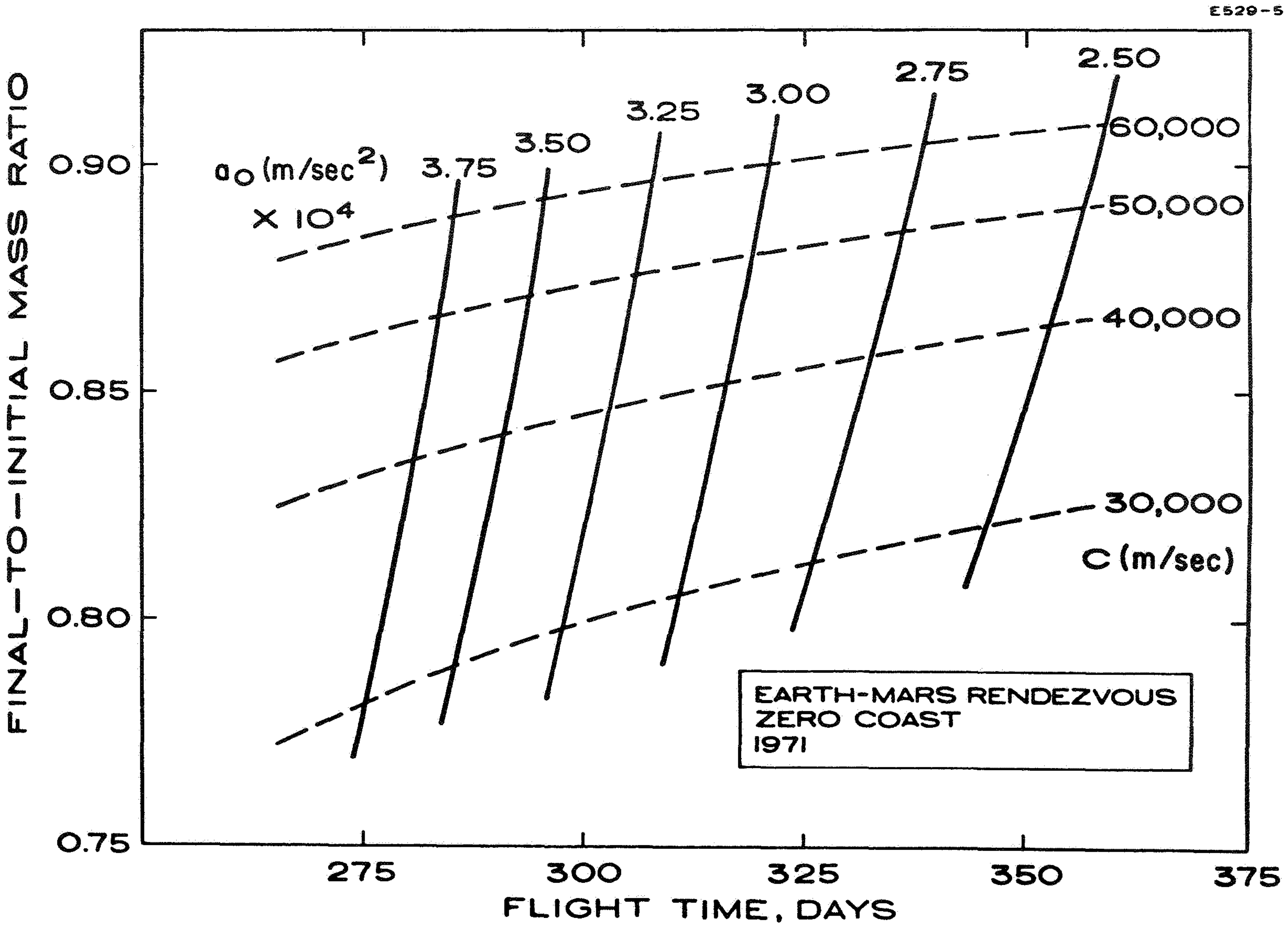

Fig. A.1-1. 1971 low thrust, high specific impulse propulsion system performance map.

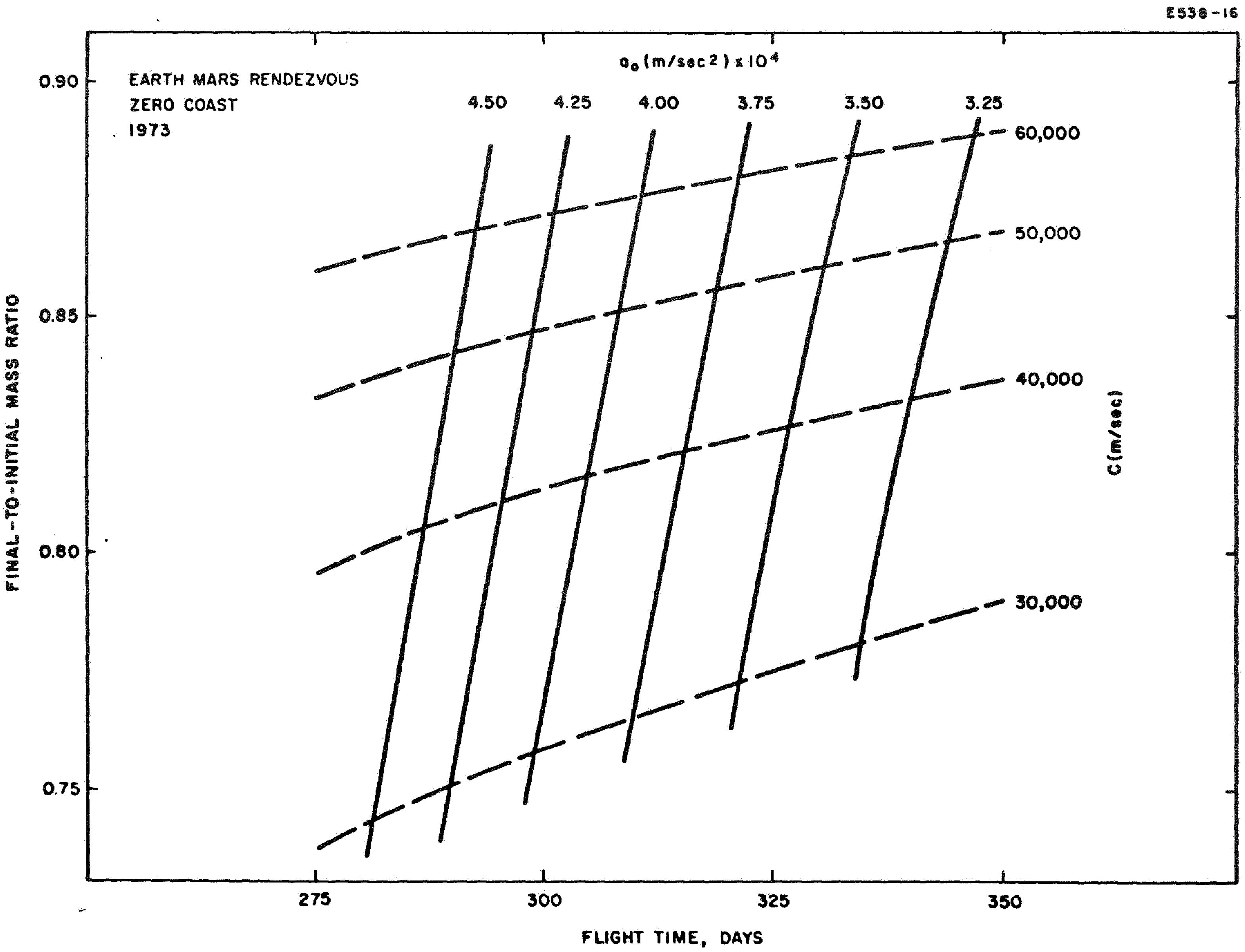

Fig. A. 1-2. 1973 low thrust, high specific impulse propulsion system performance map.

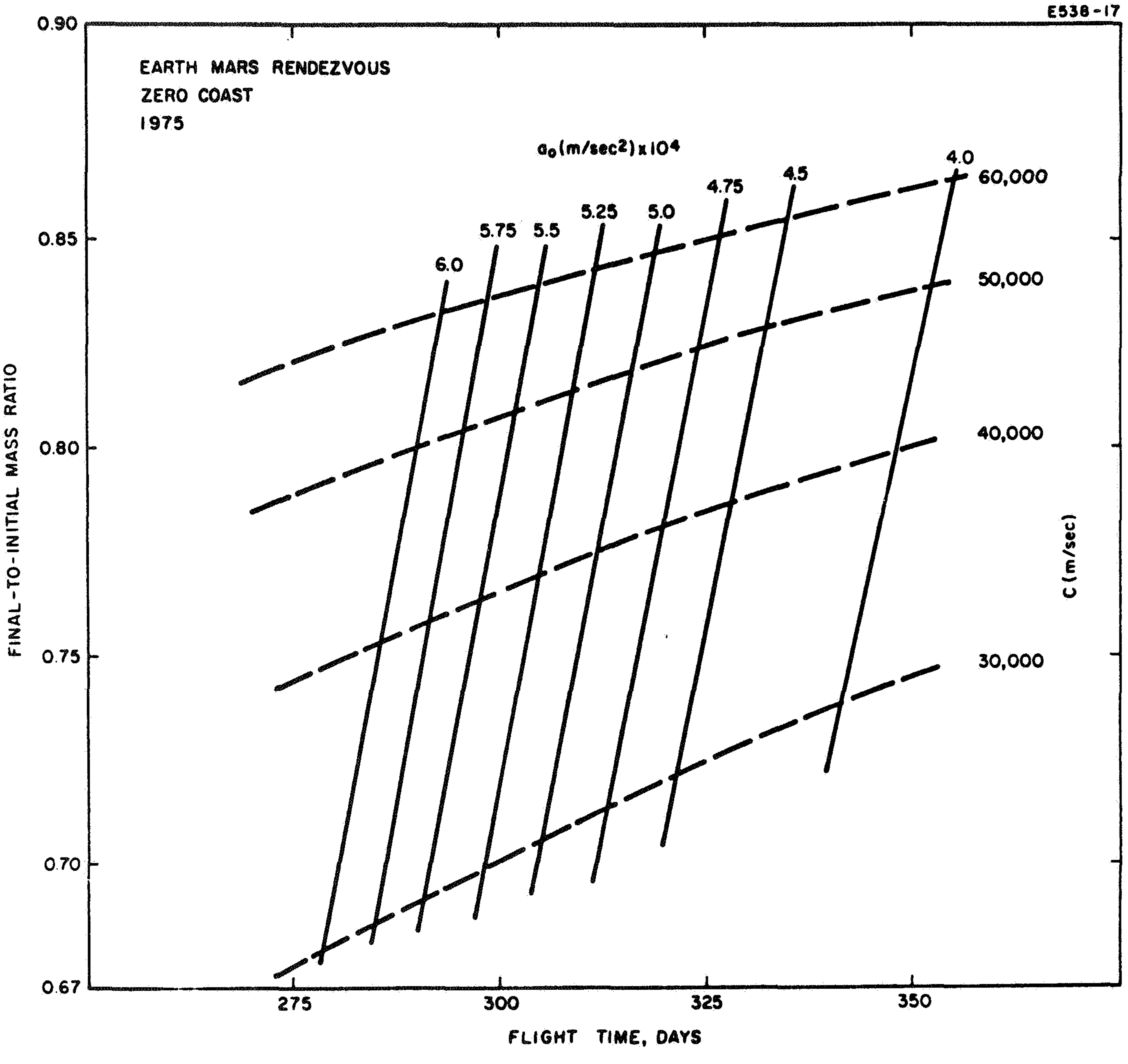

Fig. A. 1-3. 1975 low thrust, high specific impulse propulsion system performance map.

trajectory analysis are shown in Figs. A. 1-1, A. 1-2 and A. 1-3 which are performance maps for low acceleration, high specific impulse propulsion systems. These figures show the final-to-initial mass ratios as a function of total flight time for a zero coast rendezvous mission for launch years of 1971, 1973, and 1975, respectively. These data which were obtained as a direct output of the JPL low thrust variable power trajectory program are plotted for various values of initial acceleration and specific impulse. The results indicate that to a first order the final-to-initial mass ratio is dependent on specific impulse and is independent of initial acceleration and that total flight time is determined by the initial acceleration and is only slightly affected by specific impulse. As stated above, these data are completely independent of propulsion system constraints and can be used to evaluate the effectiveness of any low thrust device.

Since for the propulsion system and spacecraft design a 1971, 350 day mission was chosen, the propulsion system performance was evaluated for operating points from 3000 - 6000 sec I_{sp} and initial acceleration levels of approximately 2.5×10^{-4} m/sec^2 (e.g., see A. 1-1). By moving up the vertical 350 day line on Fig. A. 1-1 to higher values of specific impulse the final-to-initial mass ratio is increased, that is, the required propellant is decreased. However, since the power in the exhaust beam of an electric thrustor is proportional to specific impulse, the power source mass increases with I_{sp}. Obviously there is a tradeoff then between power and propellant and, therefore, an optimum I_{sp}. Optimum I_{sp} is defined here as that specific impulse at which the sum of the propulsion system and propellant masses are minimized. The total power required by the propulsion system is proportional to the specific impulse divided by the engine efficiency, thus one more effect that must be considered in determining $(I_{sp})_{opt}$ is the variation of engine efficiency with specific impulse.

The total engine efficiency as a function of specific impulse for both the Cs contact and Hg bombardment thrustors is shown in a later section (i.e. Fig. B. 1-3). These curves are meant to represent state-of-art devices and not ultimate performance capability. In addition these performance figures are felt to be consistent with 10,000 hr engine life.

With the data in Fig. B. 1-3 and the performance maps shown in Figs. A. 1-1, A. 1-2, and A.1-3; the optimum specific impulse, payload capability, and the power requirement for a given initial spacecraft weight can be determined for each type of thrustor system.

Figure A. 1-4 presents the payload capability and the optimum I_{sp} for both the contact and bombardment engines for the 1971, 350 day, zero coast rendezvous mission. The specific weight of the propulsion system is assumed to be 75 lb/kW. In each case the power requirement for a 11,700 lb spacecraft is given. The term payload mass on this figure as well as those to follow is defined as that mass placed in some elliptical orbit about Mars less the mass of the electric propulsion system. For the bombardment engine, the maximum payload capability is about 57% at an I_{sp} of 4000 sec. The payload falls off slightly at $I_{sp} > 4000$ sec. The power requirement at 4000 sec I_{sp} is about 46 kW increasing to 60 kW at 6000 sec I_{sp}. Therefore, even though only a small payload penalty is paid for operating at a specific impulse greater than the optimum, a relatively large increase in power is required. However, operation at 3000 sec I_{sp} provides little or no payload loss while lowering the power requirement to 40 kW.

In the specific impulse region shown the effect of increasing I_{sp} for the contact engine is an increase in payload capability and a decrease in power requirement. The optimum I_{sp} for the contact engine will occur at about 6200 sec providing a payload ratio of about 52% and a power requirement of 60 kW.

The effect of total flight time on payload, optimum I_{sp}, and power requirement is shown in Fig. A. 1-5. The optimum specific impulses for the three flight times shown all lie between 3000 - 4000 sec with the payload mass ratio dropping from 57% for 350 days to 48% for 300 days. The power requirement for the 300 day mission is 50 kW.

The reduction in payload capability for launch years of 1973 and 1975 is given in Fig. A. 1-6. Also presented is the effect of launch year on

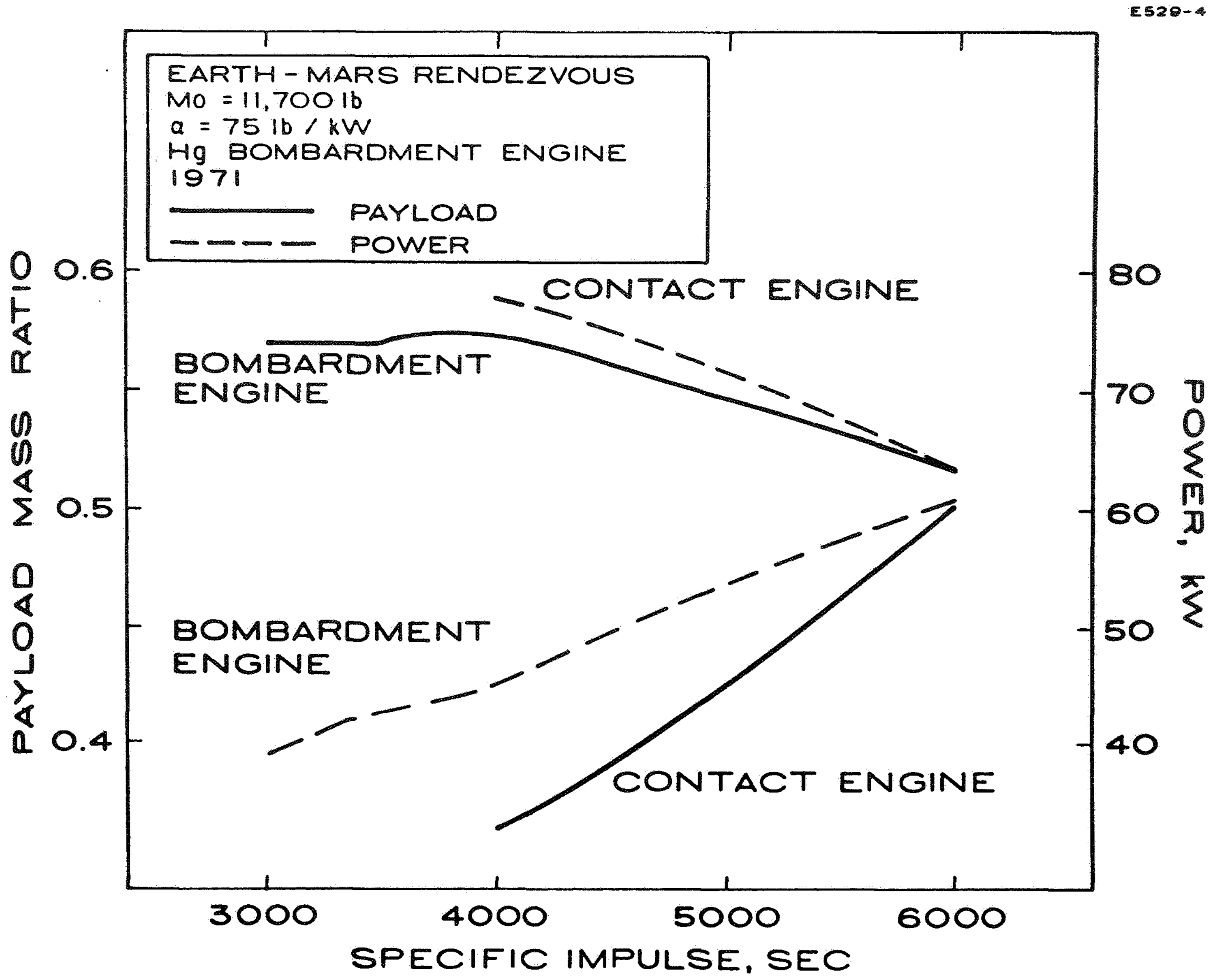

Fig. A. 1-4. Mercury bombardment and cesium contact ion engine performance capability.

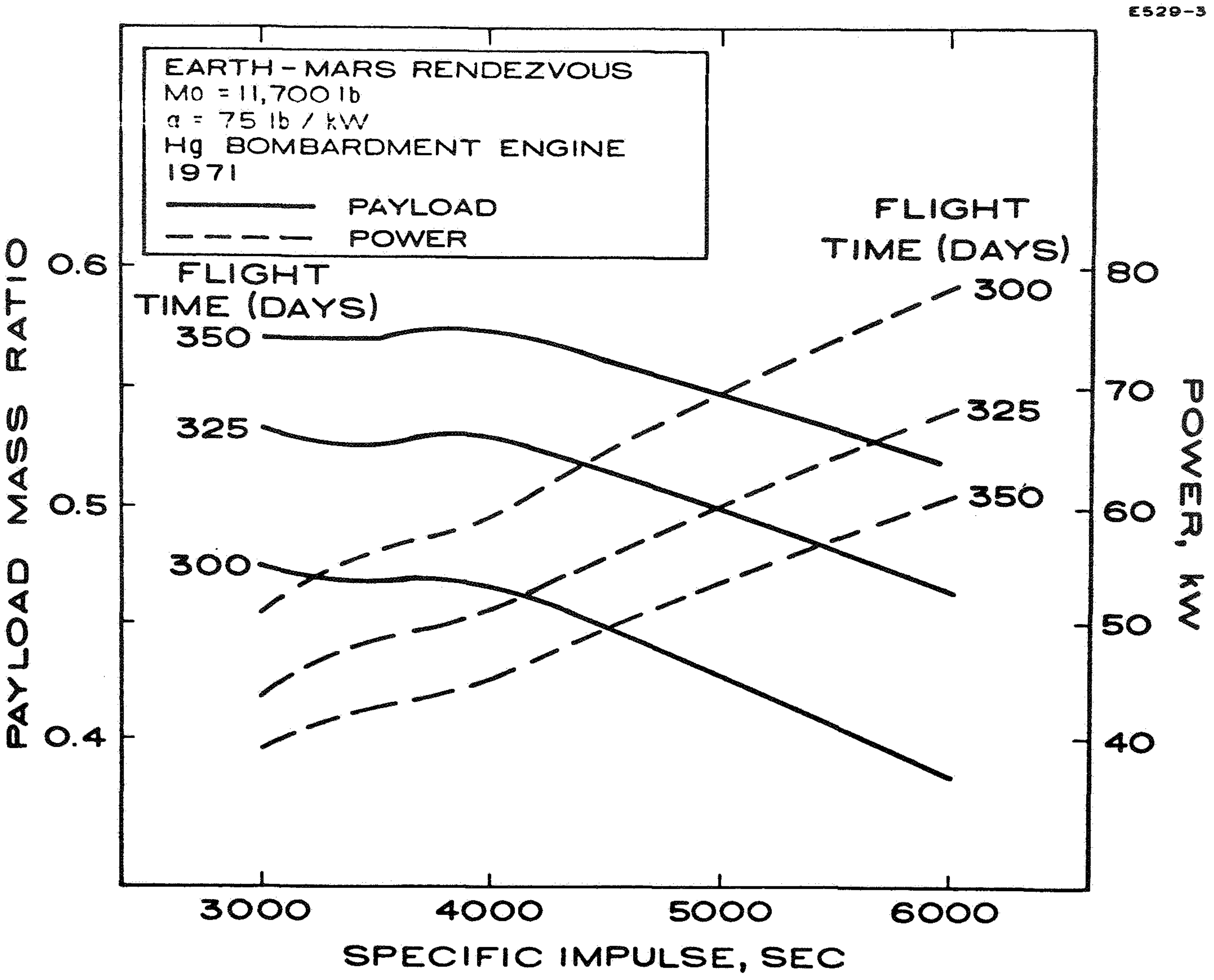

Fig. A.1-5. Effect of total flight time on ion engine performance.

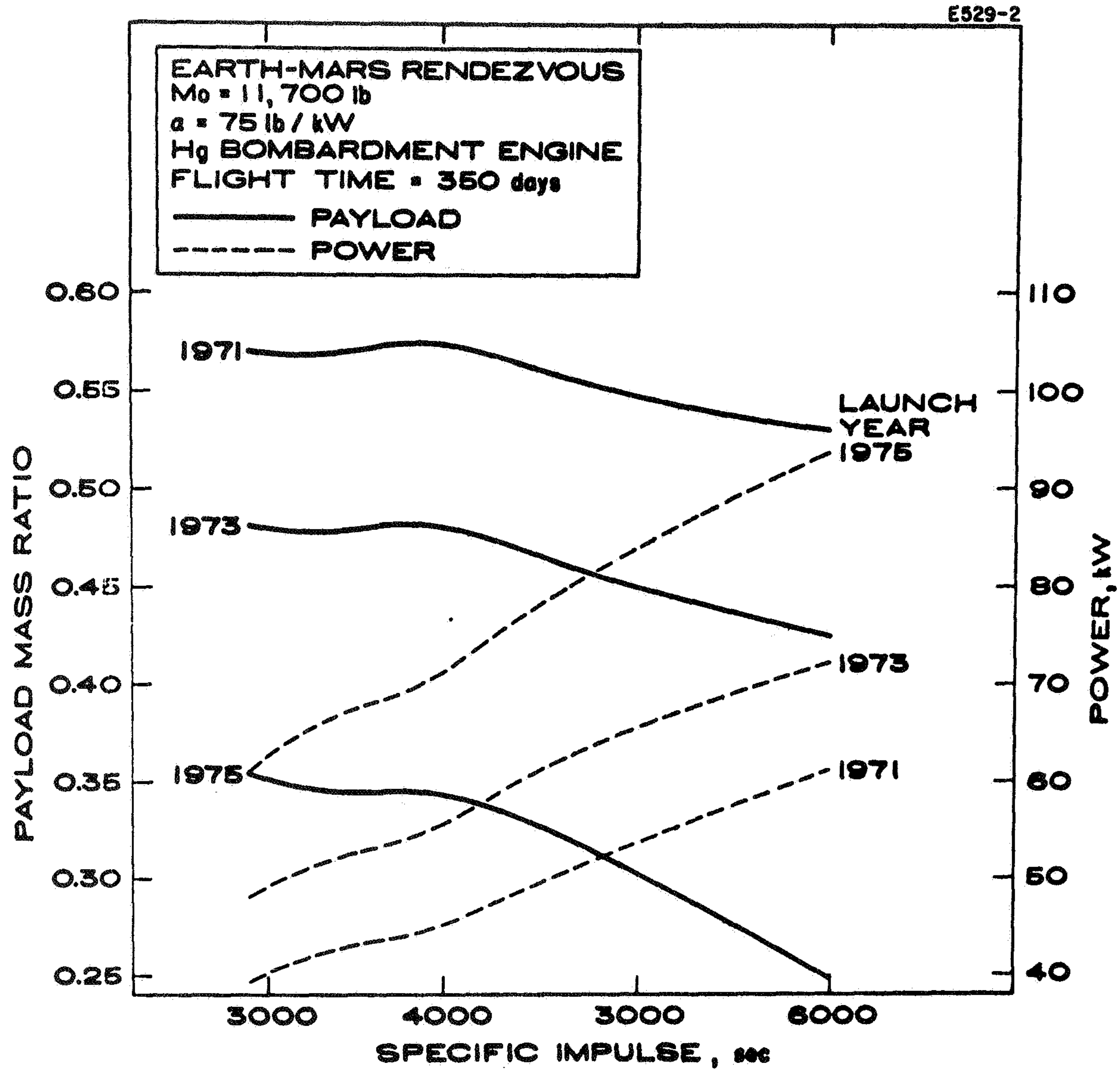

Fig. A. 1-6. Effect of launch year on ion engine performance.

the system design parameters. The optimum I_{sp} remains in the 3000 to 4000 sec region while the power requirement increases to about 60 kW for the 1975 launch year. The payload mass ratio for 1973 is 47% as compared to 35% for 1975. Again, these data are for a 350 day zero coast rendezvous mission. It is possible that for the 1975 mission a flyby profile would be more desirable. This possibility will be evaluated.

The penalty paid as a function of launch window is shown in Fig. A. 1-7. As shown, about a 2% loss in payload is sustained if a 30 day launch window is required. For the 30 day launch window, the power requirement increases from 46 kW to 48 kW.

Figure A. 1-8 shows the total heliocentric angle through which the spacecraft must travel. As measured from the initial sun-probe line, the total angle is about 270 degrees.

An important consideration in the spacecraft design is the required thrust vector direction. The variation of thrust angle is also shown in Fig. A. 1-8. Measuring from the sun-probe line, the thrust angle varies continuously from 75° - 60° -110° - 95°. Since a continuously varying thrust angle is undesirable from a spacecraft design standpoint, the payload penalty for approximating the curve shown by two discreet thrustor positions will be determined.

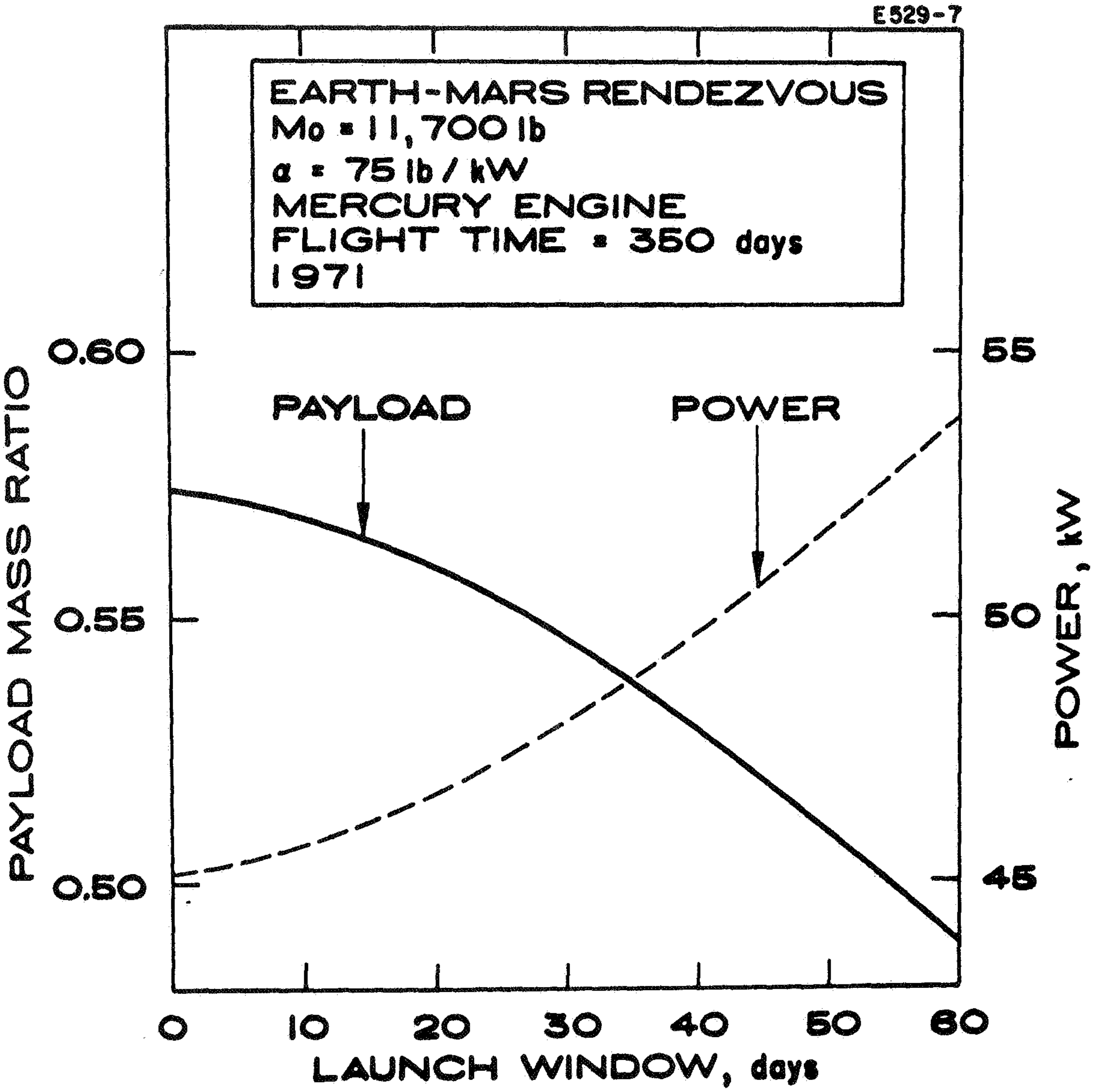

Fig. A. 1-7. Effect of launch window on ion engine performance.

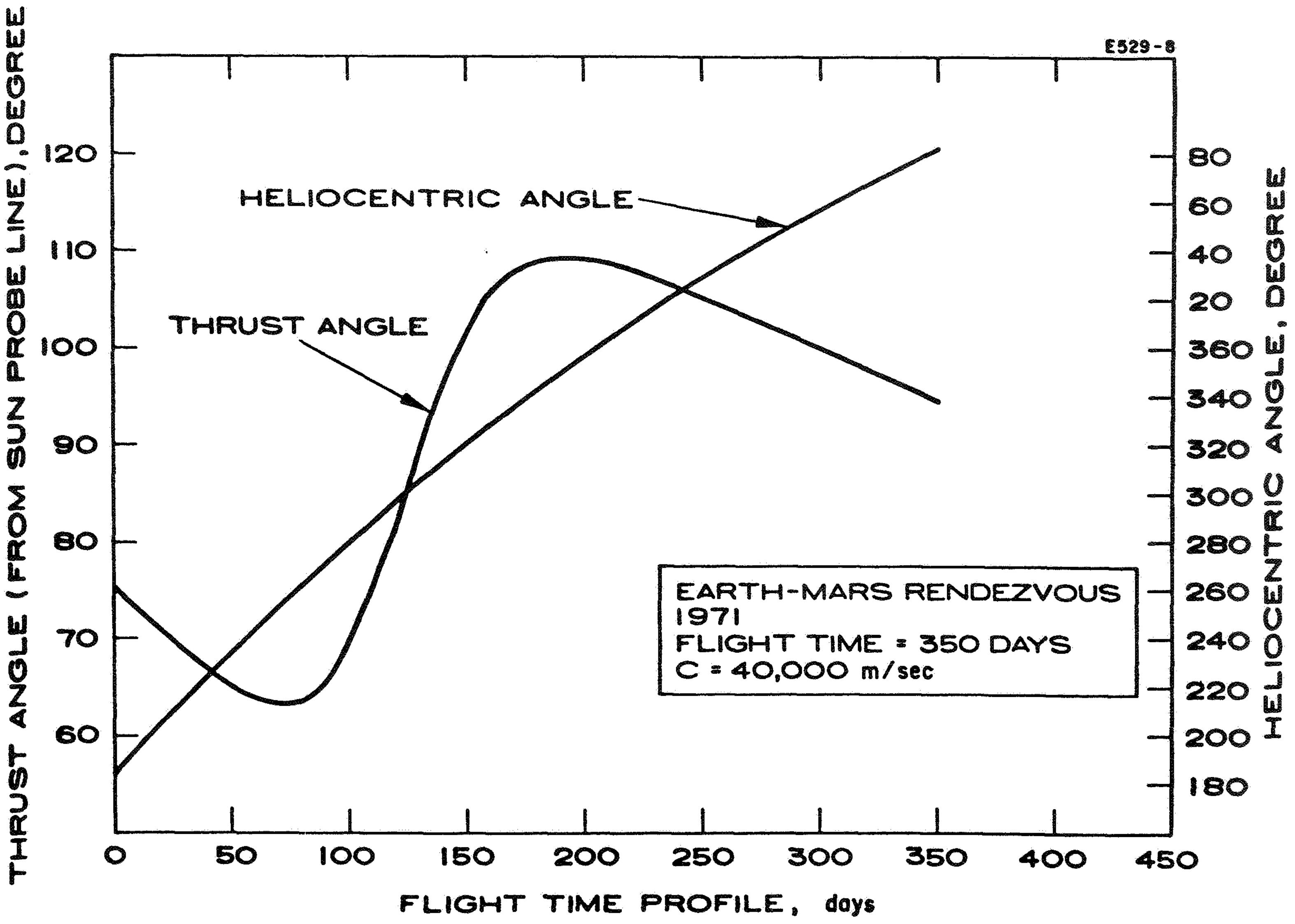

Fig. A. 1-8. Thrust vector orientation and heliocentric angle time profiles.

2. All-Chemical Spacecraft Performance Analysis

Payload capability of a Mars orbiter using all-chemical propulsion is summarized in this section. Four major parameters have been considered in maximizing the orbiter mass, as follows:

a. Geocentric injection energy requirement (C_3),

b. Hyperbolic excess speed at Mars (V_{hp}),

c. Near Earth geometry - characterized by the declination angle of the departure asymptote (ϕ_s), and

d. Near Mars geometry - characterized by the angle between the hyperbolic excess approach velocity at Mars and the Mars-Sun line (ζ_p)

The actual determination of orbiter mass capability is further dependent on the size of Martian orbit selected, and characteristics of retro-propulsion system to be used.

It has been customary to use the minimum value of C_3 for a given firing period to arrive at the maximum spacecraft weight leaving the Earth for flyby missions. For orbiter missions, however, the amount of retro propellant required for injection into a planetary orbit must be included in the overall process of maximizing the remaining orbit weight. Furthermore, the presence of a landing capsule must also be included in the analysis. Therefore, it would be advantageous to use a transfer trajectory with a low hyperbolic excess speed at Mars. Since the trajectory having low C_3 at geocentric injection is not the same as that having a low hyperbolic excess speed at Mars, and since separation of the capsule introduces a staging computation, investigation of maximum payload capability for a Mars orbiter has to be carried out for specific combination of booster vehicles, retro propulsion system performance, and dimensions of the final orbit about the planet Mars.

The main result herein deals with missions using Saturn IB/Centaur booster combination, and covers the 1969-1975 period. Some fragmentary results are also given for missions using Atlas/Centaur booster (only for the year 1971). These results are required for comparison with the mission capability of a solar powered electric propulsion system using the same booster combinations.

Due to the limited amount of time available for the generation of the aformentioned performance data, the following conditions are adopted to provide the basis of performance comparison.

a. A 1000 pound capsule will be assumed to be aboard the orbiter using the Saturn IB/Centaur booster. This capsule is to be separated from the orbiter well before retro application--this allows for a substantial reduction in retro propellant required to place the remaining orbiter in the desired orbit.

b. No capsule will be carried aboard the orbiter using the Atlas/Centaur booster.

c. The nominal Martian orbit will have a periapsis altitude of 4,000 km. and an apoapsis altitude of 50,000 km. These values have been chosen from orbital lifetime considerations.

d. The retro propulsion system will be assumed to have a specific impulse of 315 seconds, and the dry weight of the propulsion system is taken to be 10 per cent of the entire propulsion system.

e. Certain allowance for velocity increment will be provided for mid-course correction and losses due to finite burning time and other causes. For the Saturn IB/Centaur booster, this allowance is taken to be 300 meters per second; for the Atlas/Centaur booster, it is taken to be 100 meters per second. It is assumed that this allowance will be completely consumed prior to capsule separation.

The useful orbiter weight will be defined as the final weight of the orbiter less the dry weight of the retro propulsion system. The following relation may be readily obtained:

$$W_i = W_f + W_d + W_c + W_o \tag{1}$$

with the subscripts i, f, d, c, o denoting respectively the injected weight, the propellant weight, the dry weight of the propulsion system, the capsule weight and the useful orbiter weight.

Let ΔV_m denote the allowance for velocity increment defined in paragraph e above, and ΔV_r denote the velocity increment required to place the orbiter into the desired Martian orbit; it follows that the amount of propellant consumed prior to capsule separation is

$$W_{f,m} = W_i (1 - e^{-X_m}); \; X_m = \Delta V_m / g I_{sp}, \tag{2}$$

and the amount of propellant required for retro is

$$(3) \qquad W_{f,r} = (W_d + W_o)(e^{X_r} - 1); \; X_r = \Delta V_r / gI_{sp.}$$

Since $W_d = \alpha(W_d + W_f) = \alpha(W_d + W_{f,m} + W_{f,r})$,

the useful orbiter weight may be expressed as

$$(4) \qquad W_o = \left[W_i(e^{-X_m - X_r} - \alpha) - W_c\,(e^{-X_r} - \alpha) \right] / (1 - \alpha)$$

For the present investigation, $\alpha = 0.1$ as postulated in paragraph d, and $W_c = 1000$ pounds or zero depending on the booster combination under consideration.

The velocity increment required to establish a Martian orbit with apoapsis distance R_a and periapsis distance R_p, assuming retro application of the periapsis, is

$$(5) \qquad \Delta V_r = \sqrt{V_{hp}^2 + (2\,\mu/R_p)} - \sqrt{2\,\mu R_a/R_p(R_a + R_p)}$$

With $\mu = 4.3 \times 10^4$ km.^{3}/sec.^{2} for Mars, this becomes

$$\Delta V_r = \sqrt{V_{hp}^2 + 11.64} - 3.20 \text{ in km./sec. for } 4,000 \times 50,000 \text{ orbit.}$$

This is the only value used in the present study. Values corresponding to other orbits are listed below for reference.

$$\begin{aligned}
\Delta V_r &= \sqrt{V_{hp}^2 + 11.64} - 2.98 \text{ km./sec. for } 4,000 \times 20,000 \text{ orbit,} \\
&= \sqrt{V_{hp}^2 + 11.64} - 2.41 \text{ km./sec. for } 4,000 \times 4,000 \text{ orbit,} \\
&= \sqrt{V_{hp}^2 + 17.60} - 4.01 \text{ km./sec. for } 1,500 \times 50,000 \text{ orbit,} \\
&= \sqrt{V_{hp}^2 + 17.60} - 3.81 \text{ km./sec. for } 1,500 \times 20,000 \text{ orbit,}
\end{aligned}$$

The injected weight (W_i) is a function of the geocentric injection energy parameter (C_3). Thus, the useful orbiter weight becomes a function of two variables, C_3 and V_{hp}, in accordance with equations (4) and (5). Results for Saturn IB/Centaur and for Atlas/Centaur are shown in Figures A.2-1 and A.2-2, as curves of constant useful orbiter weight. Since values of C_3 and V_{hp} are functions of launch date and arrival date, curves of constant useful

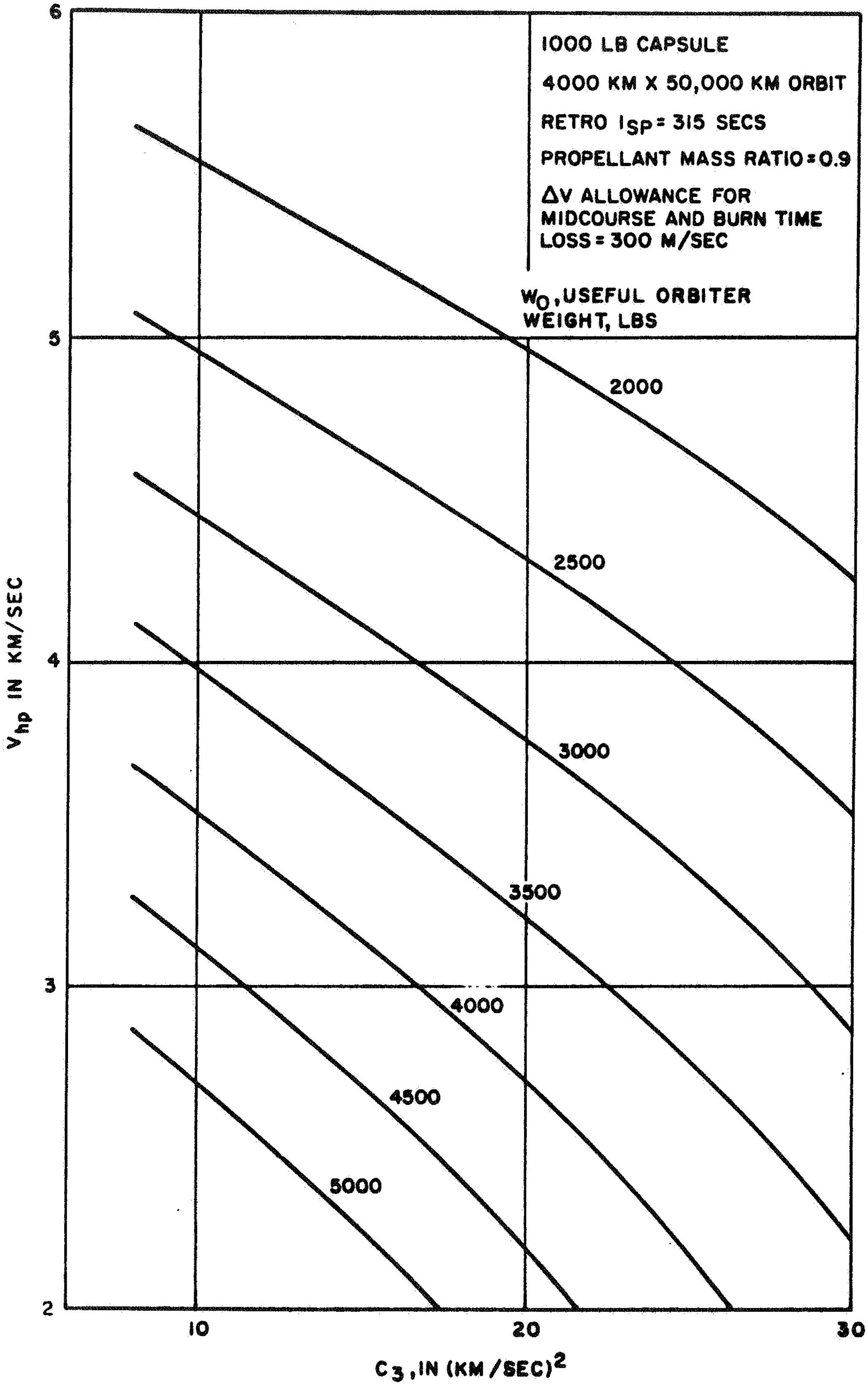
1000 LB CAPSULE
4000 KM X 50,000 KM ORBIT
RETRO I_{SP} = 315 SECS
PROPELLANT MASS RATIO = 0.9
ΔV ALLOWANCE FOR MIDCOURSE AND BURN TIME LOSS = 300 M/SEC
W_O, USEFUL ORBITER WEIGHT, LBS
2000
2500
3000
3500
4000
4500
5000
6
5
4
3
2
V_{hp} IN KM/SEC
10
20
30
C_3, IN (KM/SEC)^2

Figure A. 2-1

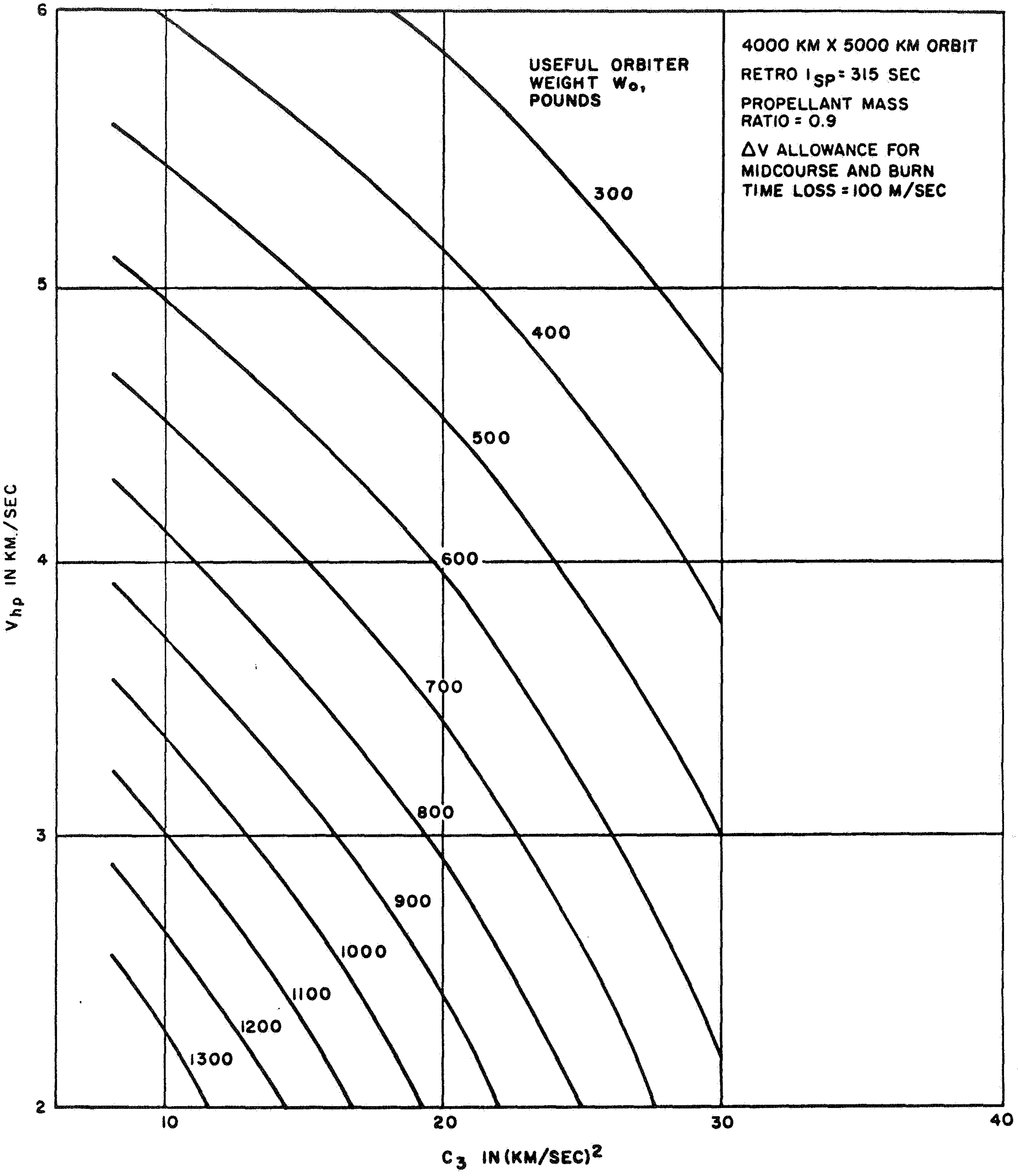
6
5
4
3
2
10
20
30
40
V_{hp} IN KM./SEC
C_3 IN (KM/SEC)^2
USEFUL ORBITER WEIGHT W_o, POUNDS
4000 KM X 5000 KM ORBIT
RETRO I_{SP} = 315 SEC
PROPELLANT MASS RATIO = 0.9
ΔV ALLOWANCE FOR MIDCOURSE AND BURN TIME LOSS = 100 M/SEC
300
400
500
600
700
800
900
1000
1100
1200
1300

Figure A. 2-2

orbiter weight can be constructed in a launch date and arrival date plane. These contours are presented in the upper portions of Figures A. 2-3a through A. 2-3h, A. 2-4a and A. 2-4b. These curves depict the maximum useful orbiter weight that may be delivered in accordance with the assumptions previously set forth.

Certain constraints placed upon the trajectories will restrict the full use of the useful orbiter weight capability as derived from considerations described in the foregoing paragraphs.

a. Restriction of Geocentric departure asymptote. When the absolute magnitude of the declination of the geocentric departure asymptote becomes greater than the latitude of the launch site, there exists a band of launch azimuths symmetric about 90° (due East) in which it is not possible to launch without performing dog-leg maneuvers. The range of this band depends upon the declination angle (Φ_s) of the departure asymptote and is shown in Figure A. 2-5 for a launch site (e. g. Cape Kennedy) at 28.3° latitude. Curves corresponding to several values of Φ_s are included in the diagrams of constant orbiter weight contours to illustrate the limitations imposed on available firing periods.

b. Restriction due to Planet Approach Geometry. For proper lighting for various experiments while the orbiter is approaching the planet Mars, the angle between the hyperbolic excess velocity vector and the Mars centered plane normal to the Mars-Sun line should be greater than 30°. This means that the angle (ζ_p) between the approach velocity vector and the Mars-Sun line must be eigher less than 60° or greater than 120°. These limiting curves, when applicable, are also included in the diagrams of constant orbiter weight contours.

The available firing period for a given useful orbiter weight may be established readily from the diagrams shown in Figures A. 2-1 through A. 2-4b. For example, refer to Figure A. 2-3c giving the results for Type I trajectories in 1971, a Saturn IB/Centaur booster would be capable of delivering 4,780 pounds of useful orbiter weight in addition to a 1000 pound capsule over a 30 day

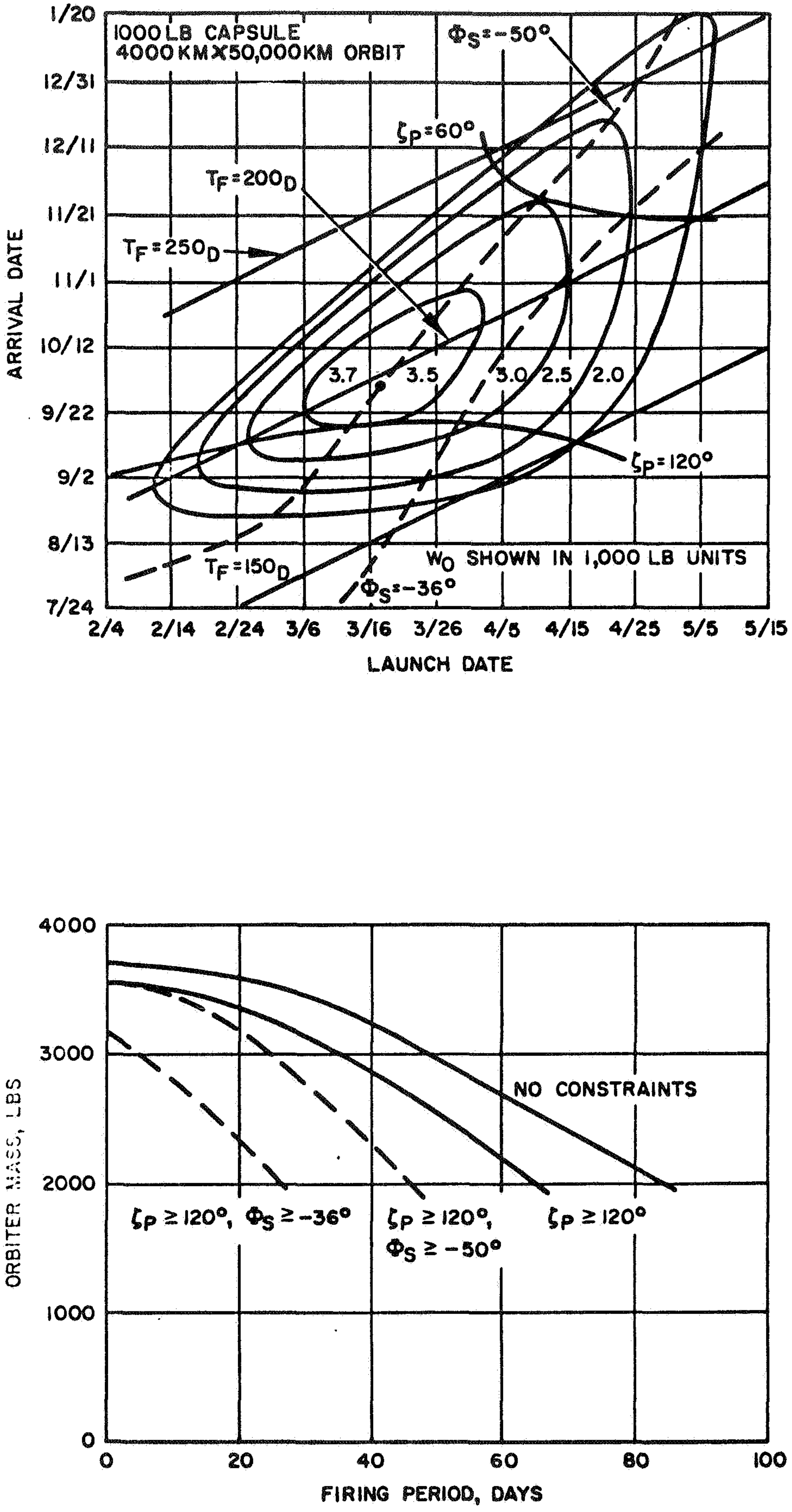

Figure A. 2-3a

ARS ORBITER CAPABILITY–SATURN IB/CENTAUR LAUNCH VEHICLE
1969 TYPE I

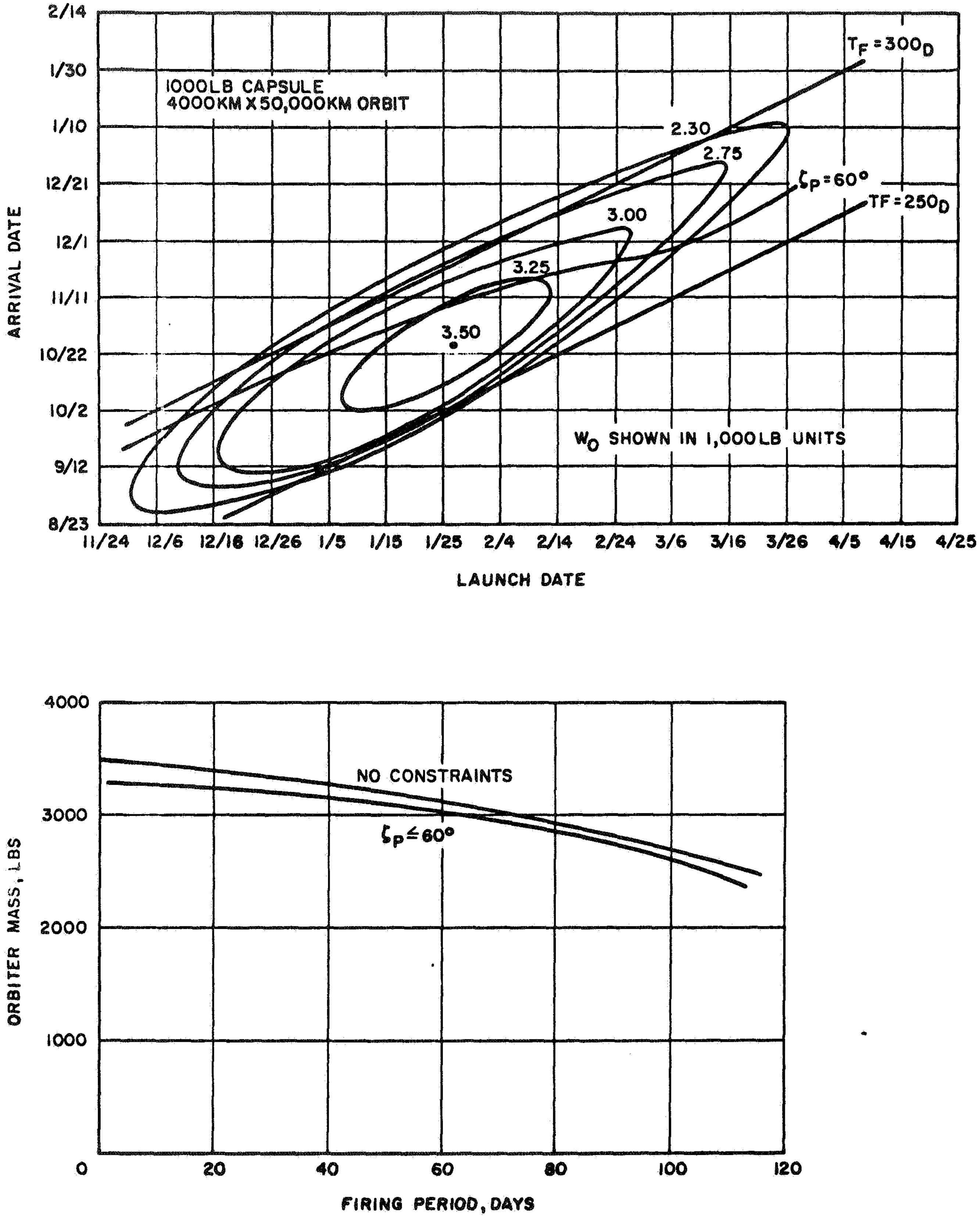

Figure A. 2-3b

MARS ORBITER CAPABILITY—SATURN IB/CENTAUR LAUNCH VEHICLE

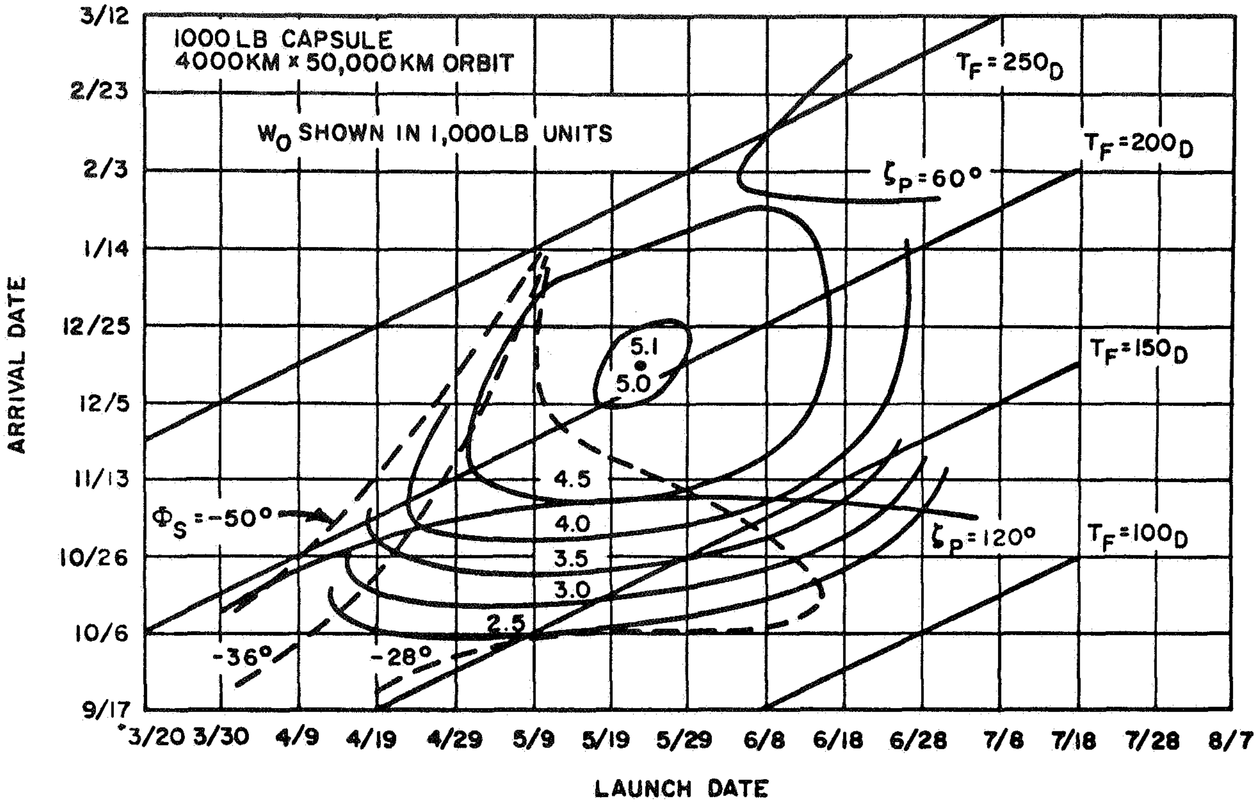

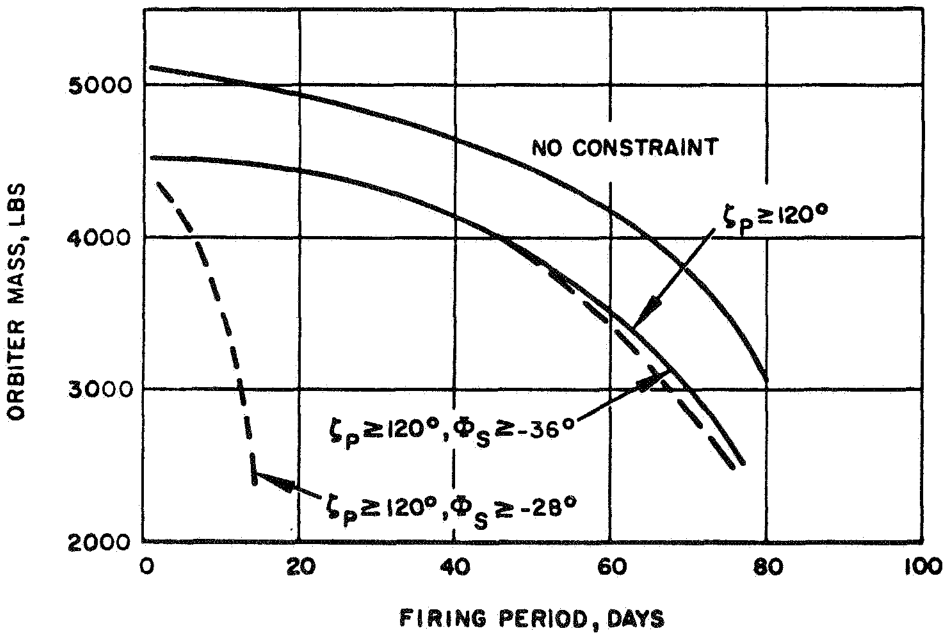

Figure A. 2-3c

MARS ORBITER CAPABILITY FOR SATURN IB/CENTAUR
1971 TYPE I

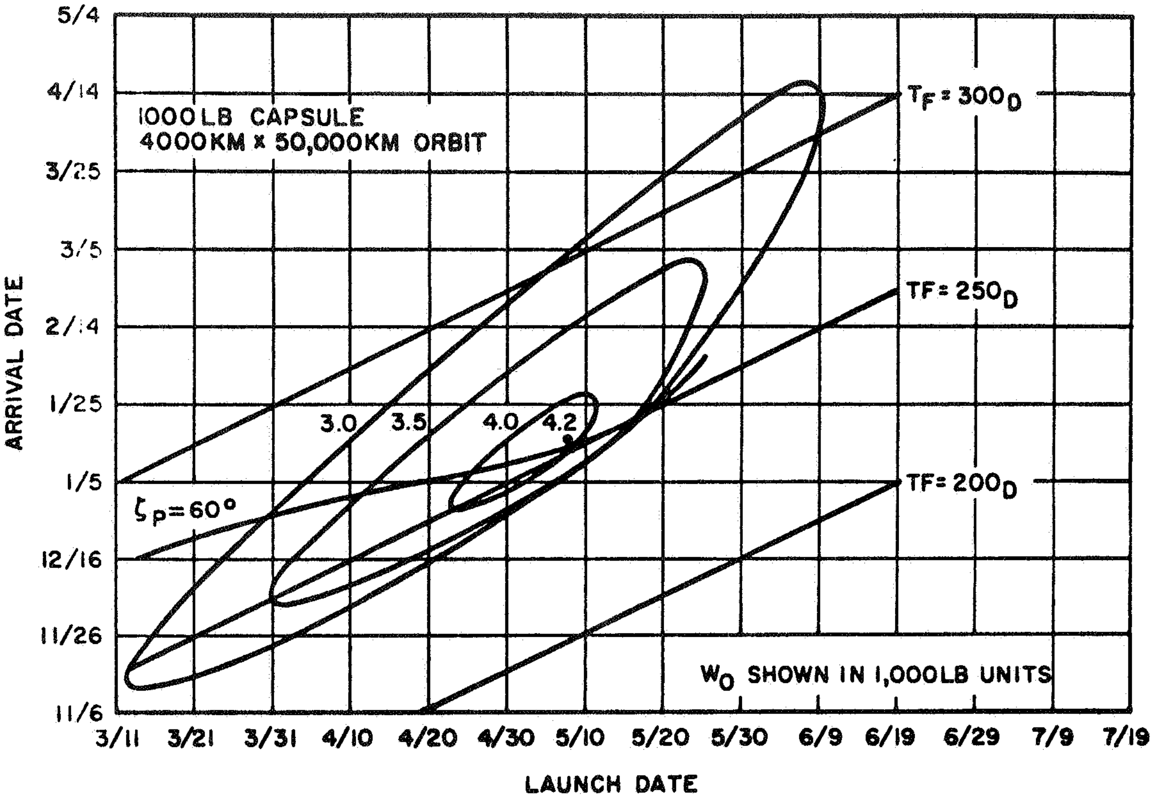
1000 LB CAPSULE
4000KM x 50,000KM ORBIT
ARRIVAL DATE
5/4
4/14
3/25
3/5
2/14
1/25
1/5
12/16
11/26
11/6
T_F = 300$_D$
TF = 250$_D$
TF = 200$_D$
3.0
3.5
4.0
4.2
ζ_p = 60°
W_0 SHOWN IN 1,000LB UNITS
3/11
3/21
3/31
4/10
4/20
4/30
5/10
5/20
5/30
6/9
6/19
6/29
7/9
7/19
LAUNCH DATE

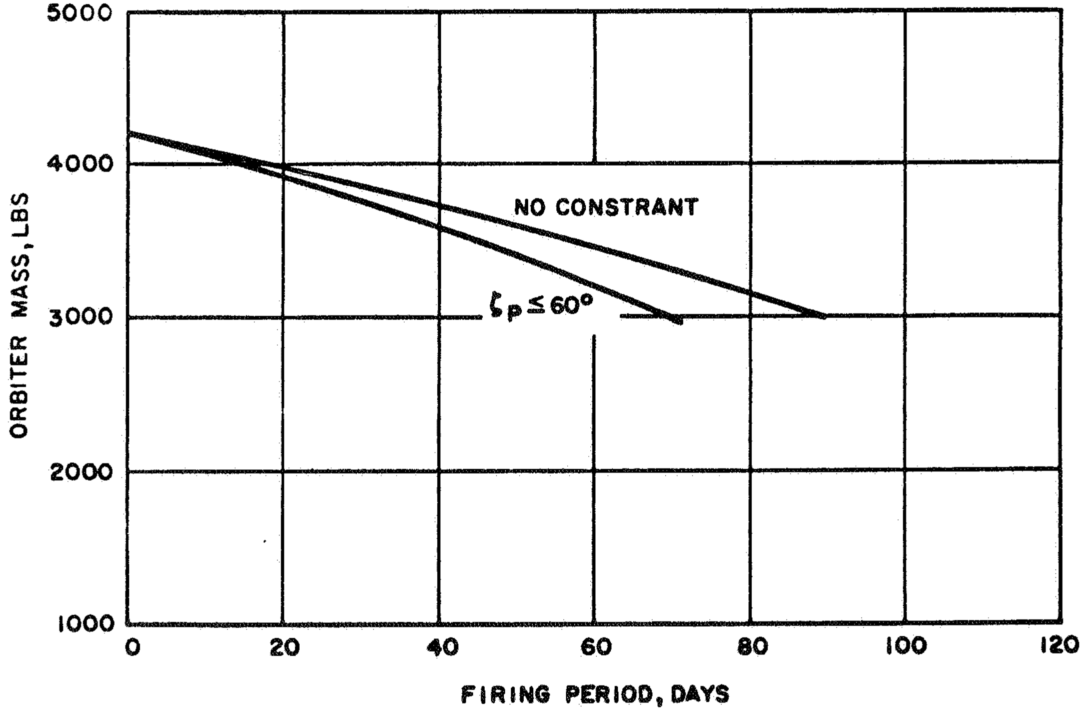
5000
4000
3000
2000
1000
ORBITER MASS, LBS
NO CONSTRANT
$\zeta_p \leq 60°$
0
20
40
60
80
100
120
FIRING PERIOD, DAYS

Figure A.2-3d

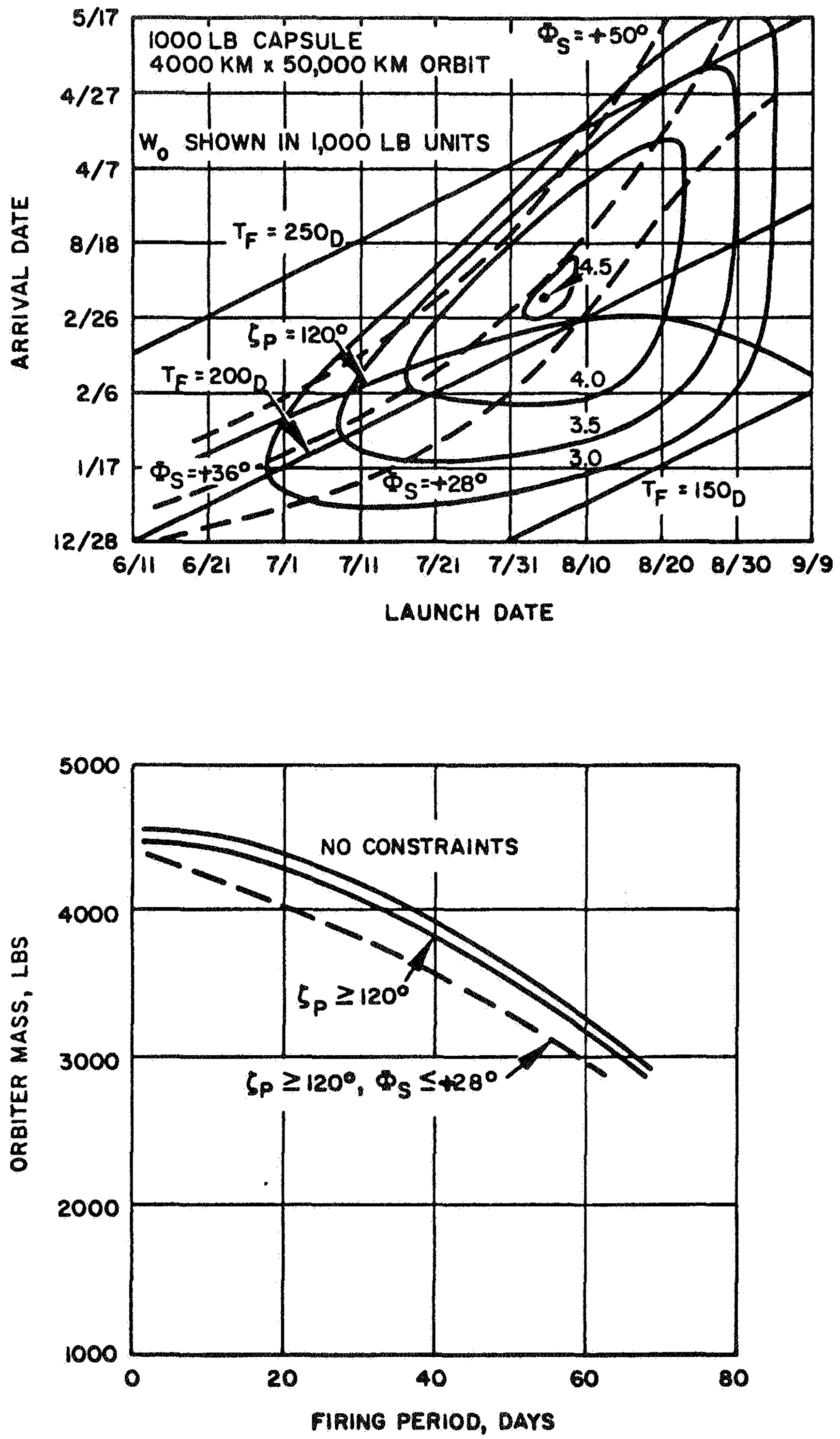

Figure A. 2 -3e

MARS ORBITER CAPABILITY-SATURN IB/CENTAUR

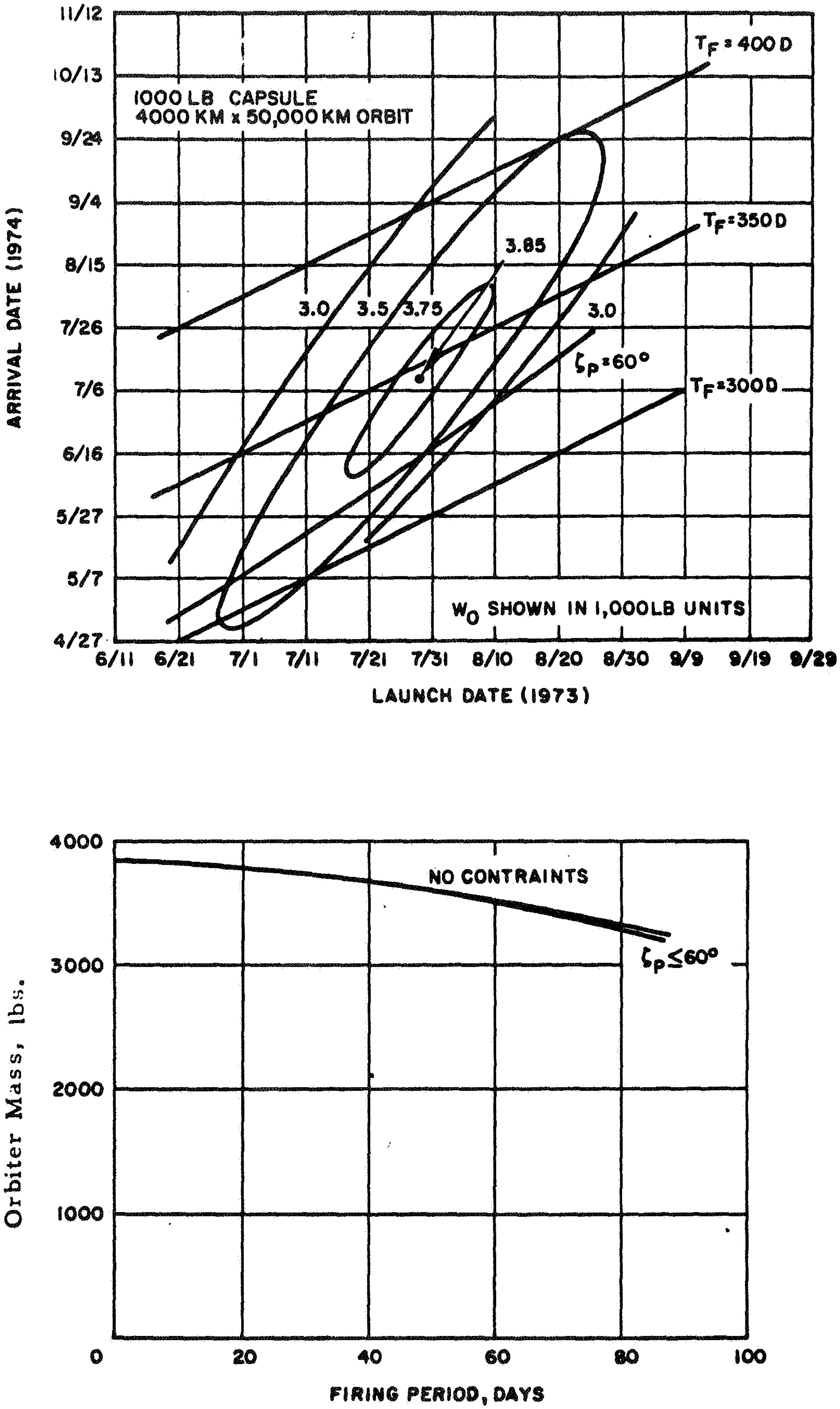

Figure A. 2-3f

MARS ORBITER CAPABILITY-SATURN IB/CENTAUR

1973 TYPE II

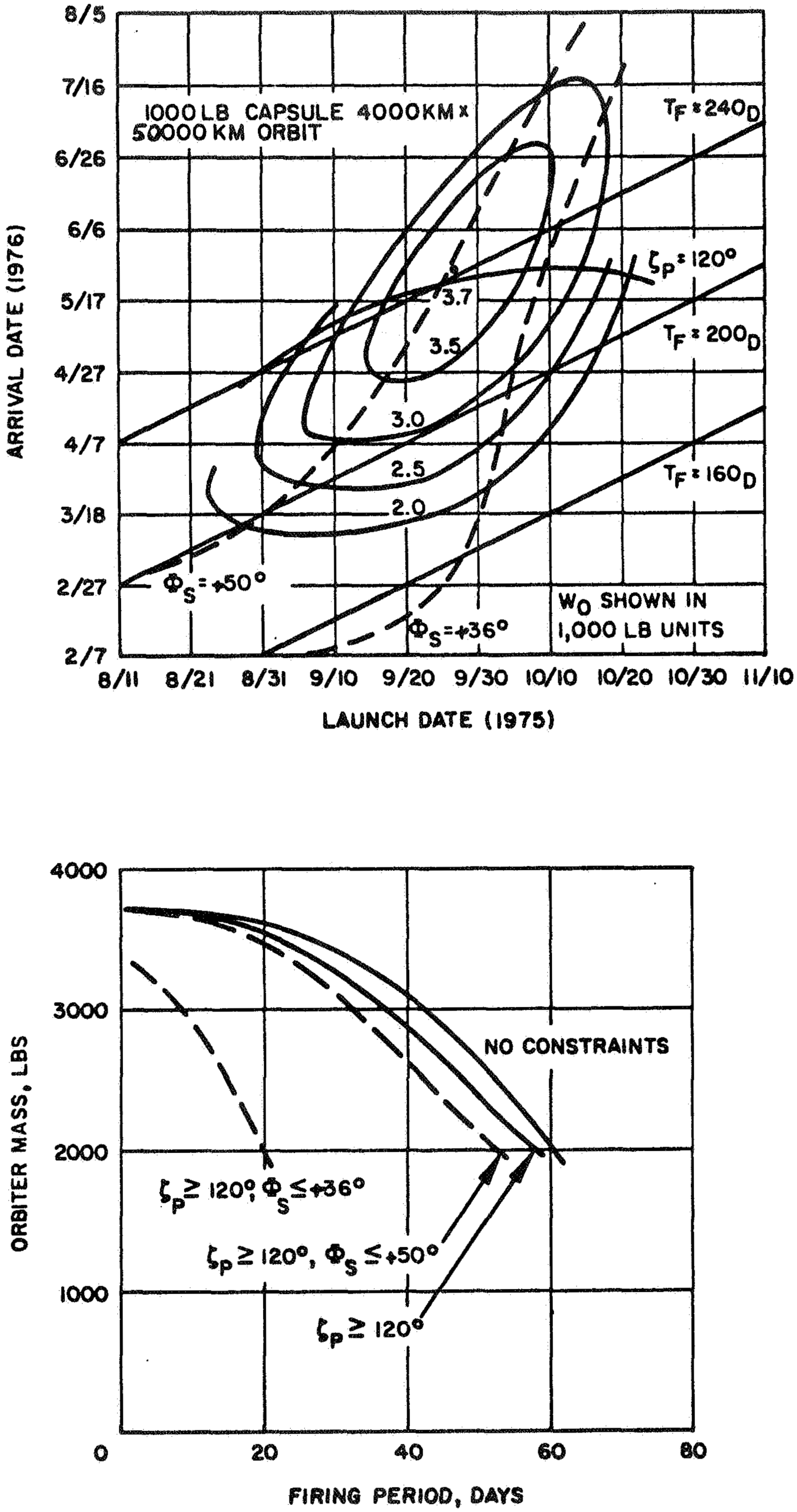

Figure A.2-3g

MARS ORBITER CAPABILITY-SATURN IB/CENTAUR

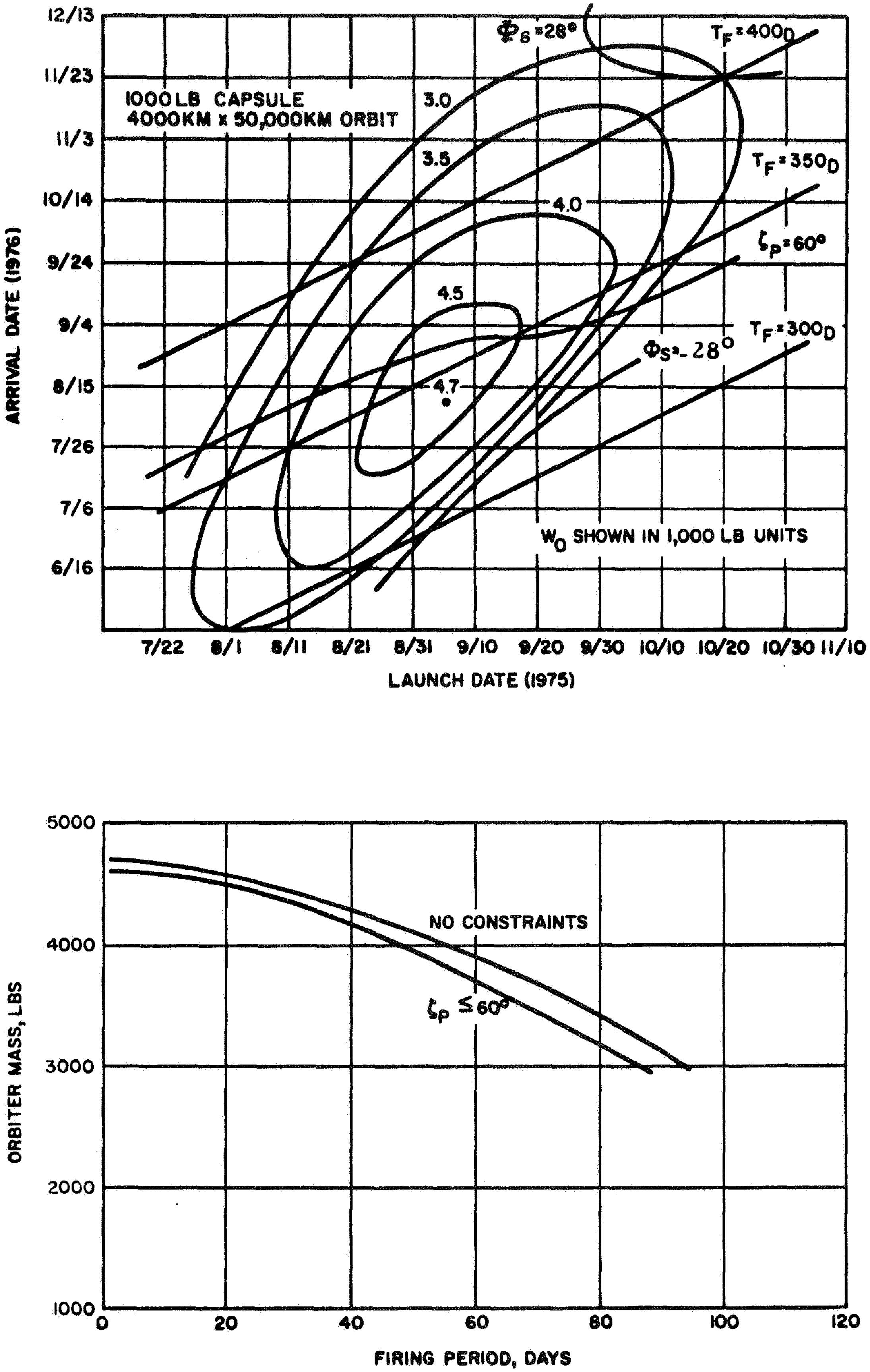

Figure A. 2-3h

MARS ORBITER CAPABILITY–SATURN IB/CENTAUR
1975 TYPE II

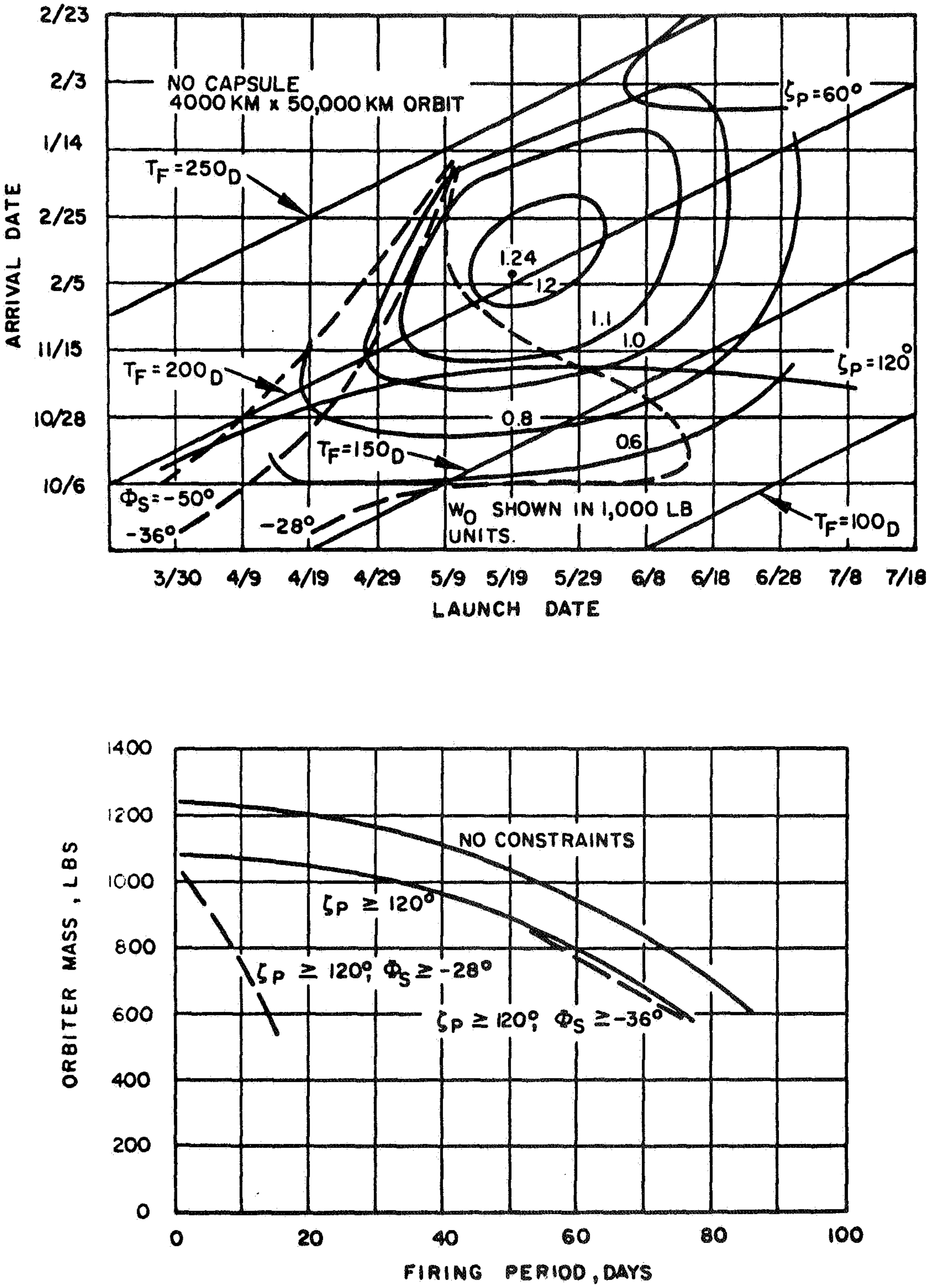

Figure A. 2-4a

MARS ORBITER CAPABILITY—/ LAS/CENTAUR LAUNCH VEHICLE
1971 TYPE I

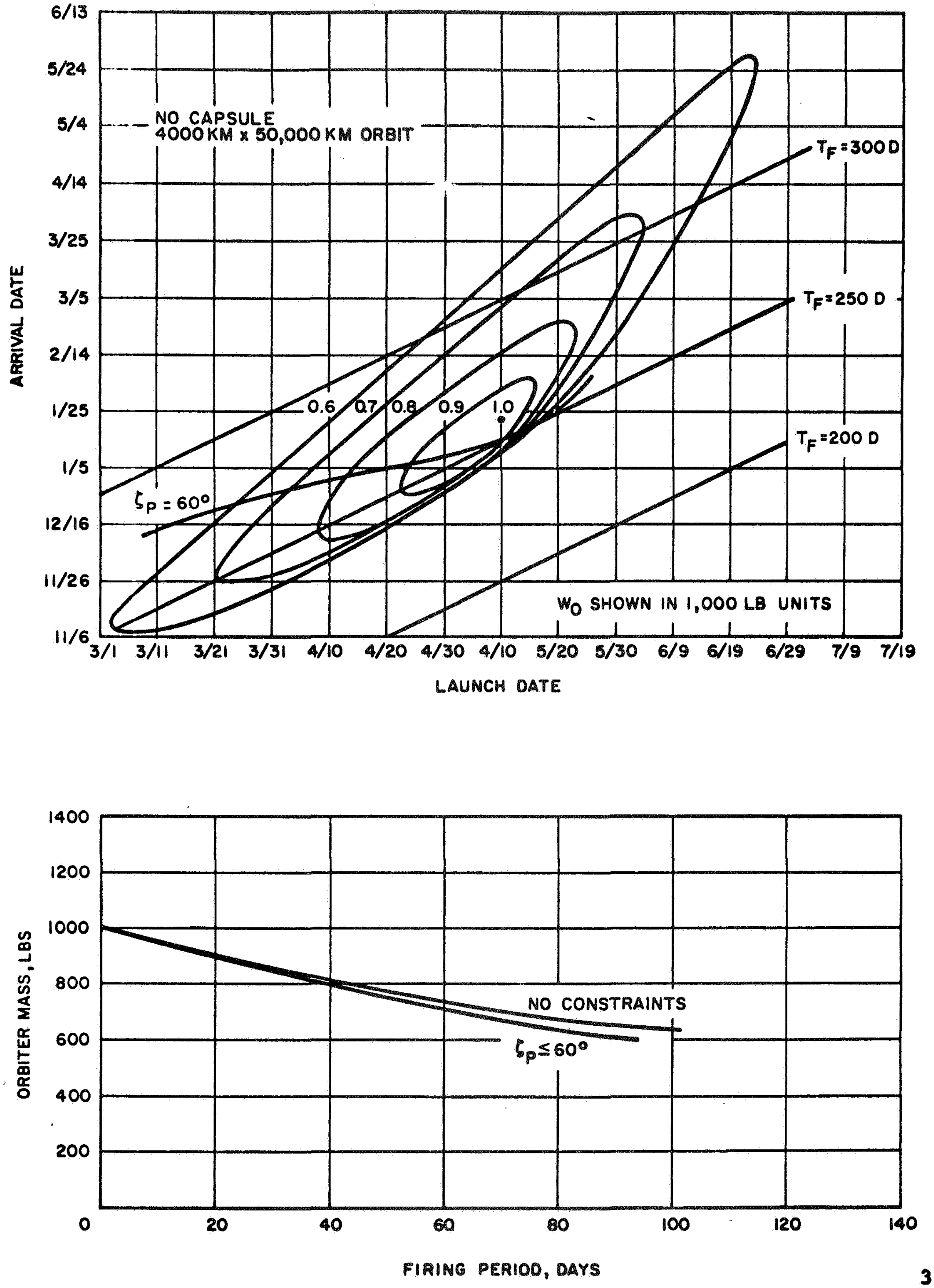

Figure A. 2-4b

MARS ORBITER CAPABILITY—ATLAS/CENTAUR LAUNCH VEHICLE
1971 TYPE II

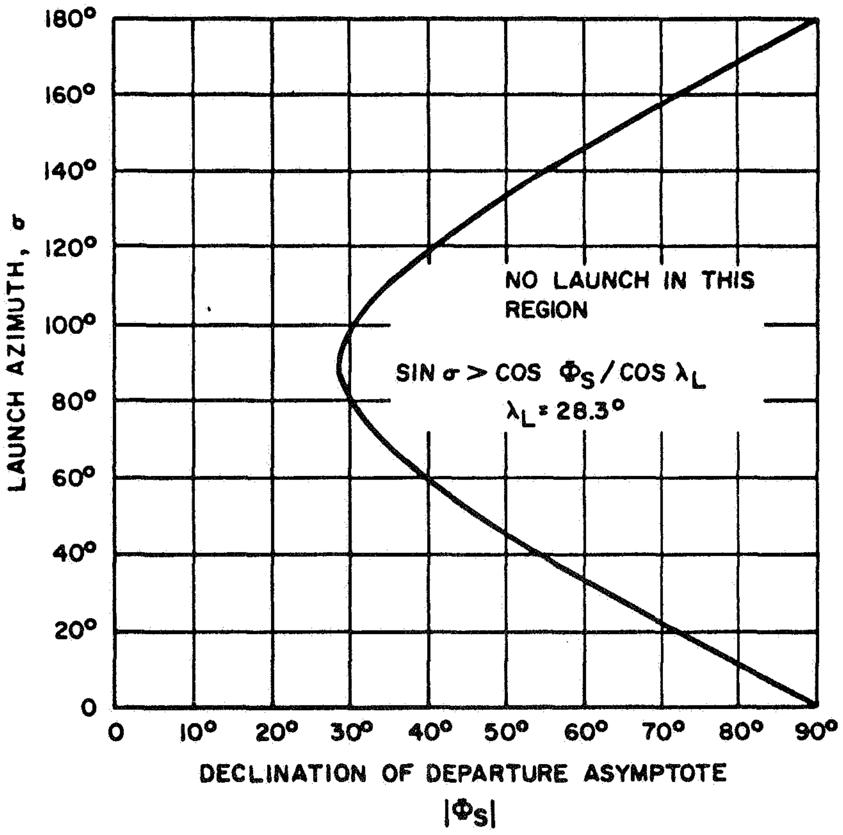

Figure A. 2-5

LIMITING LAUNCH AZIMUTH AND DECLINATION OF DEPARTURE ASYMPTOTE AT CAPE KENNEDY firing period when all limitations due to departure and approach constraints are ignored. Consideration of lighting constraint at arrival would reduce the useful orbiter weight capability to about 4,300 pounds. A departure declination angle greater than -36° has no effect on this capability. However if departure declination angle has to be greater than -28°, then a 30 day firing period cannot be maintained unless the orbiter weight is reduced to a value less than 2,500 pounds.

A short summary of useful orbiter weight is presented in Table 1 for the Saturn IB/Centaur booster for various constraints and a 30 day firing period. It may be noted that Type I trajectories in the 1969-1975 period are more sensitive towards near-earth and near Mars constraints than Type II trajectories. The main disadvantage of Type II trajectories is the long flight time requirement. However, if long flight time can be tolerated, the present study indicates that a 4,000 pound useful orbiter load may be feasible for 1971, 1973 and 1975 opportunities. The payload capability is slightly smaller for the 1969 opportunity, but it still can be more than 3,000 pounds.

TABLE I. Mars Orbiter Capability for Saturn IB/Centaur Booster with Various Constraints and a 30 Day Firing Period

Traj.	Lighting Constraint	No	$60^{o} \geq \zeta_p \geq 120^{o}$	$60^{o} \geq \zeta_p \geq 120^{o}$	Flight Time Days
Type	Launch Constraint	No	No	$36^{o} > \Phi_s > -36^{o}$	
I	1969	3,450 lbs	3,120 lbs	1,750 lbs	200-150
	1971	4,780	4,300	4,300	190-170
	1973	4,160	4,070	4,000	210-200
	1975	3,420	3,260	<2,000	230-160
II	1969	3,320	3,200	3,200	280-270
	1971	3,850	3,750	3,750	260-250
	1973	3,730	3,730	3,720	360-320
	1975	4,450	4,350	4,350	390-360

NOTE: 1000 lb. capsule separated prior to placement in an orbit with 4,000 km. periapsis altitude and 50,000 km. apoapsis altitude, with retro specific impulse of 315 seconds and dry weight ratio of 0.1. Φ_s of $\pm 36^{o}$ corresponds to a launch azimuth of 114° with a firing window of 1.3 hours.

3. Performance Comparison

During the course of the study, the missions which will be considered will include those which provide:

a. maximum payload for some specified flight time

b. minimum gross weight for a specific payload and flight time

c. minimum flight time for a specific payload.

As previously indicated, the low thrust missions investigated during the first month were restricted to trajectories providing a maximum payload for a specified flight time.

The design mission profile, established for the purpose of determining the spacecraft design requirements, is a Mars orbiter mission in which the spacecraft is injected into a parabolic orbit by the Saturn IB/Centaur launch vehicle ($C_3 = 0$) followed by application of low-thrust for 350 days which provides a velocity at Mars encounter such that the spacecraft is captured by the Mars gravitational field. At this time a retro-rocket supplies an additional velocity increment sufficient to permit the spacecraft to attain a Mars orbit having a peri-apsis of 4,000 KM and an apo-apsis of 50,000 KM. It further is assumed that a 1,000 lb. lander capsule is ejected a few days prior to the retro-phase and the bulk of the solar array is jettisoned prior to retro-retaining only the portion required to furnish 1.1 KW of power in the Mars orbit.

Presented in Figure A.3-1 is a comparison of the solar-electric powered spacecraft Mars orbit weight capability with that of the all-chemical powered spacecraft for the 1971 launch opportunity. As previously noted, the solar-electric powered phase of the mission is the zero-coast rendezvous Mars trajectory; and it can be seem that, although it has not yet been established as the optimum mission (on the basis of maximum payload for a specified flight time) for the electric propulsion spacecraft, a payload advantage of at least 700 pounds is indicated over the entire launch window investigated. Further, it should be noted that if departure declination angle for the all-chemical powered spacecraft has to be greater than -28°, then for a 30 day firing period the orbiter weight is reduced to a value less than 3500 lbs., which is only about 50 per cent of that for the solar-electric powered spacecraft.

1971 LAUNCH OPPORTUNITY

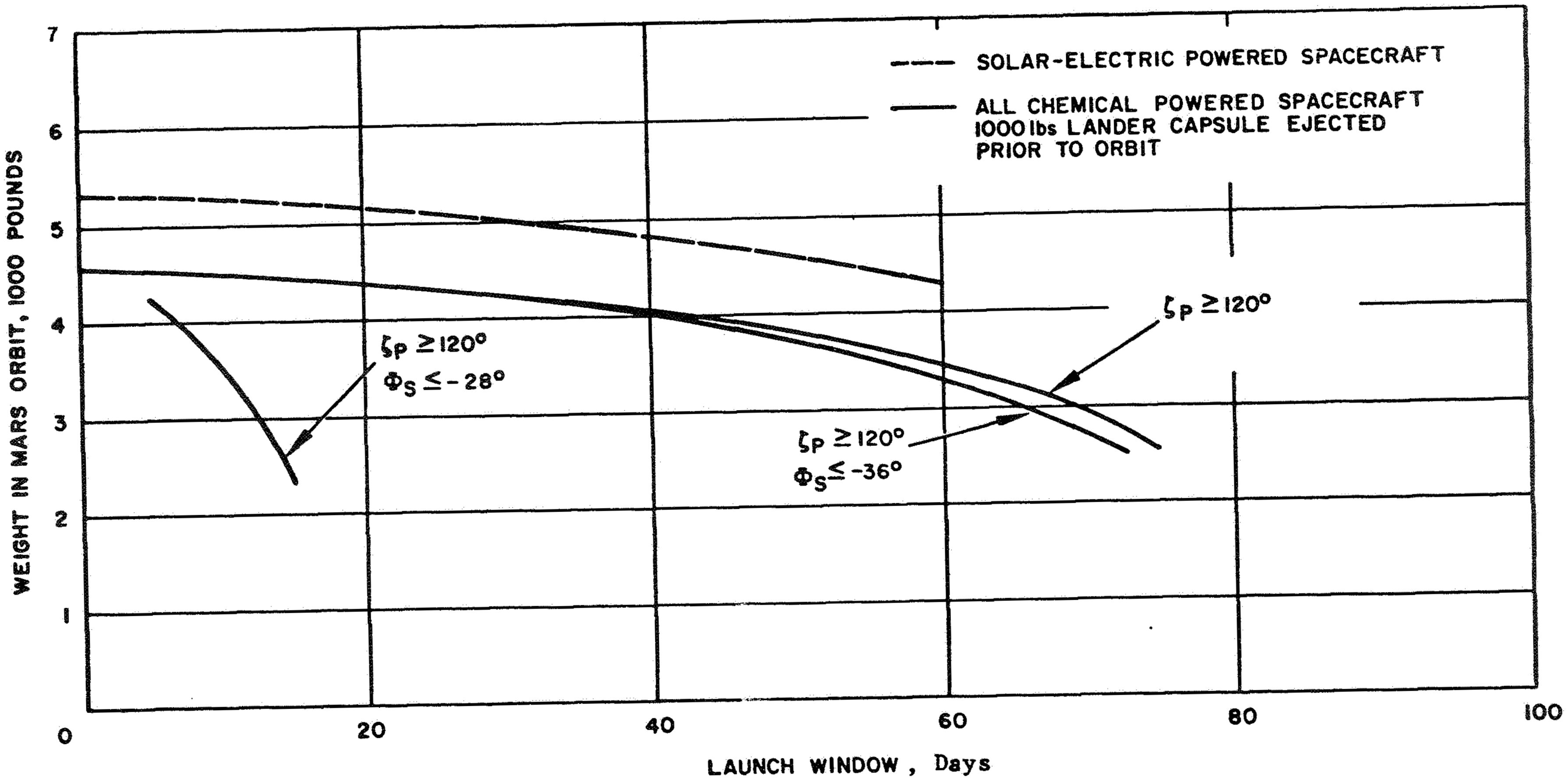

FIGURE A. 3-1

MARS ORBITER WEIGHT CAPABILITY COMPARISON

To give an insight into possible electric propulsion spacecraft payload advantages for the 1973 and 1975 launch opportunities, several fly-by low-thrust trajectories were run and the results compared with the all-chemical spacecraft Mars mission capabilities.

For the 1973 launch opportunity (Figure A. 3-2), and a 30 day launch window, the solar-electric powered spacecraft, (indicated as SEP spacecraft) has the capability of placing 5100 lbs. of useful weight into the design Mars orbit; whereas, the all chemical propelled spacecraft, with lighting constraint only, has a 4070 lbs. orbiter capability, and with $\leq 28^{\circ}$ declination restriction, only a 3800 pound orbiter capability.

Although for Type I trajectories in 1975, the lighting constraints cause only a small reduction in Mars orbiter capability for a 30 day launch period, the launch constraint would limit the orbiter capability to around 1,000 lbs. Therefore, the comparison is also made on the basis of a Type II trajectory (see Figure A. 2-3). It should be noted, however, that even on the basis of this comparison, wherein the all-chemical powered spacecraft mission is of 350 day duration (SEP spacecraft mission time is 400 days) the SEP spacecraft still has over a 400 pound orbiter payload weight advantage. It again should be pointed out that SEP mission has not yet been established as the optimum for the maximum payload for the specified conditions. The parametric trajectory studies are continuing, and optimized mission capabilities will soon be available for more detailed comparisons.

1973 LAUNCH OPPORTUNITY

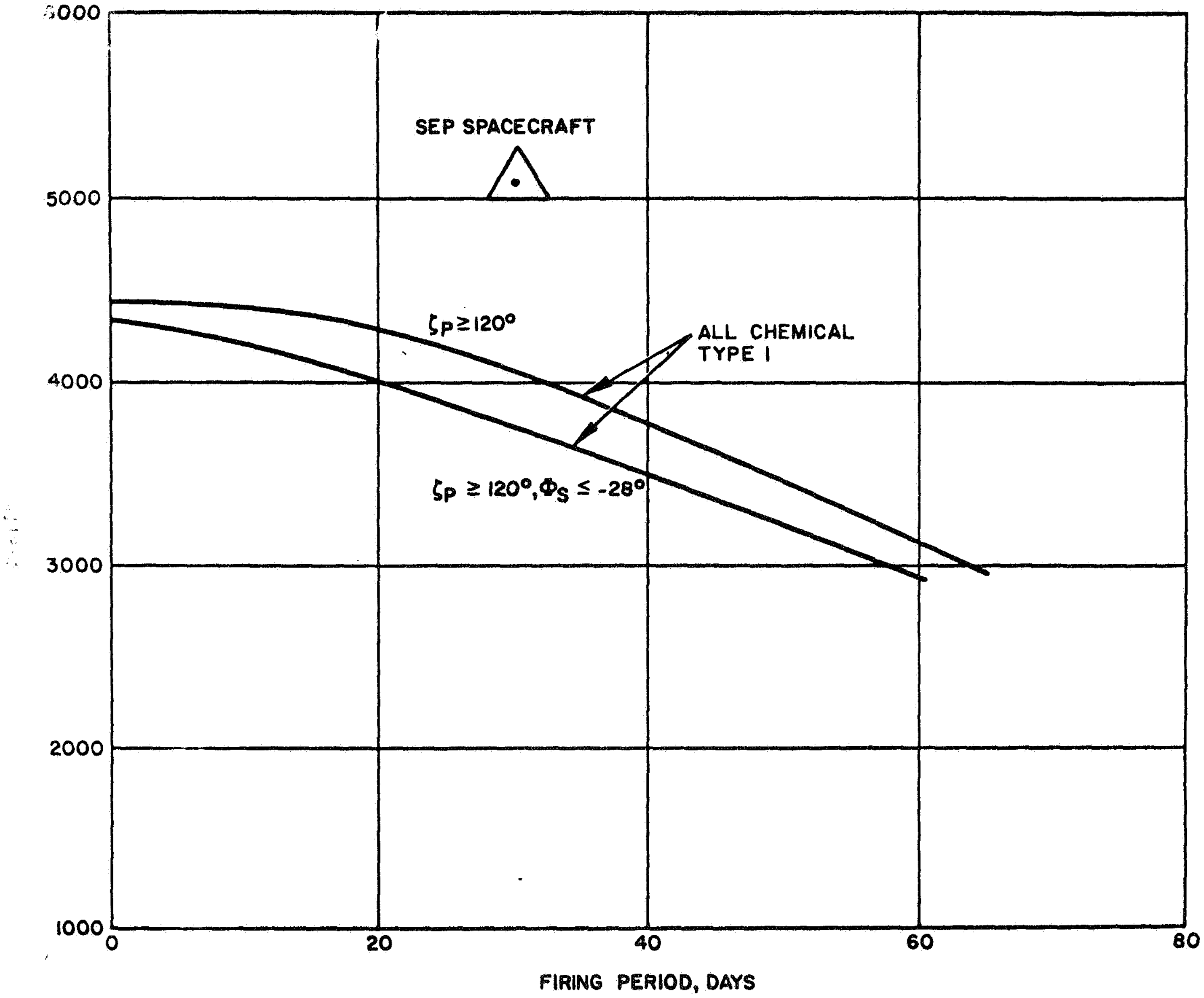

FIGURE A. 3-2

ECTS OF LAUNCH AND LIGHTING CONSTRAINTS ON ORBITER WEIGHT CAPABILITY

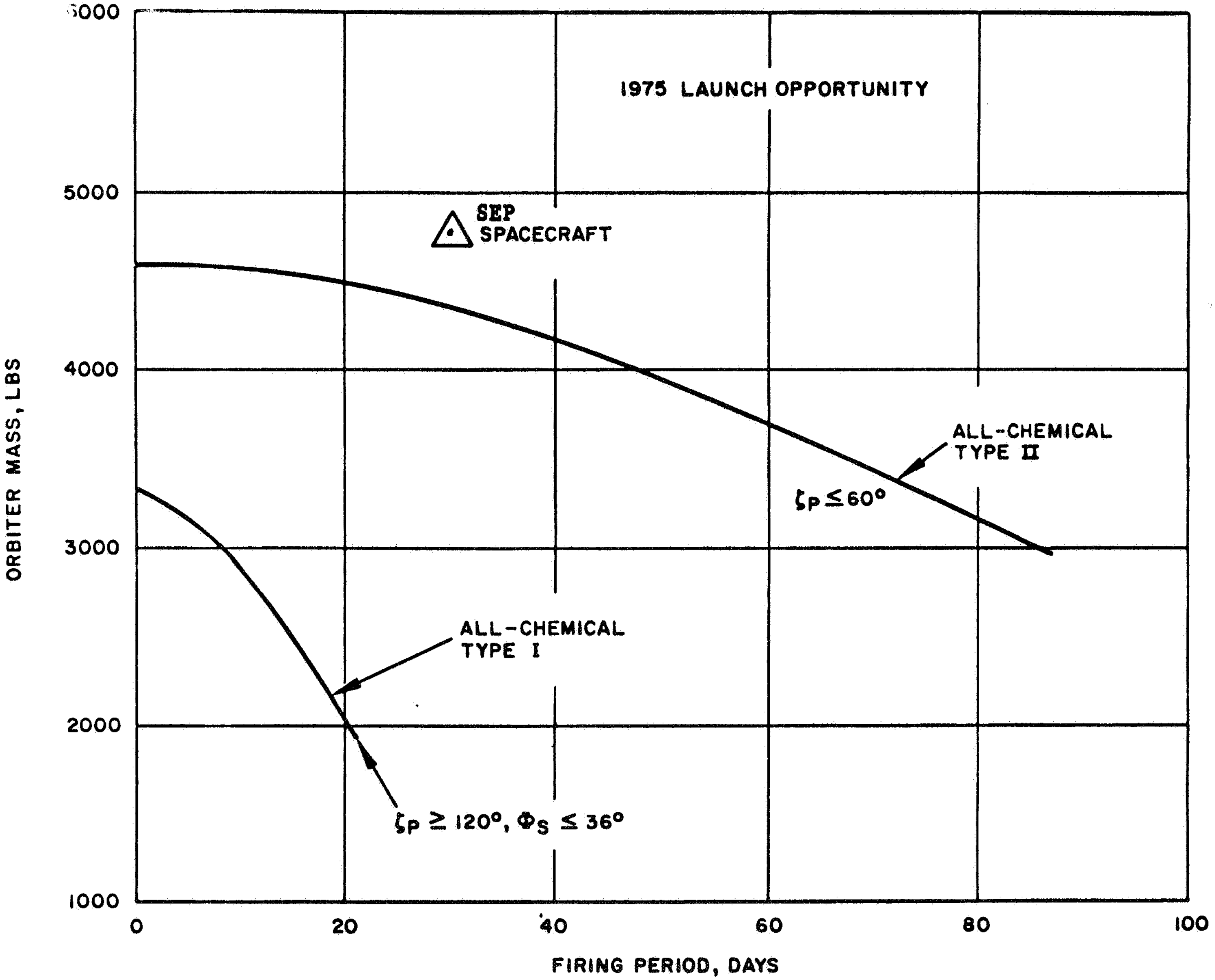

FIGURE A. 3-3

EFFECTS OF LAUNCH AND LIGHTING CONSTRAINTS ON ORBITER WEIGHT CAPABILITY

B. PROPULSION SYSTEM STUDIES

The propulsion system studies which have been performed to date have consisted of (1) an evaluation of the state-of-the-art of the major subsystems and components involved in the ion propulsion system, (2) a preliminary reliability analysis to determine the optimum thrustor module size for a high power propulsion system, and (3) a conceptual design of a 50 kW ion propulsion system employing Hg bombardment thrustor units. These initial studies which were meant to be a first iteration of the overall program have served to provide data required by the low thrust mission analysis and spacecraft design studies as well as to uncover many of the problem areas which must still be faced.

1. Component Evaluation and Parametric Study

The component evaluation and parametric study is meant to establish the present day characteristics such as performance, life, weight, size, and power requirements of the major subsystems of ion propulsion systems and to develop, for subsequent tradeoff studies, the relationships among the critical system design parameters. The major subsystems considered in the first month effort are the thrustor, feed system and power conditioning equipment.

a. Thrustor

A study has been made to establish the operating characteristics of both the Cs contact and Hg bombardment ion engines. The significant factors in evaluating ion thrustor performance are:

1) Current Density Capability
2) Accel-Decel Ratio Capability
3) Power Efficiency, and
4) Propellant Utilization

These parameters are inter-related, for example, the operating current density may be limited by accel-decel ratio, and the power efficiency of an ion engine may be affected by its propellant utilization.

Current Density Limit

The current density of the mercury engine appears to be limited by impingment at the central regions of the accel electrode. From an analysis of Ref. 1, it appears that the ratio of total beam current to engine diameter squared must be limited to 1 mA/cm^2 in order to achieve a life of one year (Fig. B. 1-1). This reference also indicates that the life of the mercury engine, operating without a decel electrode, is greatly affected by higher accel-decel ratios. This is due to the moving out of the virtual decel, hence extending the region of charge exchange. The possibility exists that using a decel electrode might increase current density capability. In addition, engines larger than 10 cm must exhibit current density distributions which are no worse than the 10 cm engine on which these results are based. Otherwise, a lower current density limit must be imposed. Acceptable current density distribution in larger engines is presently being accomplished by the use of cross-feed (20 cm engine, Ref. 5) and multiple cathodes (50 cm engine, Ref. 4).

At low specific impulses the current density limit of the present cesium contact engine (emitter width = .220"), is determined by the maximum accel-decel ratio at which the engine can perform. Since the total accelerating voltage requirement is set by current density, for a given current density, lower specific impulse requirements force the accel electrode to carry larger fractions of the total voltage. For a specific impulse of 5500 seconds, the accel-decel ratio must be at least five in order to operate at 15 mA/cm^2. In order not to exceed this value of accel-decel ratio, the current density must drop off when going to lower specific impulses. A current density of 15 mA/cm^2 may be maintained at values of specific impulse below 5500 seconds by decreasing the emitter width. Unless the neutral efflux can be reduced, it is questionable whether 15 mA/cm^2 can be exceeded even at higher values of specific impulse, because of life considerations of the accel electrodes. Figure B. 1-2 shows the predicted life of the accel electrodes as limited by charge exchange erosion. These results are based on the use of nickel as the accel electrode material, and indicate that for 1% neutral fraction 6200 hrs

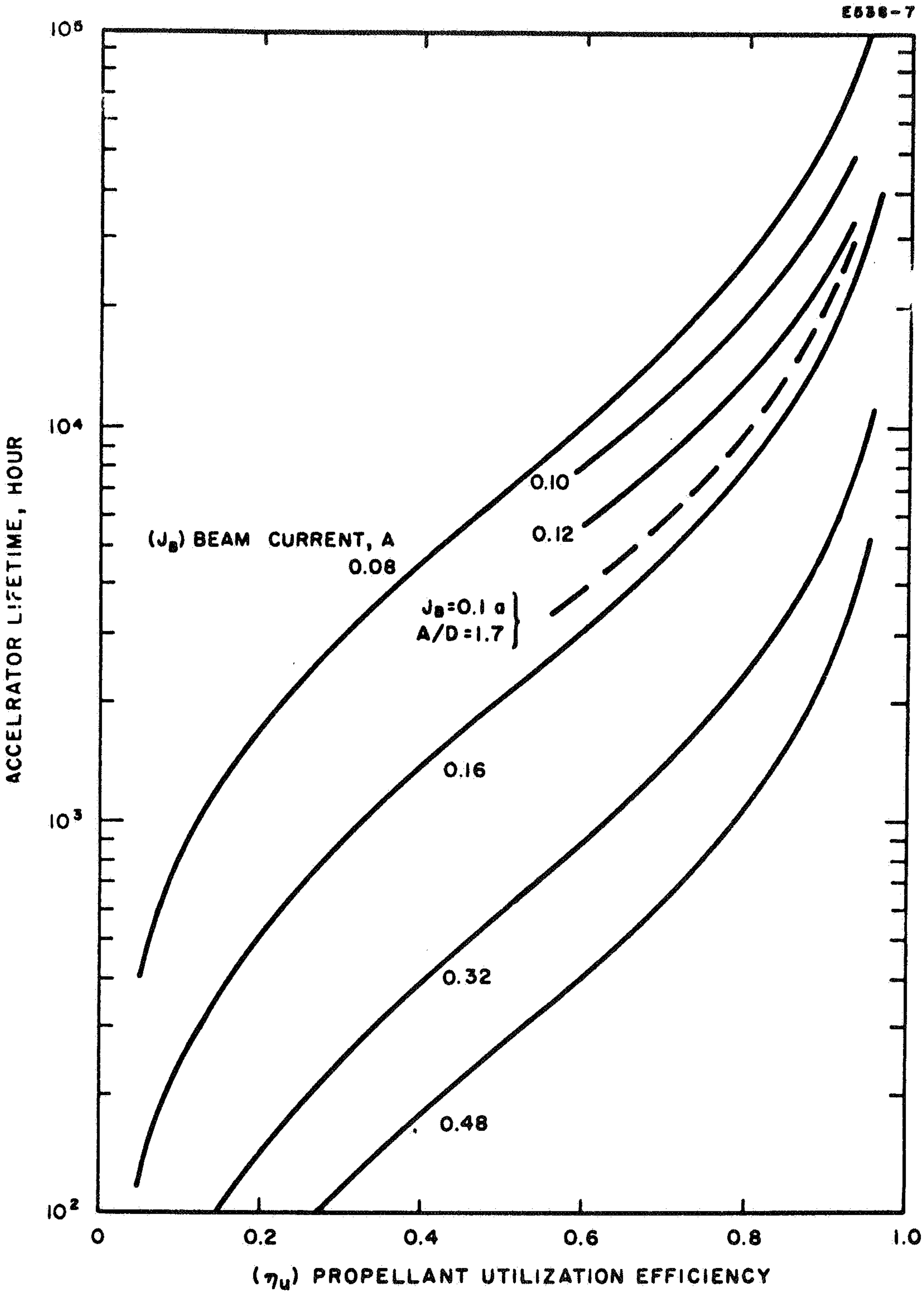

Fig. B.1-1. Mercury bombardment engine accel electrode life due to charge exchange ion erosion.

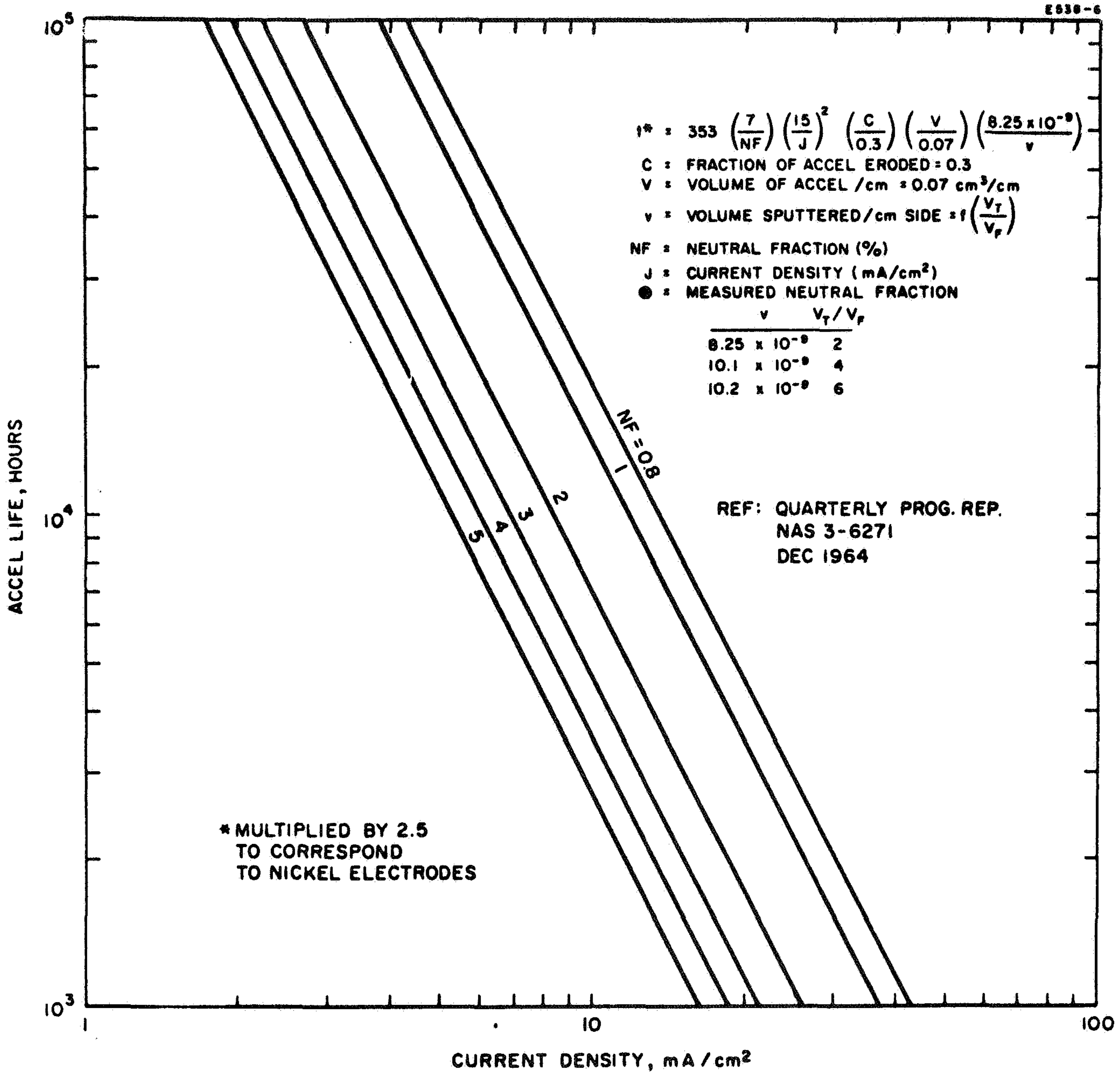

Fig. B. 1-2. Cesium contact engine accel electrode life due to charge exchange ion erosion.

life may be achieved at a current density of 15 mA/cm^2. This life may, however, be prolonged by the use of a diverter electrode (Ref. 11). Current density capability is one of the key factors in determining engine size and weight as well as performance, since the more current produced by each unit of emitting area, the less the required emitting area per unit thrust.

Accel-Decel Ratio

Of all the data reported for the mercury engine in Ref. 1, 5, 7, and 8; accel-decel ratios have seldom exceeded three, and there has been little data at over 2.5 . If this represents the limit of engine operation, a problem exists in extrapolating small engine performance (10-20 cm) to large engines for a low specific impulse value. This is so because the present 50 cm engines have greater electrode spacing and hence require over twice the total voltage of the 20 cm engine for the same current density (Ref. 4 and 9). It remains to be established, then, what the minimum electrode spacing of larger engines can be (consistent with hole size). When the electrode spacing is established the maximum current density at low specific impulses can be determined consistent with an accel-decel ratio not exceeding three.

If the accel-decel ratio of the contact engine is not to exceed five, the emitter must be made narrower in order for high current densities to be maintained at low specific impulse. The present contact engine has been designed to operate at specific impulses greater than 5500 seconds. A narrower emitter will provide high performance at specific impulses under 5500 seconds.

Power Efficiency

For the cesium contact engine, power losses are associated with maintaining the temperature of a porous tungsten slab in the neighborhood of 1400 K. This power requirement is on the order of 10 W per emitting cm^2. The ionizer heating power is essentially constant over a wide range of current densities (five to twenty-five mA/cm^2). Therefore, for any given specific impulse engine efficiency is a strong function of current density. Figure B. 1-3 is a plot of engine efficiency versus specific impulse

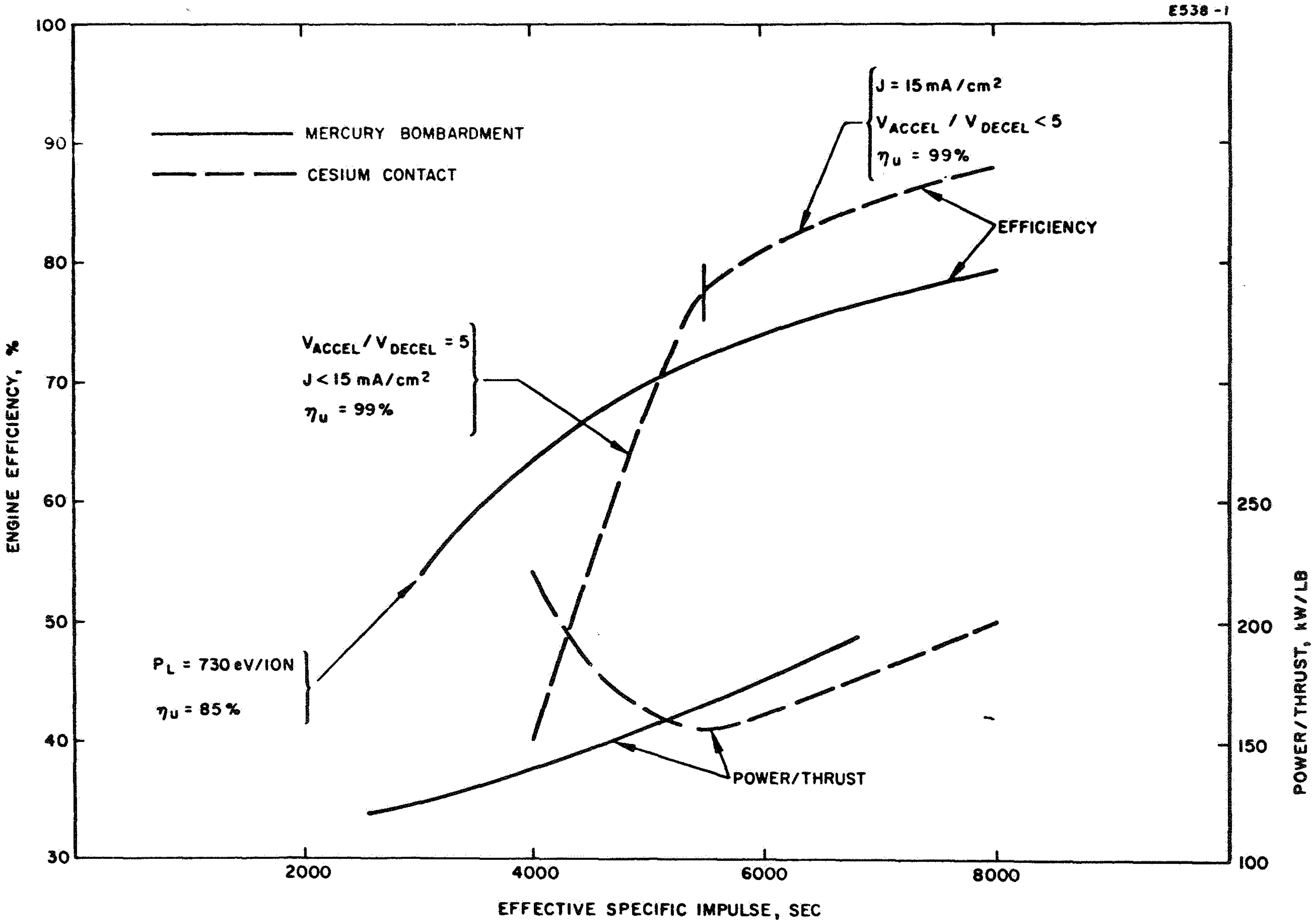

Fig. B. 1-3. Engine efficiency and power/thrust for cesium contact and mercury bombardment engines.

for the cesium contact engine. The sharp drop off in engine efficiency below 5500 seconds is due to the decrease in current density required to limit the accel-decel ratio to 5. The corresponding power to thrust curve is also shown in Fig. B. 1-3.

The major power loss of a mercury bombardment engine is in the arc discharge. This power is proportional to beam current, so that the mercury engine power efficiency does not suffer because of low current density, as in the case of the cesium contact engine. The arc power required for a given current is dependent on propellant utilization and total voltage. Typical optimized values for 80% propellant utilization are 500 eV/ion (Ref. 2 and 3). The power required for cathode emission is expected not to exceed 120 eV/ion (Ref. 9). If a permanent magnet is not used, the total power (including neutralizer) should be about 730 eV/ion. The curve showing mercury bombardment engine efficiency versus specific impulse in Fig. B. 1-3 is plotted on this basis. The power to thrust curve associated with this engine efficiency is also shown in Fig. B. 1-3.

Propellant Utilization

In the mercury bombardment engine, propellant efficiency is a function of arc power. Figure B. 1-4 shows the dependence of propellant utilization on arc power (Ref. 3). At about 80%, the trade off becomes poor, requiring excessive arc power for a small gain in propellant utilization.

In the case of the cesium contact engine, neutral fraction is determined by the inherent properties of the ionizing surface. Pure tungsten has a limit of somewhat less than 1% at 15mA/cm^2, whereas the porous effect will raise this value slightly. The neutral fraction of the cesium engine does not effect its power efficiency, as in the case of the mercury engine. The main concern here is the effect on electrode life (Fig. B. 1-2). It is possible that materials other than tungsten might be used in the future to fabricate porous ionizers, in an effort to lower the inherent neutral fraction of the pure material (Ref. 10). Also, there may be benefit in fabricating ionizers with more pores per unit area, to reduce the porous effect on increasing neutral fraction.

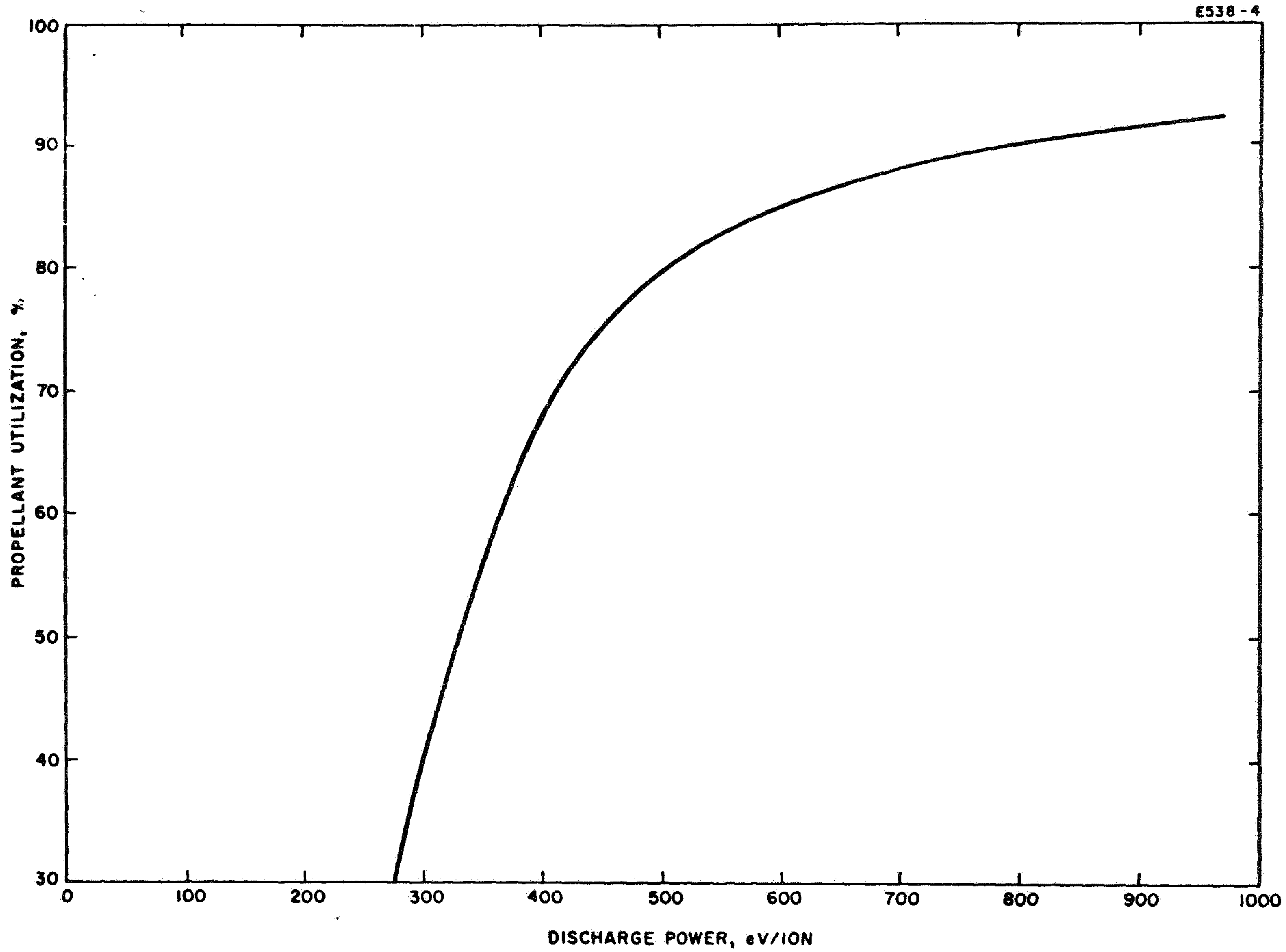

Fig. B.1-4. Mercury bombardment engine propellant efficiency versus arc discharge power.

Mechanical Aspects

The basic unit considered here for a cesium engine module is a 24 strip unit with an ionizer length of at least 3. 5 inches and no more than 10 inches. There are 2 inches of overhand on both edges because of the electrode structure. The overall unit appears as in Fig. B. 1-5. The projected flight system weight is 14 lbs at 3. 5 inches, and 40 lbs at 10 inches. The emitting areas are 110 cm^2 and 330 cm^2, respectively. It becomes quite inefficient, weight-wise, to build a unit of less than 24 strips, since the supporting structure (insulators, base plates, etc.) weight drops off much slower than the number of strips. Figure B. 1-6 shows the engine weight versus input power, based on these considerations.

Individual modules for a mercury bombardment engine system should be sized between 10 and 50 cm in diameter. Reference 6 shows that an engine of 5 cm is inferior to larger engines, and 50 cm units are the largest for which present data exists. Moreover, until it is determined whether the larger size engines can be operated at low specific impulse (because of the higher voltage requirement due to increased electrode spacing) 50 cm should be considered an upper limit. Projected flight system weight for the 20 cm bombardment engine is 6 lbs, and that for a 50 cm engine, 24 lbs. Figure B. 1-7 shows engine weight versus input power, based on the above.

b. Feed System

Feed system analysis has led to the prediction of flight system weight associated with the storage and delivery of propellant (cesium or mercury). The basic feed system unit is that shown in Fig. D. 2-2. This system is currently under development. The major components are:

1) Reservoir and Flow Valve
2) Vaporizer
3) Flow Meter

Initially two types of reservoirs were considered: The positive expulsion and capillary storage systems. The capillary storage technique requires the storage tank to be filled with a felt metal material which holds

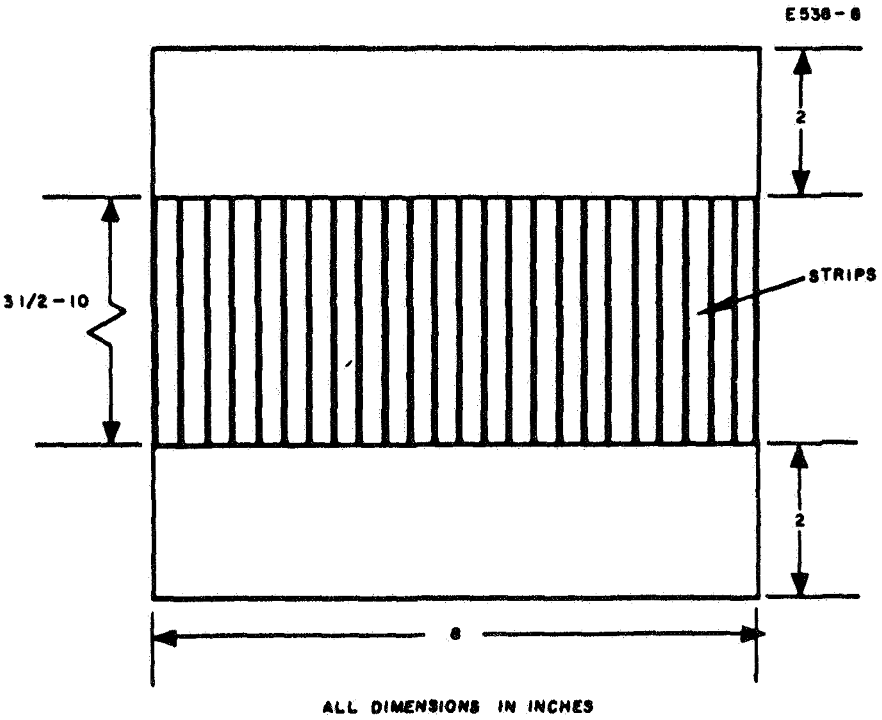
E538-6
2
STRIPS
3 1/2 - 10
2
6
ALL DIMENSIONS IN INCHES

Fig. B.1-5. Cesium contact engine basic module frontal area.

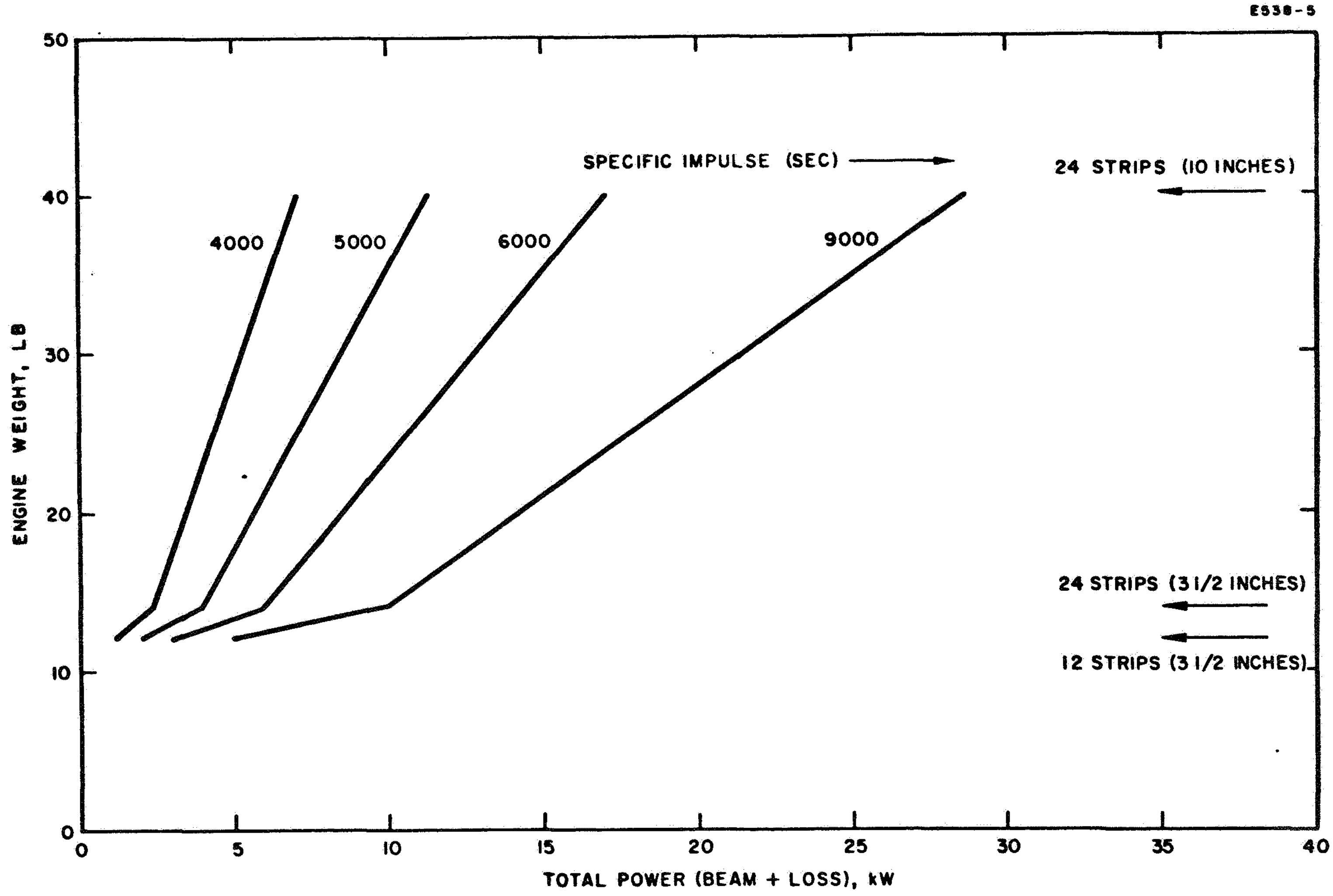

Fig. B. 1-6. Cesium contact engine thrustor weight versus total input power (beam plus loss).

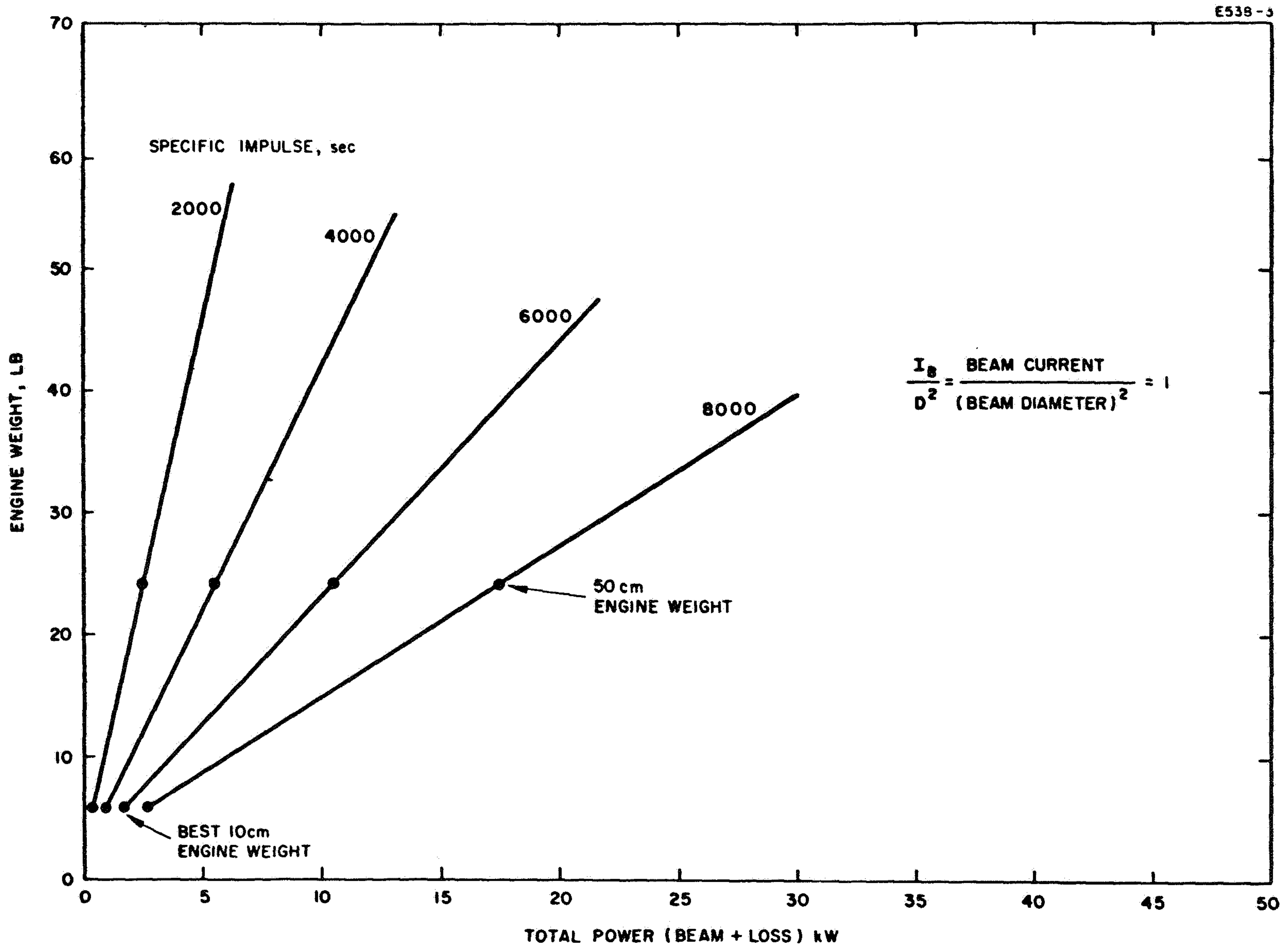

Fig. B. 1-7. Mercury bombardment engine thrustor weight versus total input power (beam plus loss).

the propellant in a zero g environment. Although this method may be useful for very small storage systems (10 lbs) the weight of the felt metal soon becomes prohibitive for larger reservoirs. Figure B. 1-8 shows the weight comparison between the capillary and positive expulsion storage systems as a function of the mercury or cesium weight contained. Thus the positive expulsion method has been chosen for engine systems where storage of 1000 to 2000 lbs of propellant is required.

The reservoir, shown in Fig. D. 2-2 is of the positive expulsion type. A high pressure supply, through a pressure regulator, keeps the stored propellant at a constant 30 psi. The weight of this unit is tabulated in Table B. 1-I, as it exists for a 40 lb mercury system (5 lb cesium system). For consideration of larger size reservoirs, this basic unit is scaled accordingly. The "S" after the component weight indicates those items whose weight increases for larger size containers. The balance of the items have a constant weight, independent of the reservoir size. Figure B. 1-8 shows the approximate weight and size of the storage system as a function of the amount of propellant it stores.

Consider, for example, the performance of the 1971, 350 day mission discussed above with a mercury bombardment ion engine system. Mission analysis has shown that the propellant to initial mass ratio is .132 (Fig. A. 1-1). Assuming an initial vehicle mass of 11,700 lbs, the mercury propellant to be stored is

$$(.132)\ (11,700) = 1550 \text{ lbs} .$$

If this mass is divided into eight separate reservoirs (equal to the number of operating engines, as shown in Section B-2), the capacity of each must be 200 lbs. Figure B. 1-8 indicates that for a 200 lb capacity (mercury), the weight of the storage reservoir is 10.5 lbs. Hence the total storage weight is

$$(8)\ (10.5) = 84 \text{ lbs}.$$

The size of each reservoir is (Fig. B. 1-8) 10 inches in diameter.

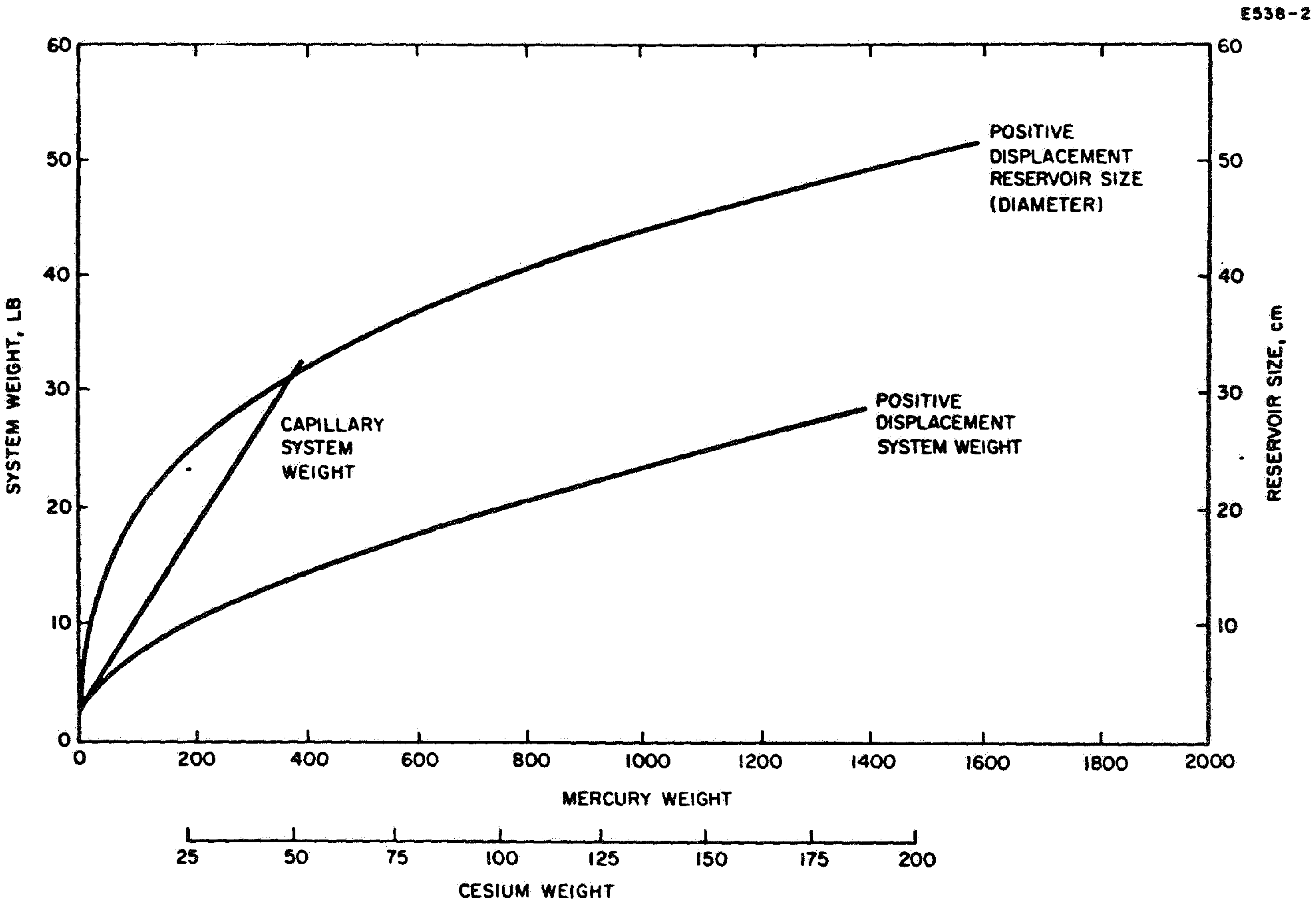

Fig. B. 1-8. Weight and size of propellant storage system as a function of propellant weight to be stored.

TABLE B. 1-I

Propellant Tankage Weights

Component	Positive Displacement System, lb	
Mercury Reservoir		
Container	0. 71	S
Flanges and Manifolds	1. 3	
Diaphragm	0. 68	S
	2. 69	
Gas Pressurization		
High Pressure Gas Reservoir	1. 0	S
Squib Valve	0. 3	
Pressure Regulator	0. 5	
	1. 8	
Mercury Control Components		
Fill Valve	0. 40	
Outlet Seal	0. 10	
Piercing Mechanism	—	
Flow Control Valve	0. 47	
	0. 97	
TOTAL	5. 5	
SCALED	2. 4	
CONSTANT	3. 1	

A cesium engine storage reservoir for the same mission requires more weight even though the mass of cesium propellant required is less than that for the mercury engine system. Due to its significantly lower density, cesium requires more storage volume per unit mass than mercury. The propellant to initial mass ratio for the cesium engine system (Fig. A. 1-1) is .09. Thus, the total cesium propellant required is

$$(.09)\ (11,700) = 1050 \text{ lbs.}$$

Consider this propellant stored in four separate reservoirs. Then each reservoir would contain 260 lbs of cesium. Figure B. 1-8 indicates an individual reservoir weight of 35 lbs. The total storage system weight for the cesium system is

$$(4)\ (35) = 140 \text{ lbs.}$$

The vaporizer under consideration is the JPL multicapillary system (Fig. B. 1-9). This system is described in Ref. 12. The liquid-vapor interface is located somewhere along the inside of the capillaries, by means of a temperature gradient. The pressure balance is maintained by the sum of the pressure drops of both the liquid and vapor phases. Increasing temperature at the downstream end moves the interface upstream, and thereby lowers the mass flowrate. It is estimated that this vaporization system will weigh about 1.5 lbs.

The flow meter device (Fig. B. 1-10) for feed system application is the variable capacitor meter (described in Ref. 12). The principle of operation is based on the displacement of a membrane under gas pressure. The resulting flow signal may be used to raise or lower the vaporizer temperature, thus producing flow control. The weight of the flow meter is also estimated at 1.5 lbs.

The final feed system consideration for a large engine system is the overall linkage from the storage reservoirs to the engines. This includes the optional switching arrangements, such that propellant from any storage tank may be supplied to any of the engines of an array. Figure B. 3-1 shows one such arrangement, where the transfer occurs in

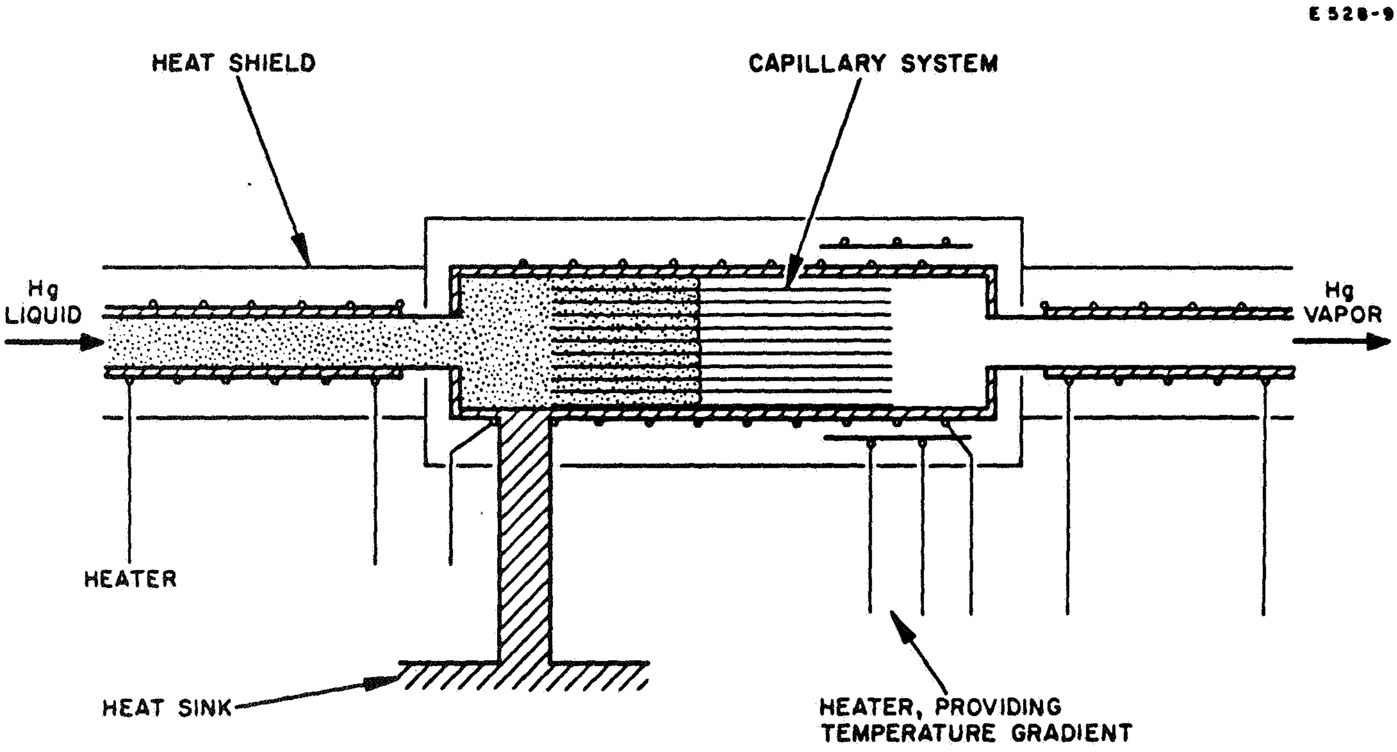
E 528-9
HEAT SHIELD
CAPILLARY SYSTEM
Hg LIQUID
Hg VAPOR
HEATER
HEAT SINK
HEATER, PROVIDING TEMPERATURE GRADIENT

Fig. B. 1-9. Vaporizer utilizing multiple capillaries with temperature gradient along capillaries.

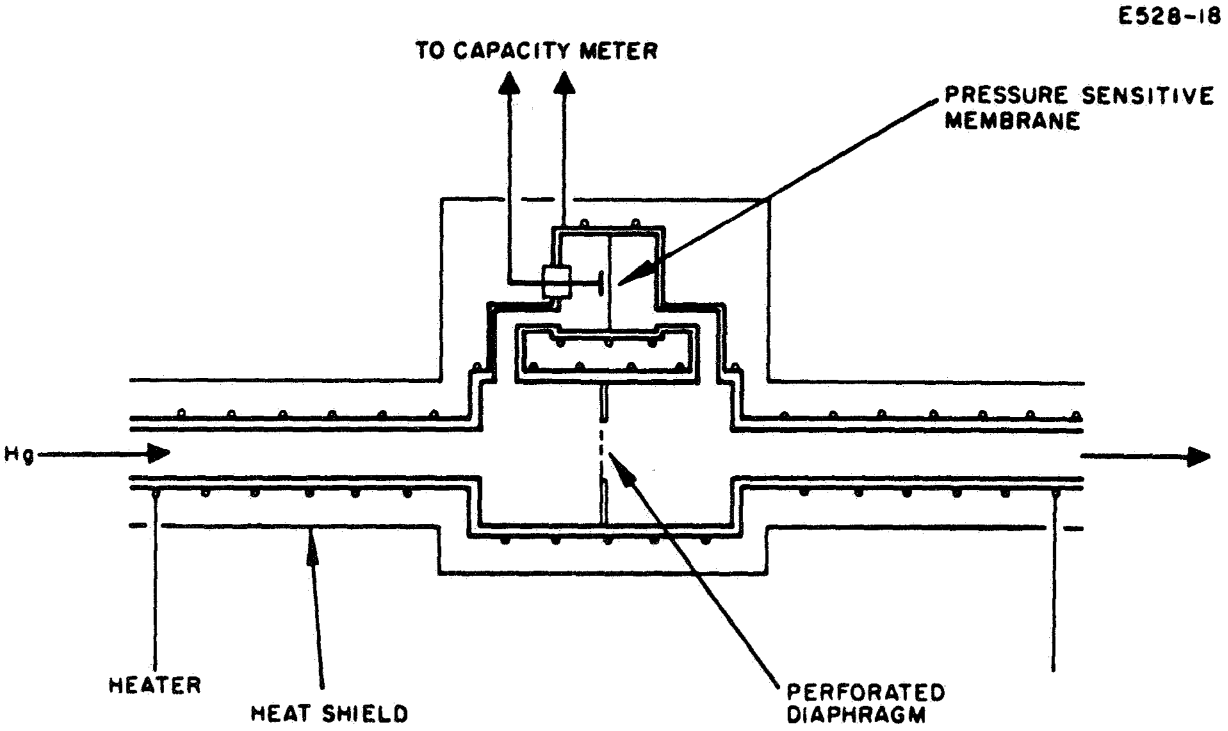
E528-18
TO CAPACITY METER
PRESSURE SENSITIVE MEMBRANE
Hg
HEATER
HEAT SHIELD
PERFORATED DIAPHRAGM

Fig. B. 1-10. Flow meter utilizing Granville-Phillips capacitance manometer.

the vapor stage. The final layout will depend on reliability and weight aspects for a particular size thrustor system. For the schematic shown, each propellant tank has its own vaporizer, and may be switched to any of several engines in an array, each with its own flow meter.

b. Power Conditioning System

Functional Requirements

An ion engine power conditioning system operating from solar cell power must perform three basic functions: (1) convert the solar panel output voltage to useable ion engine voltages, (2) control and regulate the ion engine voltages, and (3) provide a power and impedance match between the solar panel power system and the ion engines. Each of these functions must be performed by the power conditioning system as the solar panel output power and voltage vary with time. For the mission under consideration, solar panel output voltage will increase as the spacecraft moves away from the sun. The solar panel output voltage increase is primarly due to the temperature-resistance characteristic of the solar cell. As the distance from the sun increases, solar cell panel surface temperatures decrease with an attendent decrease in solar cell internal impedance. In addition solar cell panel output power will decrease as the spacecraft proceeds towards Mars. The drop off in solar panel power is assumed proportional to $R^{-1.7}$. The voltage-current characteristics of a 50 kilowatt solar cell power system are shown in Fig. B. 1-11. The voltage-current characteristics are shown for the solar panel power system operating at 1.0, 1.25, 1.5, and 1.7 astronomical units from the sun. Figure B. 1-12 is a plot of solar panel power-voltage characteristics for the same conditions assumed in Figure B. 1-11. As shown by the load lines in Fig. B. 1-12, the electrical power obtainable from the solar cell array is a strong function of the load resistance. In effect, the load resistance will be required to vary from 0.2 ohms to 0.7 ohms if the maximum power available from the solar panel system is to be utilized. Solar panel voltage, maximum output power, current and optimum load resistance versus mission time are shown in Fig. B. 1-13 for the mission under consideration. From these curves it can be seen that three control functions

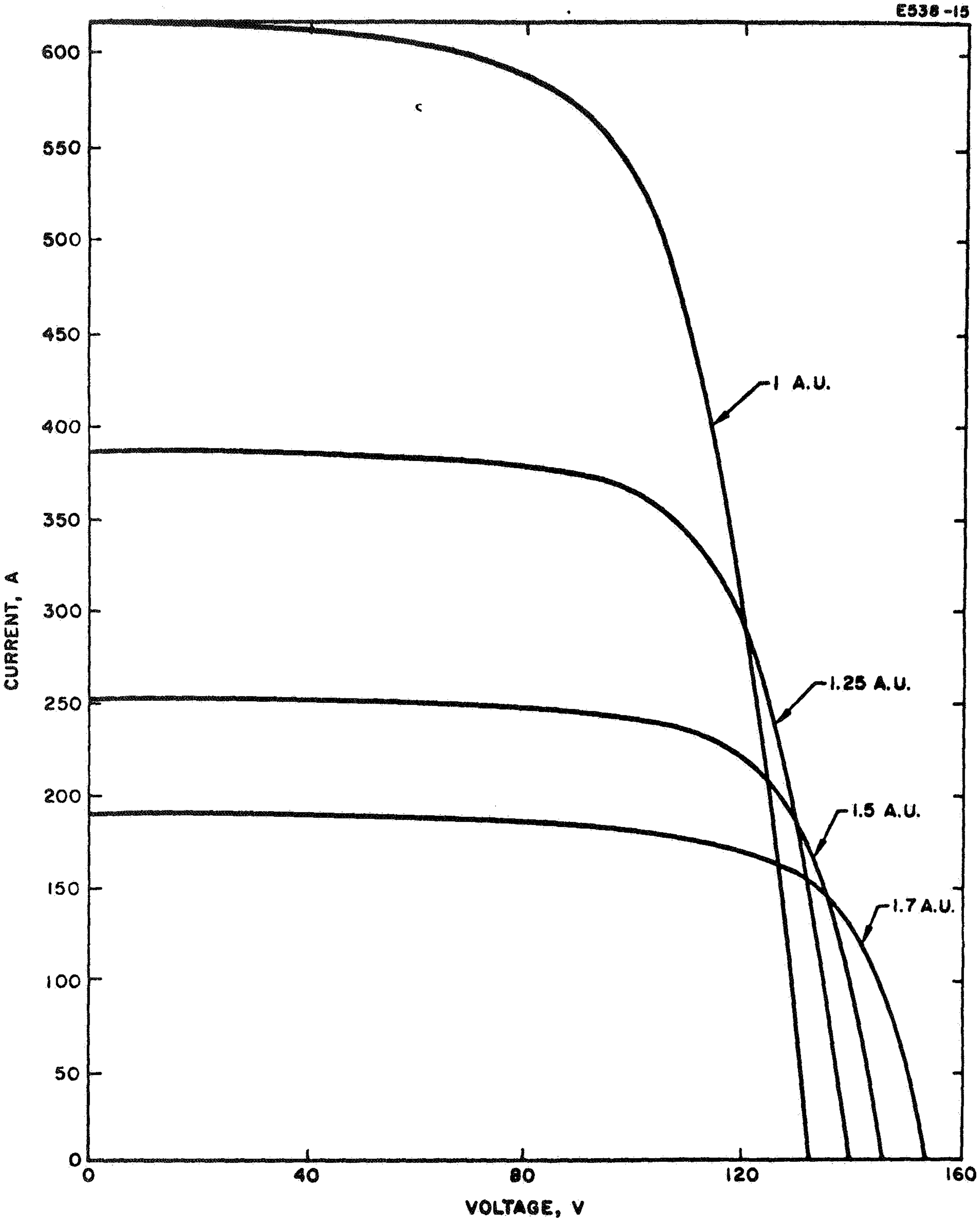

Fig. B.1-11. Solar array I-V characteristics.

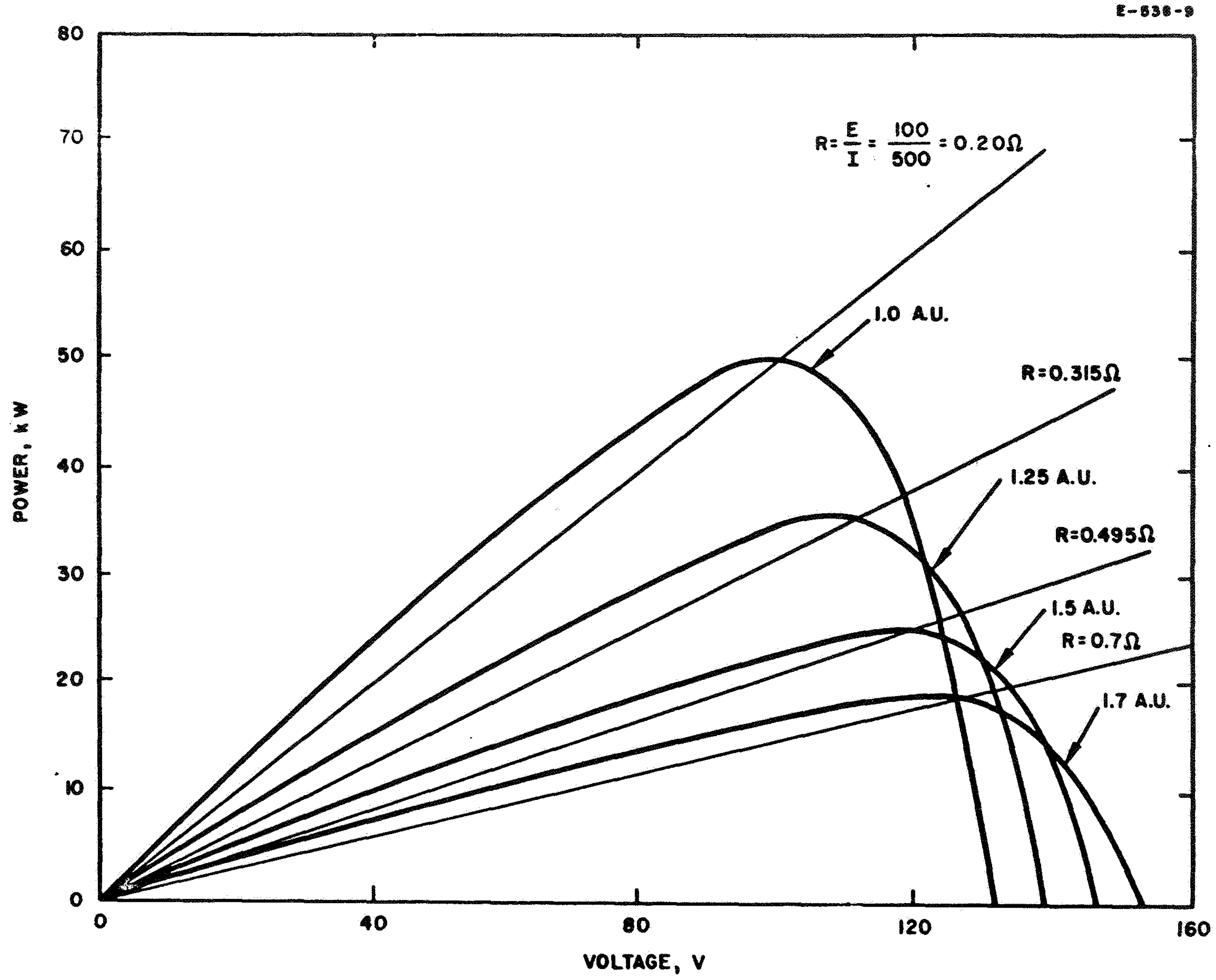

Fig. B. 1-12. Solar array power-voltage characteristics.

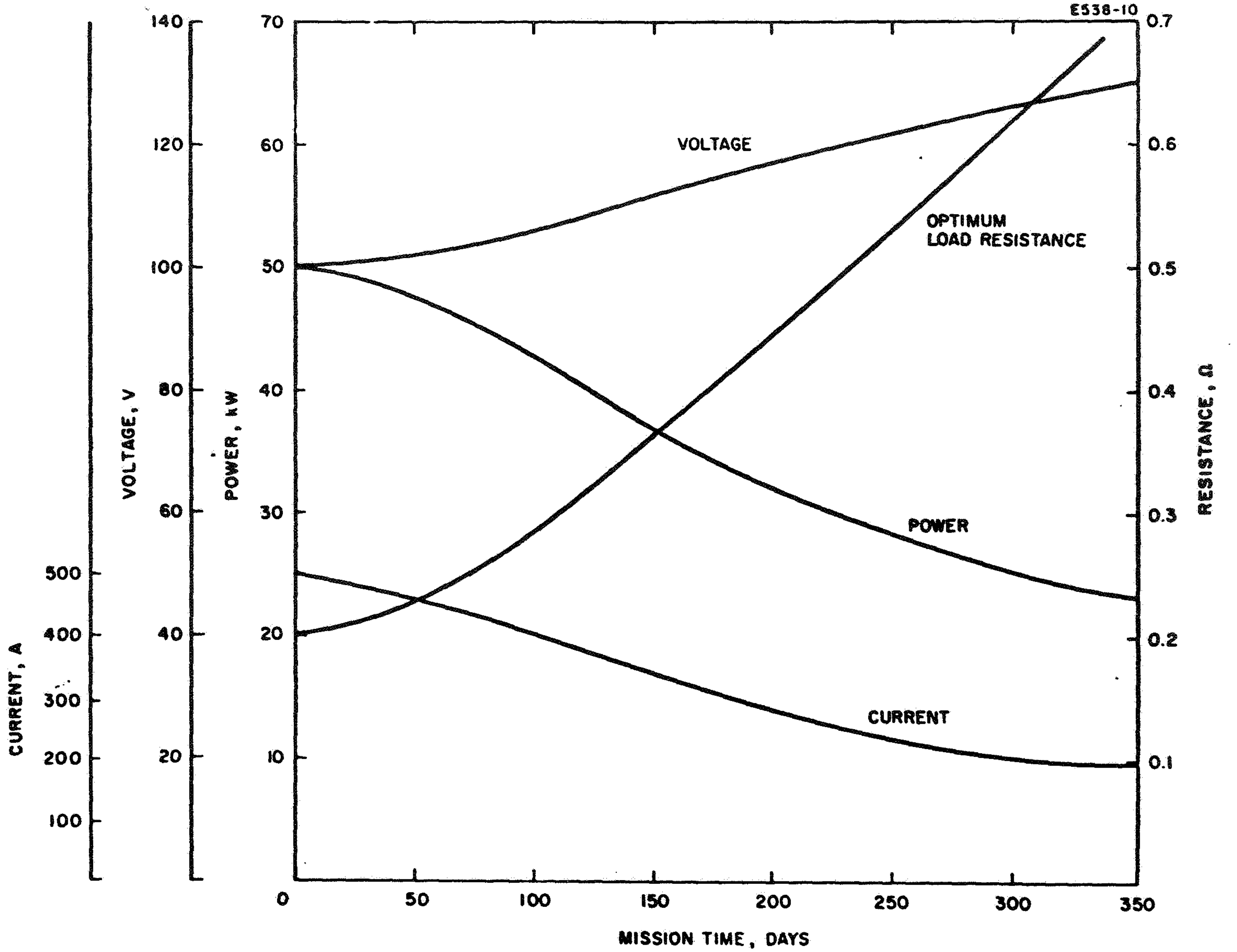

Fig. B.1-13. Solar array electrical output characteristics.

are necessary: (1) the solar panel load resistance must increase with time in order to maintain maximum power output (2) the power conditioning output voltage must be regulated in order to minimize the variation in engine thrust and I_{sp} and (3) the input power required by the load must decrease with time.

Power Conditioning Design Evaluation

For this study, the power conditioning system design must meet the following criteria:

1. The power conditioning system must match the power source (solar cell output) to either the cesium surface contact or mercury electron bombardment multi-module ion engine thrustor systems.
2. The power conditioning system must be capable of operating at a 50 kilowatt power level in a space environment.
3. The power conditioning design must be based on existing technology and components.

The basic power conditioning design goals are:

1. Specific weight < 15 lbs/kilowatt
2. Power efficiency > 90%
3. Operating life > 10,000 hours
4. Mission reliability > 0.97
5. Modular design to permit the use of redundant or standby circuit techniques to meet circuit reliability goals.
6. Circuit simplicity (minimum electronic part count)
7. Compatibility with spacecraft mounting and heat rejection system.

Using the criteria and design goals listed above, two power conditioning designs have been evaluated. A description of these designs and the initial results of the evaluations are presented in the sections that follow.

SERT-II Design Approach: Figure B. 1-14 is a block diagram of a 6 kilowatt ion engine power conditioning system design developed under NASA contract NAS 3-3565 (and identified as the SERT-II system). Four inverter systems are employed to step up or convert the solar cell output voltage to useable ion engine voltages. Two of these inverters are used for the main beam

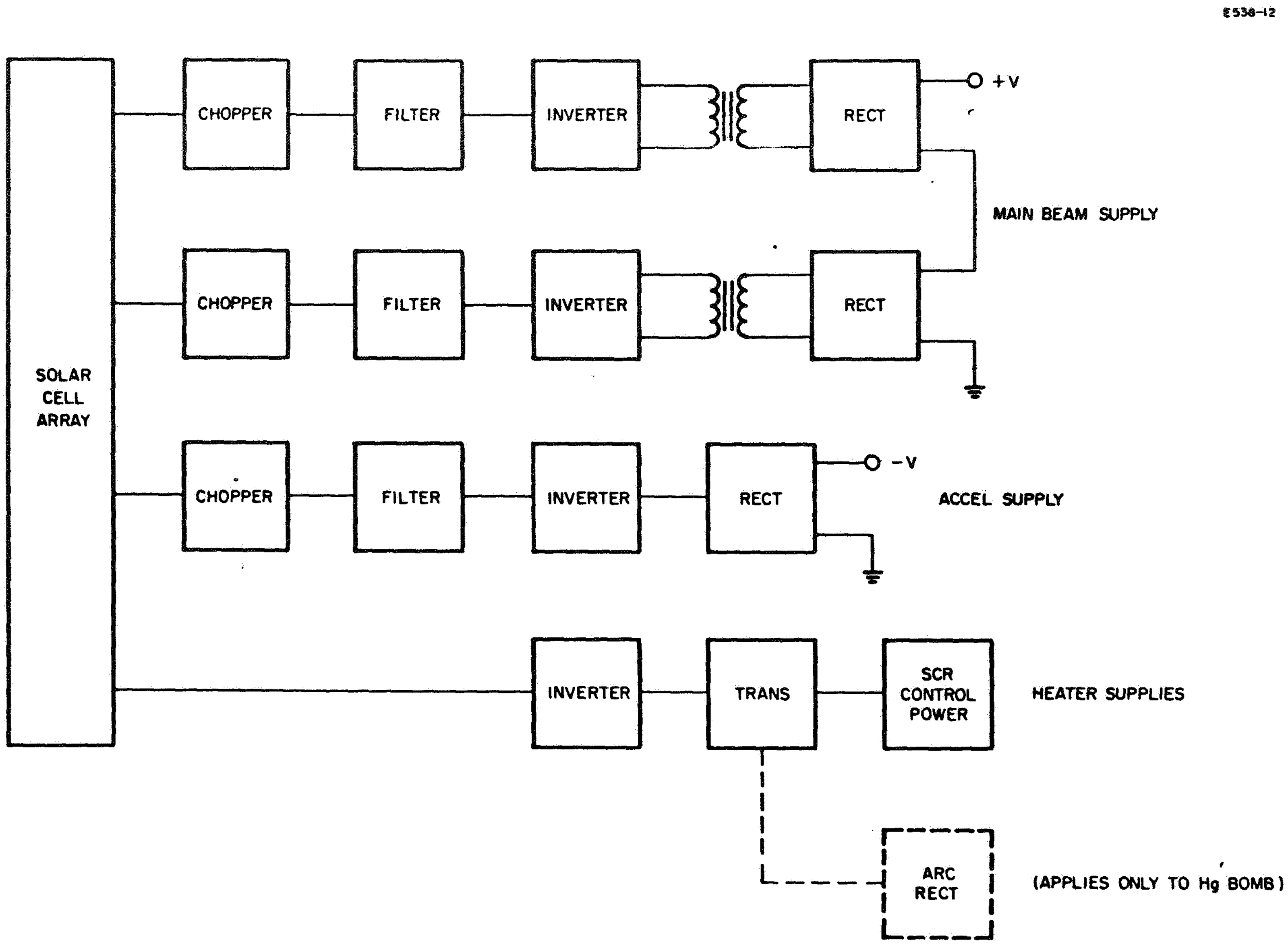

E538-12
SOLAR CELL ARRAY
CHOPPER
FILTER
INVERTER
RECT
+V
MAIN BEAM SUPPLY
CHOPPER
FILTER
INVERTER
RECT
CHOPPER
FILTER
INVERTER
RECT
−V
ACCEL SUPPLY
INVERTER
TRANS
SCR CONTROL POWER
HEATER SUPPLIES
ARC RECT
(APPLIES ONLY TO Hg BOMB)

Fig. B.1-14. SERT II, 6 kW power conditioning system.

supply, one for the accelerator supply and one for the arc discharge supply and heater systems. A conventional chopper regulator system is employed to regulate and control the power conditioning output voltages. With this circuit the dc input voltage to the inverter can be varied between 100 and 0 volts by employing chopper pulse width modulation, varying the dc input voltage to the inverter system directly controls the output voltage. This system has been employed on SERT-I and works very satisfactorily. However, for SERT-I a battery supply is used as the source of power. With a battery system, chopper regulation is very efficient since the power system is in effect a stored energy system. When the chopper is turned off no power is lost. In comparison, the solar power system is not a stored energy system; if a chopper regulation system is employed with solar cells the off time effectively results in lost power to the system. For example, if the chopper system operates with a 50 percent duty cycle the power conversion efficiency would also be 50 percent. Of course, this effect can be minimized by operating several chopper systems out of phase with each other. However, if a chopper regulation system is used some type of energy storage or buffer system will be required between the solar panel and the inverter. The buffer system requirement would increase the overall power conditioning system weight and circuit complexity.

The advantages of the SERT-II design are: (1) a good technology base supported by actual engine operating experience with the SERT-I equipment and (2) a design which is well underway.

The disadvantages of the SERT-II design are: (1) low inverter frequency (1 KC), (2) energy storage system required, (3) liquid cooling system required which is subject to meteoroid puncture and pump failure, (4) high specific weight when cooling system is included, (5) not compatible with standby and partial parallel circuit redundancy techniques, (6) design power level is relatively inflexible and (7) one power conditioning system is required for each ion engine system.

Multi-module Design: The design philosophy of this circuit concept is to construct a relatively high power system by using many common low power modules. The low power level of the individual modules will allow higher frequency operation with available transistors than would be possible with a single high power module, thereby achieving a saving in system weight yet maintaining high power efficiencies. A basic inverter system is employed in each module to convert the solar cell output voltage to chopped 20,000 cps ac. The output is then rectified in a bridge circuit. As shown in Fig. B.1-15, a commutating diode has been included at the rectifier output. The purpose of this diode is to provide a current path that bypasses a module when it is turned off so that the series string is not interrupted. The commutating diode allows the transformer secondary to be bypassed when the module is turned off, and yet is nondissipative when the module is operating.

The multi-module power conditioning design concept is based on three equal wattage module unit designs. Each module is identical in every respect except for the turns ratio on the output transformer (i.e., the voltage output). Two of these modules, the main beam and accelerator supply modules, are expected to operate at approximately a 93% overall power efficiency. The low voltage module systems, arc and heater supplies, are expected to operate at 77% power efficiency. For a 4000 sec I_{sp} ion engine system the power conditioning system will be required to convert approximately 80% of the solar power to high voltage and 20% to low voltage. On this basis, the total heat generated by the power conditioning system would be:

High voltage systems (beam and accel supplies)

Total System Power x % at high voltage x (1 - efficiency)

50 kW x .80 x .07 = 2.8 kW

Low voltage systems (arc and heater supplies)

Total System Power x % at low voltage x (1 - efficiency)

50 kW x .20 x .23 = 2.3 kW

Total heat generated by 50 kW power conditioning system . 5.1 kW

As now planned the power conditioning modules will be assembled in an array that will permit the heat loss from each power conditioning module system to be directly dissipated by radiation only. For this work it is assumed that the power conditioning array will be shadow shielded from the

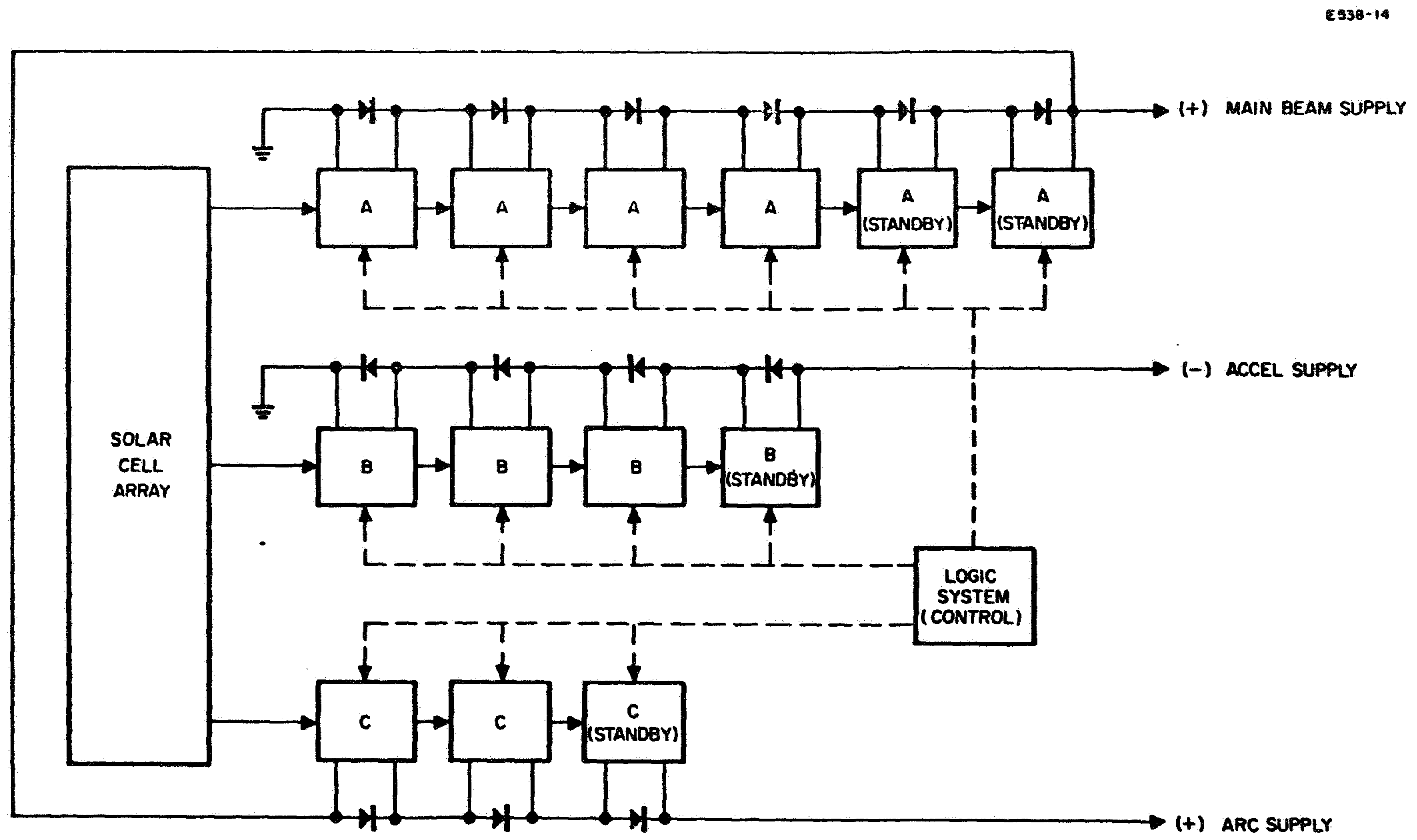
E538-14
SOLAR CELL ARRAY
A
A
A
A
A (STANDBY)
A (STANDBY)
(+) MAIN BEAM SUPPLY
B
B
B
B (STANDBY)
(−) ACCEL SUPPLY
LOGIC SYSTEM (CONTROL)
C
C
C (STANDBY)
(+) ARC SUPPLY

MODULE TYPE A (MAIN BEAM) 100V 1A DC
B (ACCEL SUPPLY) 1000V 0.1A DC
C (ARC SUPPLY) 5V 24A DC

NOTE: DIODES SHOWN ARE USED TO PREVENT A CIRCUIT FAILURE IN THE EVENT OF AN INVERTER OPEN CIRCUIT

Fig. B. 1-15. Multi-module power conditioning system.

sun and that each power conditioning array will radiate to space over a solid angle of 2π steradians. The area of each power conditioning module is to be designed to maintain a radiating temperature of 70° C for the power dissipated in each module. The high voltage modules will generate approximately 10 watts of thermal power and will require a radiator area of 4" x 5". The low voltage modules will generate approximately 23 watts of thermal power and will require a radiator area of 6.5" x 7". On this basis, the total radiating area of the power conditioning system would be: (assuming 100 watt modules)

High voltage systems (beam and accel supplies)

$$\frac{\text{Power at high voltage}}{\text{power/module}} \times \frac{\text{radiating area}}{\text{module}}$$

$$\frac{50 \times 10^{3}\,\text{W} \times .80}{100\,\text{W}} \times \frac{4\,\text{in} \times 5\,\text{in}}{144\,\text{in}^{2}/\text{ft}^{2}} = 55.5\ \text{ft}^{2}$$

Low voltage systems (arc and heater supplies)

$$\frac{\text{Power at low voltage}}{\text{power/module}} \times \frac{\text{radiating area}}{\text{module}}$$

$$\frac{50 \times 10^{3}\,\text{W} \times .20}{100\,\text{W}} \times \frac{6.5\,\text{in} \times 7\,\text{in}}{144\,\text{in}^{2}/\text{ft}^{2}} = 31.6\ \text{ft}^{2}$$

$$\text{Total Radiator Area} = 87.1\ \text{ft}^{2}$$

The advantages of the multi-module design concept are (1) high reliability because the modular design is well suited to standby and parallel circuit redundancy techniques, (2) low specific weight, (3) high power efficiency, (4) high inverter chopping frequency, (5) low ripple, (6) insensitivity to input solar panel supply voltage level, (7) direct radiation of heat due to power conversion losses and (8) output power level is flexible and engine system power can be optimized without being limited by the power conditioning.

The disadvantages of the multi-module design concept are (1) one power conditioning system will be required for each engine system, (2) the same standard module is not applicable to the high voltage and low voltage supplies and (3) voltage regulation will result in either some power waste or some voltage variation depending on the type of regulation used.

Voltage Regulation Methods: As pointed out previously the solar panel output voltage will increase 20 to 30 percent during the course of a mission. To maintain constant ion engine I_{sp} the ion engine bus voltages must remain at a fixed voltage even though the output voltage of the solar cells is increasing. Further, the voltage regulation function must be performed with a minimum of power loss. Several methods of voltage regulation have been studied; two methods involve regulating the output of the solar panel system and two methods would be accomplished within the power conditioning system.

The two methods for regulating the output voltage of the solar panel system are zener diode regulation and solar cell switching. Zener diodes placed in parallel with the solar panel outputs would limit the output voltage to the break over voltage of the zener diodes. The diodes can be chosen to limit the output to the nominal value at the beginning of the mission (100 volts for the present study). The disadvantage to this system is that it is a form of dissipative regulation and would result in an increasing power waste as the mission progressed (Fig. B. 1-16). Initially there would be no loss of power but by the end of a 350 day mission approximately 40% of the available power would be wasted.

The solar panel output voltage can be regulated without a power dissipation penalty by solar cell switching. The solar panel is comprised of many solar cells connected in parallel and series. As the individual solar cell voltages increase the total panel output voltage can be maintained constant by switching some cells from a series to parallel configuration. The disadvantages of this system are the complexity of the switching matrix and the problems associated with switching high dc currents.

Voltage regulation within the power conditioning system can be accomplished by chopper regulation or, for the multi-module system design, by switching out individual modules. The characteristics and disadvantages of a chopper regulation system are described in the section on SERT-II system design.

The multi-module design concept of obtaining a high voltage by series connecting the outputs of numerous low voltage modules permits incremental

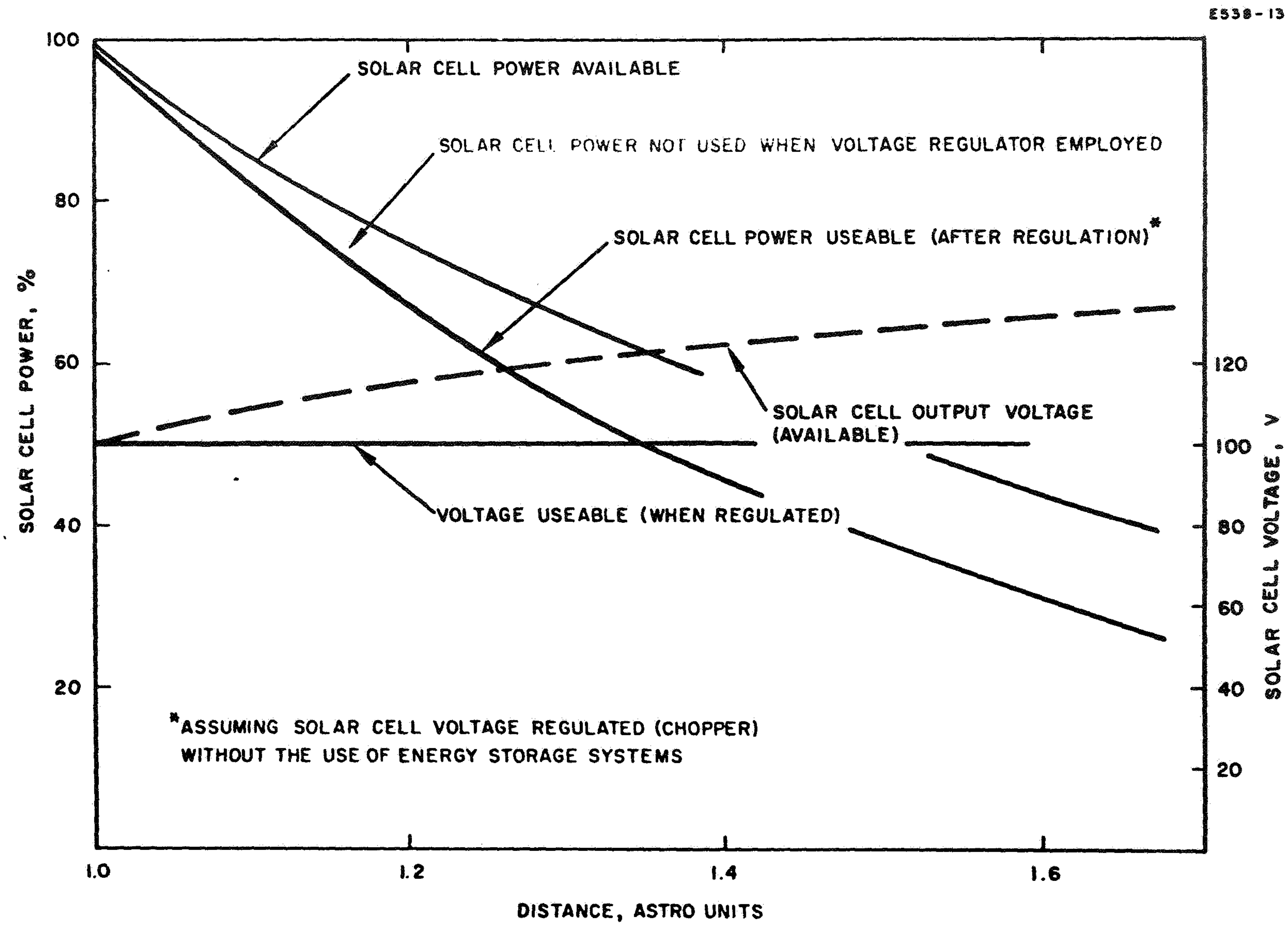

Fig. B.1-16. Solar array power-voltage characteristics.

voltage regulation by switching off individual modules. This method is particularly suited to the high power beam supply where a fairly large number of the low power modules operating at a relatively low output voltage will be required. The voltage increment that occurs when one module is switched off is, of course, dependent on the number of modules in series. As mentioned in the section on the multi-module system design each module will have a commutating diode across the output so that the series path is not interrupted when one or more modules are turned off.

Besides providing a solution to the problem of maintaining an essentially constant voltage across the ion engine, the modularized power conditioning system along with a modularized thrustor system offers an attractive means of load and power matching. Consider, for example, an ion engine system as pictured in the following schematic:

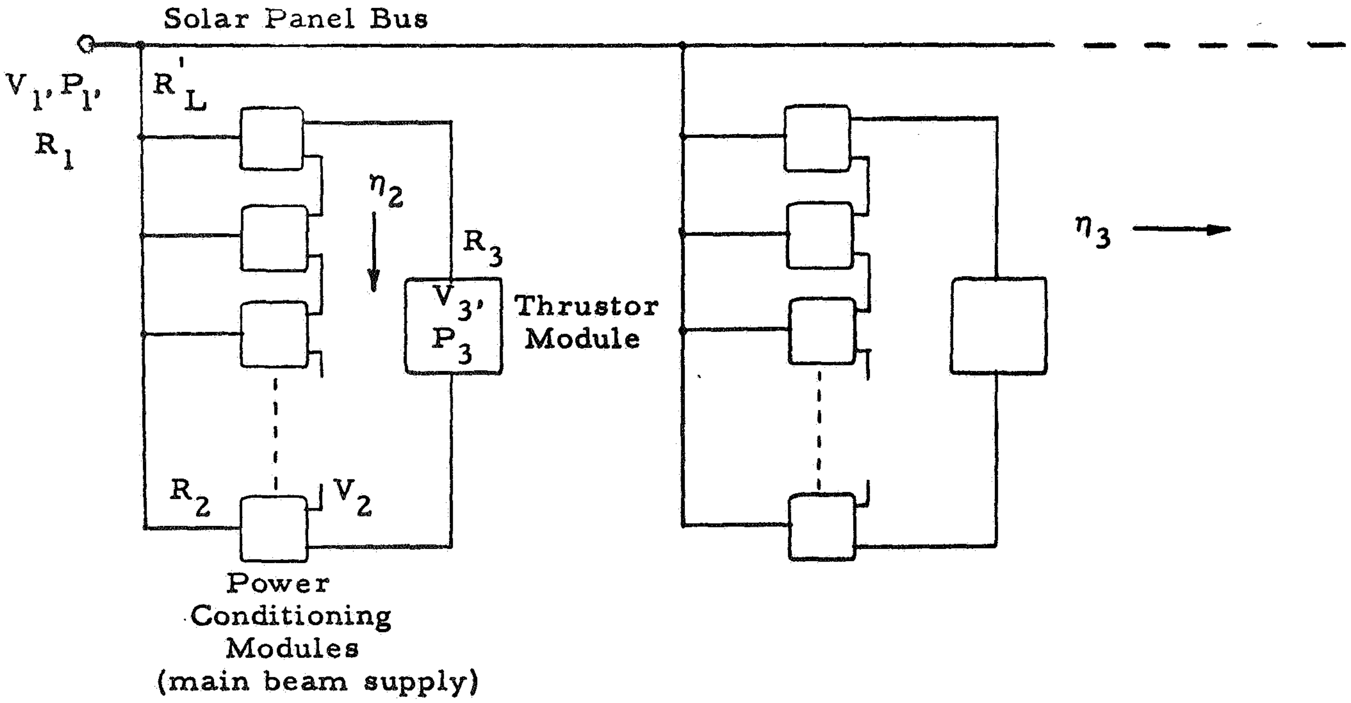
Solar Panel Bus
$V_1, P_1,$
R_1
R'_L
η_2
R_3
V_3, P_3
Thrustor Module
R_2
V_2
Power Conditioning Modules (main beam supply)
η_3

where $V_1(t)$ = Solar panel bus voltage

$P_1(t)$ = Solar panel power (max)

$R_1(t)$ = Optimum load resistance

$R_L(t)$ = Reflected load resistance (total system)

$R_L'(t)$ = Resistance of single thrustor plus its power conditioning modules

$R_2(t)$ = Resistance of single power conditioning module

$V_2(t)$ = Voltage output of single power conditioning module (where $V_2 = V_1$)

$\eta_2(t)$ = Number of power conditioning modules per thrustor

V_3 = Thrustor beam voltage

P_3 = Single thrustor power

R_3 = Single thrustor resistance

$\eta_3(t)$ = Number of thrustors

I_3 = Thrustor beam current

These parameters are related as follows:

$$R_3 = \frac{V_3^{\,2}}{P_3} \quad ; \quad R_L'(t) = \frac{R_2(t)}{\eta_2(t)}$$

$$I_3 = \frac{P_3}{V_3} \quad ; \quad R_L(t) = \frac{R_2'(t)}{\eta_3(t)}$$

$$R_2(t) = \frac{V_2(t)}{I_3} \quad ; \quad R_1(t) = \frac{V_1^{\,2}(t)}{P_1(t)}$$

It can now be shown by proper manipulation of the above relationships that at any time t where the available power is equal to an integer times the rated thrustor power (i.e., $P_1(t) = \eta_3(t)\, P_3$) and the required thrustor voltage is an integer times the power conditioning module output (i.e., $V_3 = \eta_2(t)\, V_2(t)$), load matching results (i.e., $R_L(t) = R_1(t)$) simply by choosing η_2 and η_3 properly for voltage regulation and power matching. Since load matching is guaranteed only at specific points along the power curve, a power waste will occur in the intervals between these points. The number of thrustors and power conditioner modules will determine the length of these intervals and, therefore, the power loss. The effect of η_2 and η_3 on the amount of power wasted as well as the variation in thrustor beam voltage is being analyzed at present. The results of this analysis will affect the choice of both thrustor and power conditioner module size. In addition the above analysis shall consider the effect of power supplies other than the main beam supply shown above.

REFERENCES

1. W. R. Kerslake, "Charge-Exchange Effects on the Accelerator Impingement of an Electron Bombardment Ion Rocket" TN D - 1657.
2. H. R. Kaufman and P. D. Reader, "Experimental Performance of Ion Rockets Employing Electron-Bombardment Ion Sources", ARC - 1960.
3. H. R. Kaufman, "The Electron Bombardment Engine", Advanced Propulsion Concepts Proceedings of 3rd USAF Symposium, October, 1962.
4. P. D. Reader, "Experimental Performance of a 50- Cm Diameter Electron-Bombardment Ion Rocket", AIAA No. 64-689, September, 1964.
5. P. D. Reader, " Experimental Effects of Propellant Introduction Mode on Electron-Bombardment Ion Rocket Performance, TN -2587.

6. R. D. Reader, "Experimental Effects of Scaling on the Performance of Ion Rockets Employing Electron-Bombardment Ion Sources", IAS/ARS No. 61-87-1781, June, 1961.

7. W. R. Kerslake, "Accelerator Grid Tests on an Electron-Bombardment Ion Rocket", TN-D 1168.

8. W. R. Kerslake and E. V. Pawlik, "Additional Studies of Screen and Accel Grids for Electron Bombardment Ion Thrustors", TN-D 1411.

9. H. J. King, Personal Communication

10. D. Berman, "Neutral Fraction from Porous Ionizers", IPD 5-3, February, 1965.

11. Ion Rocket Engine Development, Contract No. NAS 3-6271, Quarterly Report No. 1, February 22, 1965.

12. Mercury Feed System Proposal (65 M-4595/A7228) Hughes Research Laboratories, March, 1965.

2. Reliability Analysis

An important question to be answered before a system design can begin is the total number of modules to be employed in building up to a high power electric propulsion system. There are several important considerations which affect the answer to this question; the foremost of which is system reliability.

As is well known the establishment of component reliability figures at high confidence levels requires costly and time consuming test programs. It is possible, however, to build up system reliability through redundancy techniques even though component reliability is either somewhat low or possibly not established. Redundancy, whether series, parallel or standby, will increase propulsion system weight. It is desirable, therefore, to determine the method by which the requisite reliability can be obtained with a minimum addition to system weight.

Standby redundancy is the only applicable technique for increasing the reliability of the thrustor system. It is well known that the reliability of a system can be increased to any desired level if enough standbys are employed. However, in order to minimize the weight penalty a computer program was developed which determines the combination of operating and standby modules such that the redundant engine system weight is a minimum for a given desired system reliability. Once the number is found, the optimum module size (from a weight-reliability standpoint) for an engine system of a given power level is defined. The development of the computer program is discussed in Ref. 1 and will be reviewed here. Assume that each engine system has a failure rate λ which can be divided into the sum of: (1) λ_p which is, to a first approximation, linearly dependent on the size or power level of the engine (e. g., area dependent effects) and (2) λ_c which is essentially independent of engine size (e. g., control system). In general λ_c covers all items which must be duplicated or added if a large engine is divided into modules.

Consider now the division of the single large unit into m modules and the reduction in size of the standby units from that of a complete single engine system to the smaller thrustor module. If the failure rate of a module is λ_m then, the failure rate of the complete operating engine system is m λ_m. Since only the chance failure region is being considered, the probability of a component failure occuring in a given Δt is not a function of the amount of time the component has already operated. It is obvious then that the replacement of a single module (should one operating module fail) is equivalent to the substitution of a complete system of m modules with failure rate m λ_m. The reliability of a redundant system consisting of m operating modules and N standby modules is then

$$(1) \qquad R_{m,N} = e^{-m\lambda_m t} \sum_{r=0}^{N} \frac{(m\lambda_m t)}{r\,!}$$

Writing the failure rate of the modularized operating engine in terms of λ_p and λ_c (for later purposes let $\lambda_R = \lambda_c / \lambda_p$), it is seen that

$$(2) \qquad m\,\lambda_m = \lambda_p + m\,\lambda_c$$

Finally, then

$$(3) \qquad R_{m,N} = e^{-(\lambda_p + m\lambda_c)\,t} \sum_{r=0}^{N} \frac{\left[(\lambda_p + m\lambda_c)\,t\right]^r}{r\,!}$$

The reliability of a redundant modularized engine system can now be found. Since the modules have not been specified they may, if desired, be thought of as any combination of thrustor, control system, feed system, and power conditioner. Modularizing a redundant engine system does not in itself guarantee a reduction in overall system weight. However, if the choice of module size is left open, a weight-reliability optimization can be performed.

The weight of a single large engine can be divided into the sum of that part which is linearly dependent on the power level and that which is independent of engine size (i. e., in a manner similar but not necessarily identical to the division of λ). The weight of a modularized engine system can then be written

$$(4) \qquad W_m = W_p + m\, W_c$$

where W_p = weight of those items dependent on engine size

W_c = weight of those items independent of engine size

For a system of m operating modules with N standbys, the weight is

$$(5) \qquad W_{m,N} = (W_p + m\, W_c) + (\frac{N}{m} W_p + N\, W_c)$$

The percentage weight increase of a redundant system over that of a single large engine can now be shown to be

$$(6) \qquad \frac{W_{m,N} - W_{1,0}}{W_{1,0}} = (m + N - \frac{N}{m} - 1) \frac{C_o}{(C_o + 1)} + \frac{N}{m}$$

where C_o is the ratio of W_c to W_p

It is now possible to determine the combination of m and N such that the redundant engine system weight is a minimum for a given desired system reliability. The results will vary depending on the values of λ_R, C_o, and $R_{1,0}$.

Typical results of the optimization study are shown in Figs. B. 2-1 and B. 2-2. These results, based on the constraint that the overall system

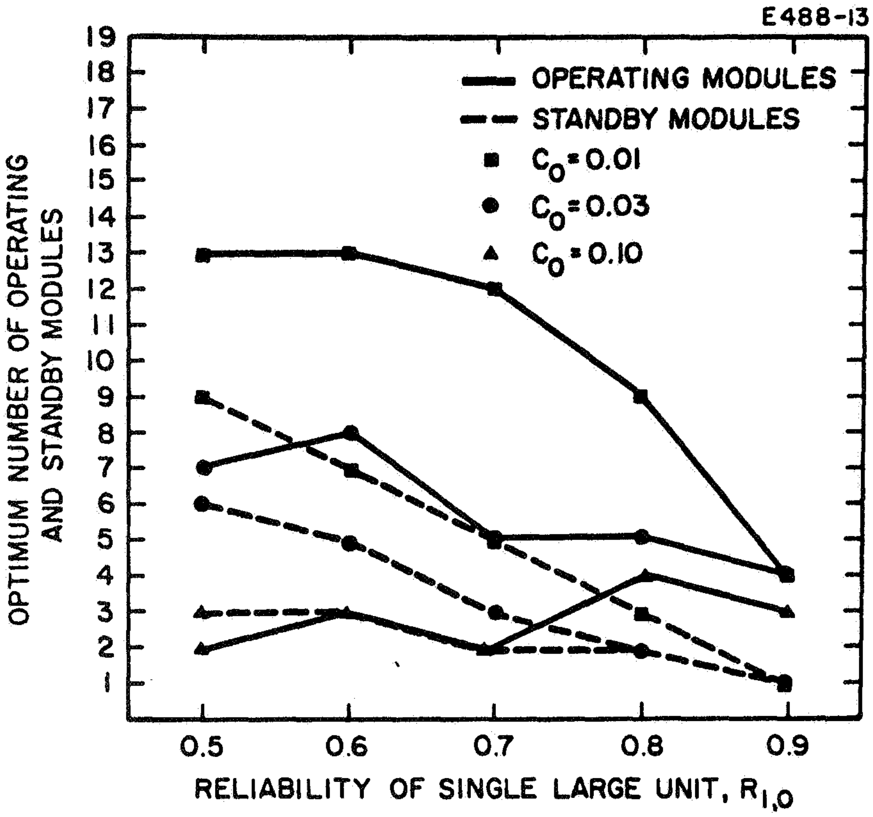

Fig. B.2-1. Optimum number of engine modules to obtain 0.97 system reliability (C_0 is ratio of weight of items independent of engine size to those dependent on engine size).

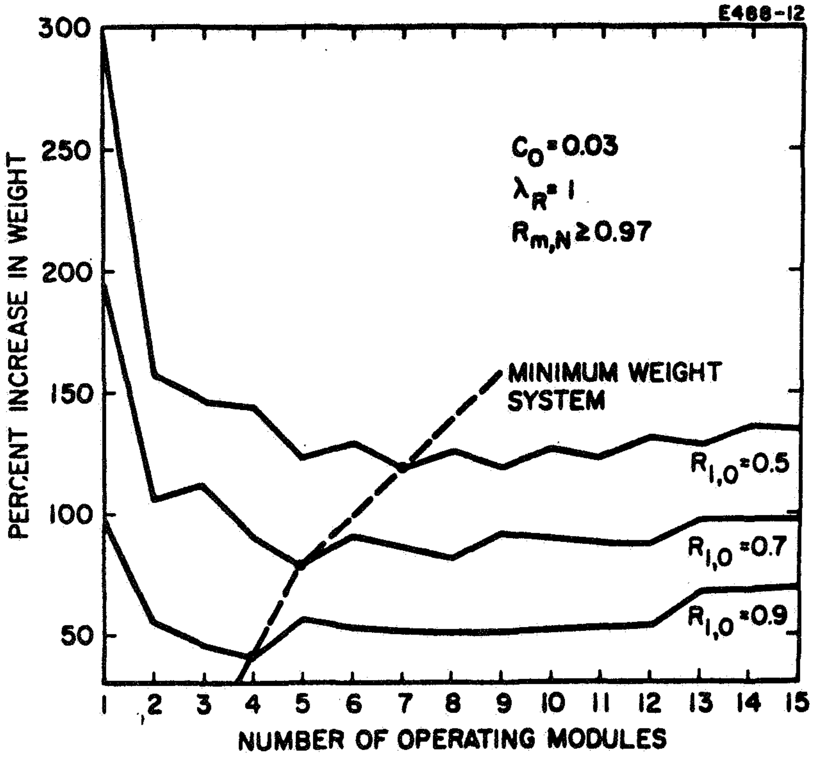

Fig. B.2-2. Weight penalty to obtain 0.97 system reliability (λ_R is ratio of failure of items independent of engine size to those dependent on engine size).

reliability be at least 0.97, are given for ranges of λ_R, C_o and $R_{1,0}$ thought to cover ion engine systems.

The optimum number of operating modules and standbys are shown in Fig. B.2-1 as a function of single large engine reliability. These data assume a λ_R of unity and are given for various values of C_o. In general the optimum number of modules decreases as the single large engine reliability increases. However, at high values of C_o (e.g., 0.1), m is relatively independent of $R_{1,0}$. In all cases, the required number of standbys decreased as the single large engine became more reliable. Both m and N decreased monotonically with increasing C_o.

Figure B.2-2 shows the weight penalty incurred when increasing the engine system reliability to 0.97 by standby redundancy techniques.

These data show the sensitivity of system weight to the number of modules for various values of $R_{1.0}$ when C_o equals 0.3. Two important conclusions can be drawn from the curves in Fig. B.2-2. First the initial division (i.e., $m = 2$) of the large engine system provides the greatest single weight savings. Second, the lower the value of $R_{1,0}$ the more significant the optimization. A final conclusion is that only a small penalty is paid if numbers of modules greater than optimum are employed. This conclusion is not general, however, since for high values of C_o, there occurs a rather definite minimum with serious weight penalties resulting if large number of modules are employed. In the design of high power engine systems where a large m may be desirable, it is important to minimize the weight of duplicated items even though they may already only be 0.1 of the total system weight.

The above analyses have assumed a constant power system. At the present time, the reliability studies are being extended to consider the variable power effect. It is expected that the initial number of standbys will be reduced for the variable power case since as the power decreases operating modules will be turned off and, therefore, available as standbys.

For example, consider that at time t_o, there are m_o operating modules and n_o standbys and that at time t_j one operating unit is switched out and becomes a standby. Thus in the interval (t_j, t_{j+1}) there are

$(m_o - j)$ operating modules and $(n_o + j)$ standby units. The probability of exactly h failures occuring during the time interval Δt is

$$(7) \qquad P_m(h, \Delta t) = e^{-(\lambda_p + m\lambda_c)\Delta t} \frac{[(\lambda_p + m\lambda_c)\Delta t]^h}{h!}$$

where m units are operating during time Δt.

The probability P_t that the proper number of operating and standby modules are available during the complete mission time profile is

$$(8) \qquad P_t = P_{\Delta t_1} \cdot P_{\Delta t_2} \cdots\cdots P_{\Delta t_k}$$

where $P_{\Delta t_1}$ = Probability that n_o or less modules fail during an interval (t_o, t_1)

$P_{\Delta t_2}$ = Probability that $n_o + 1 - j_1$ or less modules fail during an interval (t_1, t_2)

.

.

.

$P_{\Delta t_k}$ = Probability that $n_o + k - \sum_{a=0}^{k} j_a$ or less modules fail during an interval (t_k, t)

Now the probability that m or less modules fail during an interval (t_j, t_{j+1}) i

$$(9) \qquad \sum_{h=0}^{m} P(h, t_{j+1} - t_j) = \sum_{h=0}^{m} e^{-[\lambda_p + (m_o - j)\lambda_c](t_{j+1} - t_j)} \frac{\{[\lambda_p + (m_o - j)\lambda_c](t_{j+1} - t_j)\}^h}{h!}$$

The reliability for a total time t of a variable power system consisting initially of m_o operating units and n_o standbys is then

$$(10)\qquad R_{m_o, n_o}(t) = \sum_{j_1=0}^{n_o} P(j_i, t_1 - t_o) \cdot \sum_{j_2=0}^{n_o+1-j_1} P(j_2, t_2 - t_1 \cdots\cdots$$

$$\sum_{j_\mu=0}^{n_o+\mu-1-\sum_0^{\mu-1} j_a} P(j_\mu, t_\mu - t_{\mu-1}) \cdots\cdots \sum_{j_{k+1}}^{n_o+k-\sum_0^{k} j_a} P(j_{k+1}, t_{k+1} - t_k)$$

or

$$(11)\qquad R_{m_o, n_o}(t) = \prod_{\mu=1}^{k+1} \left(\sum_{j_\mu=0}^{n_o+\mu-1-\sum_0^{\mu-1} j_a} P(j_\mu, t_\mu - t_{\mu-1}) \right)$$

where

$$(12)\qquad P(j_\mu, t_\mu - t_{\mu-1}) = e^{-\left[\lambda_p + (m_o - \mu + 1)\lambda_c\right](t_\mu - t_{\mu-1})}$$

$$\frac{\left\{\left[\lambda_p + (m_o - j + 1)\lambda_c\right] (t_\mu - t_{\mu-1})\right\}^{j_\mu}}{j_\mu !}$$

and $j_o = 0$

At the present time Eq. 11 is being programmed to replace Eq. 3 so that the optimum number of modules for the variable power case can be defined.

Ref. 1 - J. H. Molitor et al, Effects of Reliability Considerations on the Design of Electric Thrustor Arrays, AIAA Paper No. 65-68

3. Conceptual Design

The ultimate goal of the propulsion system studies is the design of a complete ion engine system which satisfies the various constraints and requirements established by the mission, reliability, solar panel, and spacecraft integration studies. The complete engine system, for both the Cs contact and Hg bombardment thrustors, consists of the thrustor array, power conditioning and engine control system, and the storage and feed system.

During this first iteration of the overall program a conceptual design of a Hg bombardment engine system was performed. This system was designed to meet the constraints as established by the 1971, 350 day zero coast rendezvous mission for a spacecraft weight of 11,700 lb, that is:

1) Power Requirement = 48 kW
2) Specific Impulse = 4000 sec
3) Propellant Weight = 1550 lb
4) Thrust Vector Orientation Variation = 60°

The choice of module size for the initial conceptual design was made on the basis of the reliability analyses presented above. A preliminary estimate of Co = 0.03 and $\lambda_R = 1$ was made for the thrustor system. In addition a single large thrustor reliability of 0.6 was assumed. Figure B.2-1 shows that for a constant power system the optimum combination of operating and standby engines is 8 and 5, respectively. It was assumed, therefore, that for the variable power system an array of 12 thrustors, 8 operating and 4 standby, would be employed.

Another important consideration in the choice of optimum module size is the efficient use of the power available from the solar panel. In order to follow this power curve, the individual thrustors must either be capable of operating with variable power input or thrustor modules must be shut off. The former, of course, complicates the system design. The latter is effective only if the module size is small enough such that the discreet power steps closely approximate the power curve. Possibly a combination of the two alternatives will be the final solution. The effect of efficient power utilization on the choice of module size is at present being studied. It is possible, for example, that the number of modules as determined by the reliability analysis should only be considered as a minimum value.

A conceptual drawing of a complete ion propulsion system which satisfies the design constraints which have been discussed above is shown in Fig. B. 3-1. It consists of 12 thrustor modules. Initially, 8 of these would be operating and 4 would be in standby to satisfy the reliability considerations. The thrustor array shown is based on a 6 kW, 50 cm, Hg bombardment engine operating at low current density(e.g. 2-3 mA/cm^2) and is 5' x 7'. The size of this array would be reduced by operating a 20 cm thrustor at higher current density, such would be the case for the Cs contact thrustors. The weight of the complete thrustor system would be about 290 lb.

Also shown in Fig. B. 3-1 is a conceptual layout of the feed system and propellant tankage. The propellant tanks each have a 200 lb liquid Hg capacity and are 10" in diameter. The total array being somewhat less than 3' x 3' . A modular concept is employed in the tankage system for two reasons (1) redundancy techniques can again be employed for increased reliability and (2) each tank contains a positive expulsion system which, if a single tank were used, would have to support a ton of Hg under launch conditions.

The rest of the feed system consists of:

1) On-off valve
2) Phase Separator (Vaporizer)
3) Feed Transfer System which switches tanks to thrustors
4) Flow Control to measure and regulate the gas flow to the engine
5) High Voltage isolation system which electrically decouples the high voltage thrustor from the feed system and propellant tanks.

Since the thrustor array must be rotated through 60°, the tanks will be mounted to the engine cluster so that flexible couplings are not required. The feed system is, therefore, shown in an exploded view.

The power conditioning system consists of 8 panels of modules, one panel consisting of the power supplies required for a single thrustor. Each panel is approximately 3' x 3' and is designed in a flat panel for radiation

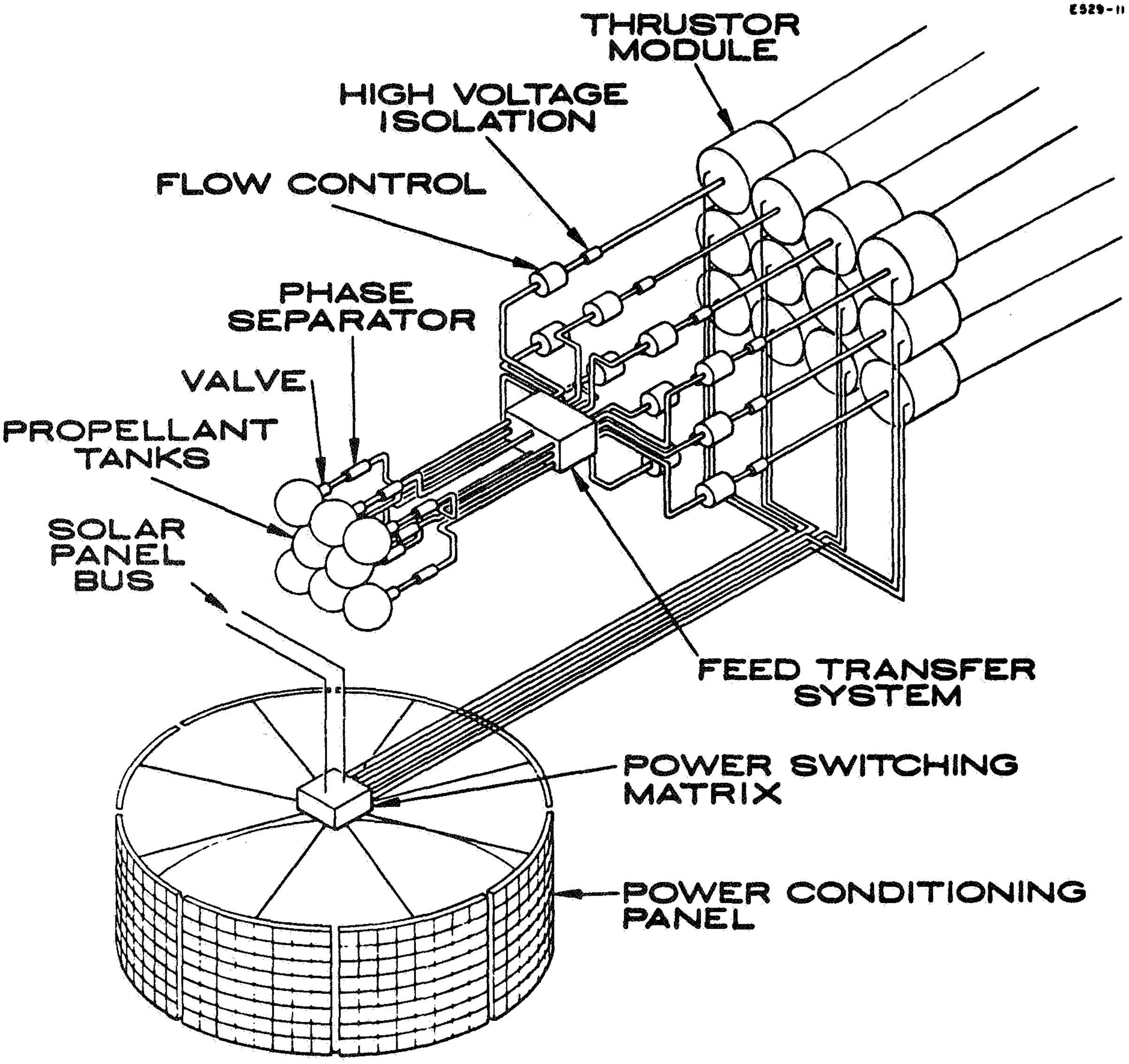
E529-11
THRUSTOR MODULE
HIGH VOLTAGE ISOLATION
FLOW CONTROL
PHASE SEPARATOR
VALVE
PROPELLANT TANKS
SOLAR PANEL BUS
FEED TRANSFER SYSTEM
POWER SWITCHING MATRIX
POWER CONDITIONING PANEL

Fig. B.3-1. Conceptual drawing of 48 kW ion engine system.

cooling. The eight panels are shown forming an 8' diameter cylinder which slips over the spacecraft structure as will be shown later. A power switching matrix provides switching between the power conditioning panels and thrustor modules. Again extra power conditioning panels could be provided to increase system reliability. However, the reliability of each panel can be made arbitrarily high by increasing the number of power conditioning modules per panel as shown in Fig. B. 3-2.

As shown, each power supply is made up of a number of low voltage, low power modules strung in series such that the required thrustor voltage and power is obtained. By placing a number of extra modules in series with those required, the reliability of the individual supplies can be increased to any desired level. The high voltage, high power beam supply is shown consisting of 47 50V, 100 watt modules. Other supplies shown are the high voltage, low power accelerator supply, the arc discharge supply, and the various heater supplies.

As indicated the 48 kW system may be approximately considered to be composed of separate 6 kW engine systems, each with its own feed system and power conditioning. It is of interest, therefore, to tabulate the components of a 6 kW mercury bombardment engine system. Table B.3-1 shows the weights broken down into the four major subsystems. The total system weight is shown to be 99 lb for a specific weight of 16.5 lb/kW. Although items such as cabling, piping, and redundancy are not included, the indications are that the engine system will come well within the 25 lb/kW goal.

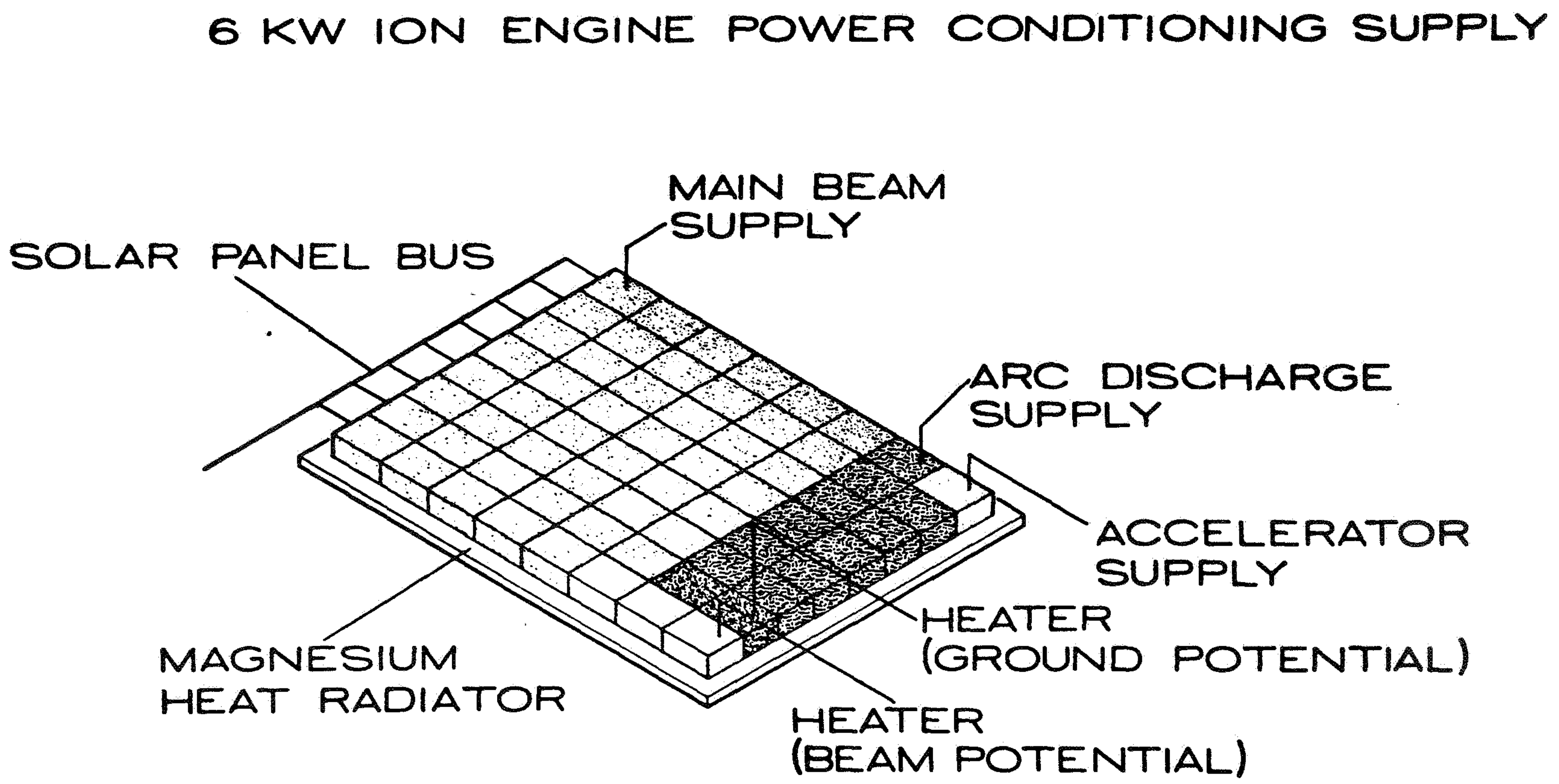
6 KW ION ENGINE POWER CONDITIONING SUPPLY
MAIN BEAM SUPPLY
SOLAR PANEL BUS
ARC DISCHARGE SUPPLY
ACCELERATOR SUPPLY
HEATER (GROUND POTENTIAL)
MAGNESIUM HEAT RADIATOR
HEATER (BEAM POTENTIAL)

Fig. B.3-2. Conceptual drawing of 6 kW ion engine power conditioning system.

TABLE B. 3-1

PRELIMINARY WEIGHT ESTIMATE

6 kW MERCURY BOMBARDMENT ENGINE SYSTEM

THRUSTOR		POWER CONDITIONING	
Accel Electrode:	8 lb	Main Beam Supply (47)*:	38.0 lb
Screen Grid:	4.5	Accel Supply (1):	0.8
Shell:	7	Arc Supply (11):	8.8
Magnet (Coil & Insulators):	2.5	Heater Supplies (5):	4.0
Miscellaneous:	2	TOTAL:	51.6 lb
TOTAL:	24 lb	(* Number of Modules)	
FEED SYSTEM		**CONTROL SYSTEM**	
Mercury Reservoir: (200 lb Propellant Capacity)	10.5	Ion Engine Control:	6
Vaporizer:	1.5	Circuit Malfunction Monitor:	3
Flow Control:	1.5	Switching Matrix:	1
TOTAL:	13.5 lb	TOTAL:	10 lb
TOTAL WEIGHT:	99.0 lb		
SPECIFIC WEIGHT:	16.5 lb/kW		

C. SPACECRAFT SYSTEM DESIGN

1. General Arrangement

The predominent factors affecting the general arrangement are the solar array concept, the orientation of the thrust vector during heliocentric transfer, the area required for thermal radiation, the large diameter communications and radar antenna, the lander capsule, and the use of a chemical engine for retro thrust. Both configurations presented herein are designed to be compatible with the Saturn IB/Centaur Nose Fairing and S/C Dynamic Envelope (furnished by JPL) presented in Figure C.1-1.

Two of the several initial Boeing solar array design concepts were selected for preliminary spacecraft conceptual designs. One concept, wherein the solar array is divided into a large number of small rigid panels which are folded and stacked during launch and are deployed in an "accordian" fashion, is referred to as the "Folding Modular" solar array and designated by Boeing as the SC-1 configuration (see Figure C.1-2). The second, wherein the solar cells are mounted on a flexible substrate and the array is rolled on a drum during launch and deployed by extendible booms, is referred to as the "Roll-Up" solar array and designated by Boeing as the SC-3 configuration (see Figure C.1-3). In Figures C.1-4 and C.1-5 are depicted artist renditions of conceptual spacecraft designs that are compatible with the two aforementioned solar array configurations. General arrangements showing both stowed and deployed positions of components are presented in Figures C.1-6 and C.1-7.

A preliminary weight breakdown for the conceptual spacecraft designs presented is shown in Table C-1. It should be noted, however, that this is not a complete weight statement. It does not include such items as the launch vehicle adapter (which could weigh as much as 1,000 lbs) the wire harnessing, and additional payload capability to bring the total launch weight up to the escape velocity capability of the Saturn IB/Centaur launch vehicle (11,700 lbs.). The weight statement, however, does include the estimated weight of all the significant subsystems considered in the general arrangements presented.

PRELIMINARY ESTIMATES

SYSTEM PERFORMANCE - 5500 SQ. FT. AT 1 A.U.

ARRAY DESIGN	UNIT/WT.* lbs/sq. ft.	CELL* TEMP. °C	POWER* WATTS/SQ.FT.	PERFORMANCE* WATTS/lb.
RIGID CONCENTRATOR	.511	63	8.1	15.8
RIGID NON-CONCENTRATOR	.750	63	9.1	12.1
SEMI-RIGID NON-CONCENTRATOR	.48	57	10	21.0

* Note these numbers represent preliminary estimates only and not to be used for other than initial configuration purposes

Part 1

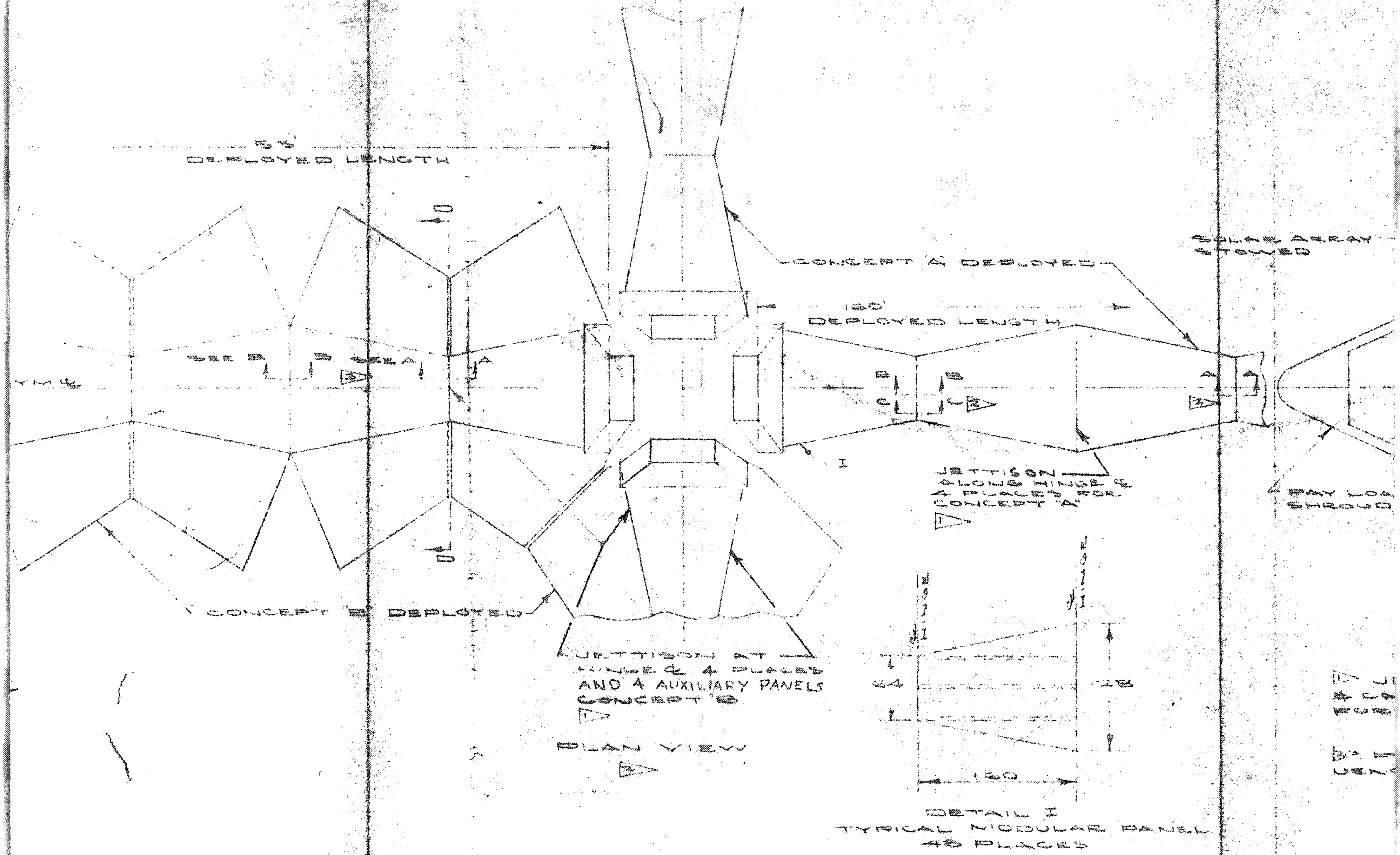
53'
DEPLOYED LENGTH
SYM ℄
SEE B
B SEE A
A
D
D
CONCEPT B DEPLOYED
CONCEPT A DEPLOYED
160'
DEPLOYED LENGTH
B
C
3
I
SOLAR ARRAY STOWED
JETTISON ALONG HINGE ℄ 4 PLACES FOR CONCEPT 'A'
1
PAY LOA
SHROUD
JETTISON AT HINGE ℄ 4 PLACES AND 4 AUXILIARY PANELS CONCEPT 'B'
1
PLAN VIEW
2
HINGE ℄
HINGE ℄
64
128
160
DETAIL I
TYPICAL MODULAR PANEL
48 PLACES

Part II

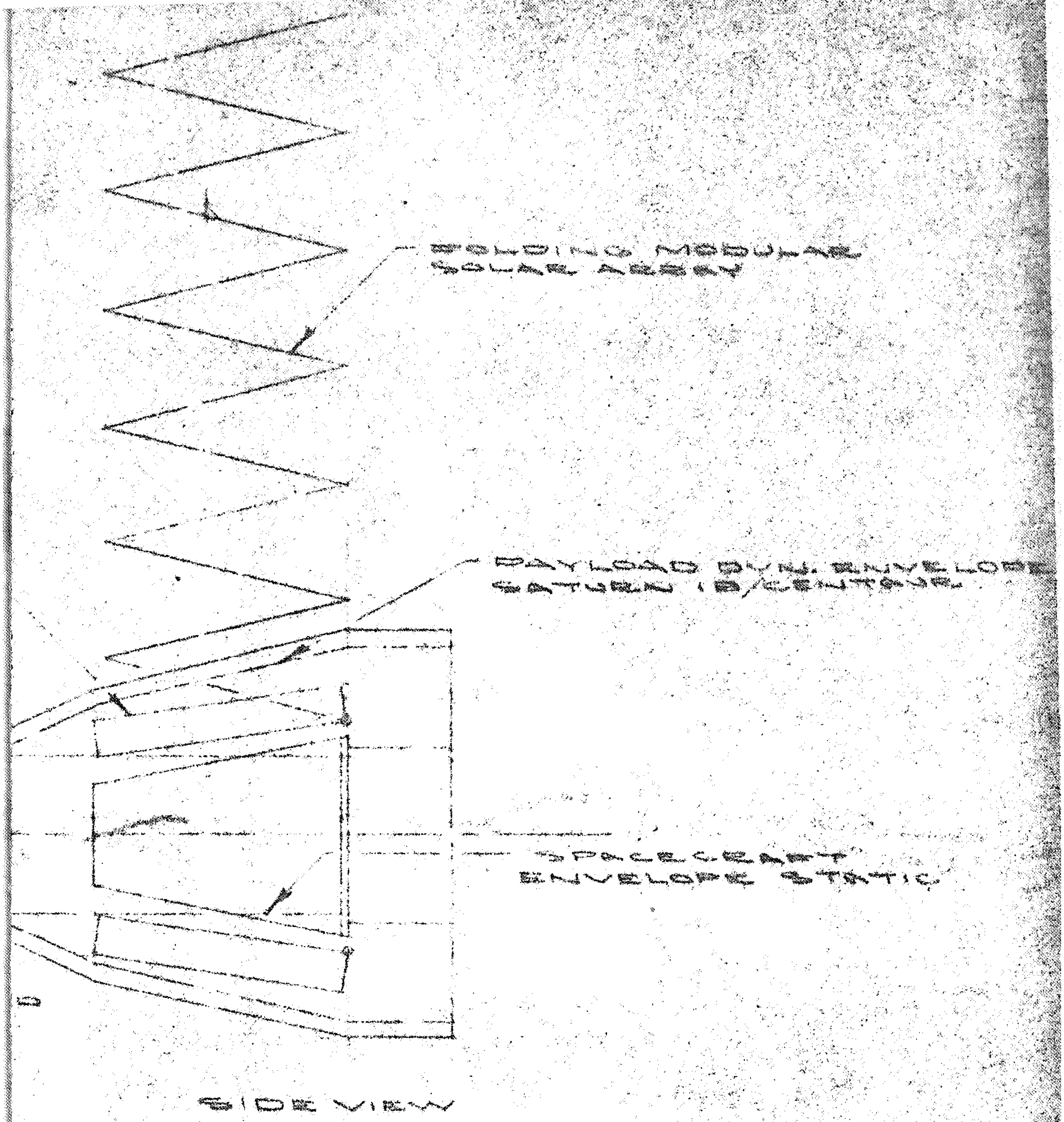
FOLDING MODULAR
SOLAR ARRAY
PAYLOAD DYN. ENVELOPE
SATURN IB/CENTAUR
SPACECRAFT
ENVELOPE STATIC
SIDE VIEW

ETTISON CONSISTS OF HINGE & LATCH DETACH
IBLE CUTTING BY PYROTECHNIC DEVICES &
CED SEPARATION BY SPRING

OR SECTION VIEWS, FUNCTIONAL SEQ-
CE & OTHER INFORMATION SEE FIG. 13

Part III

FOLDING MODULAR
SOLAR ARRAY
SC-1 CONFIGURATION

FIGURE C.1-2

1/100 SIZE

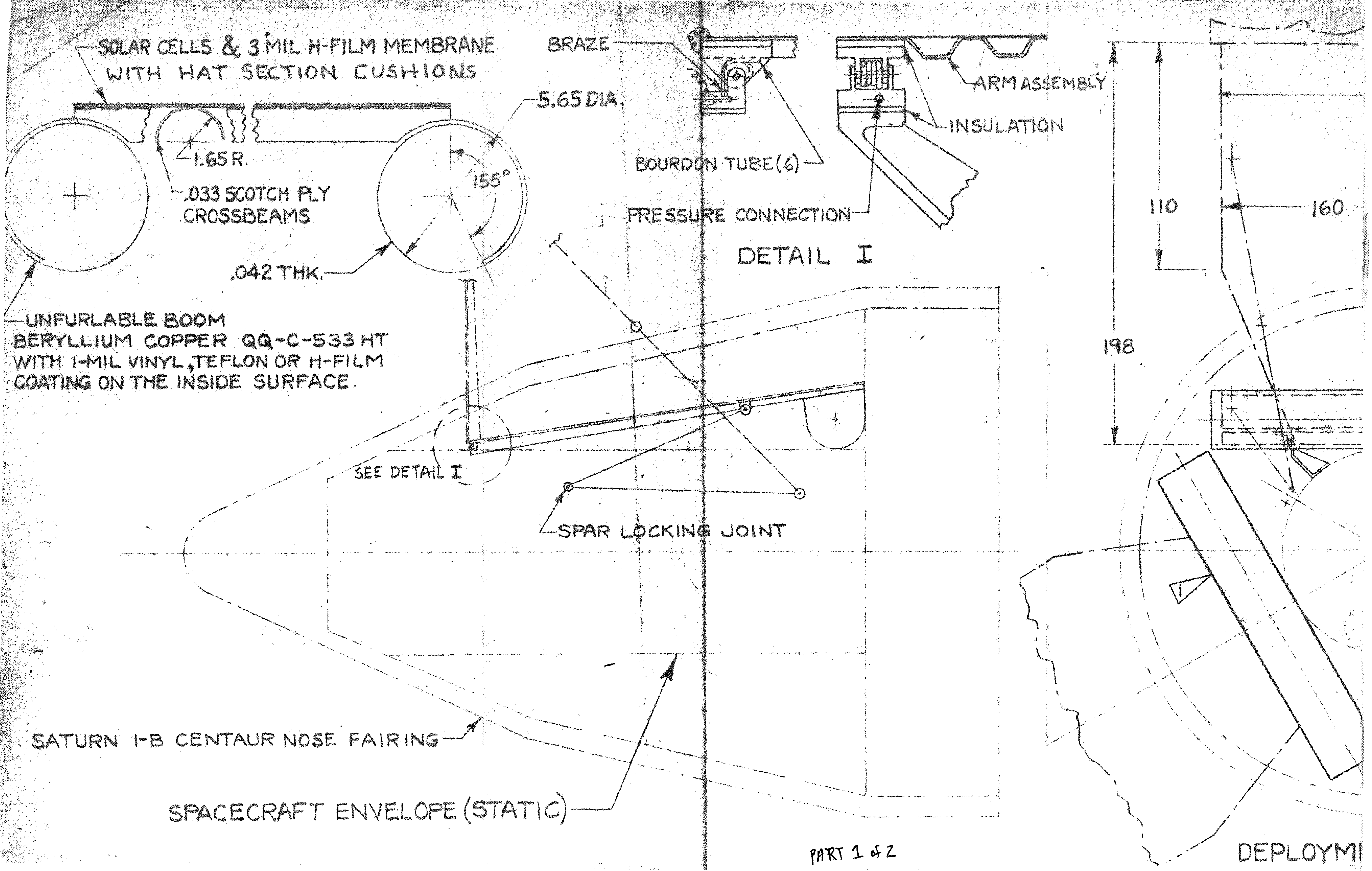
SOLAR CELLS & 3 MIL H-FILM MEMBRANE WITH HAT SECTION CUSHIONS
5.65 DIA.
1.65 R.
.033 SCOTCH PLY CROSSBEAMS
155°
.042 THK.
UNFURLABLE BOOM BERYLLIUM COPPER QQ-C-533 HT WITH 1-MIL VINYL, TEFLON OR H-FILM COATING ON THE INSIDE SURFACE.
BRAZE
BOURDON TUBE (6)
PRESSURE CONNECTION
ARM ASSEMBLY
INSULATION
DETAIL I
110
160
198
SEE DETAIL I
SPAR LOCKING JOINT
SATURN I-B CENTAUR NOSE FAIRING
SPACECRAFT ENVELOPE (STATIC)
DEPLOYM

PART 1 of 2

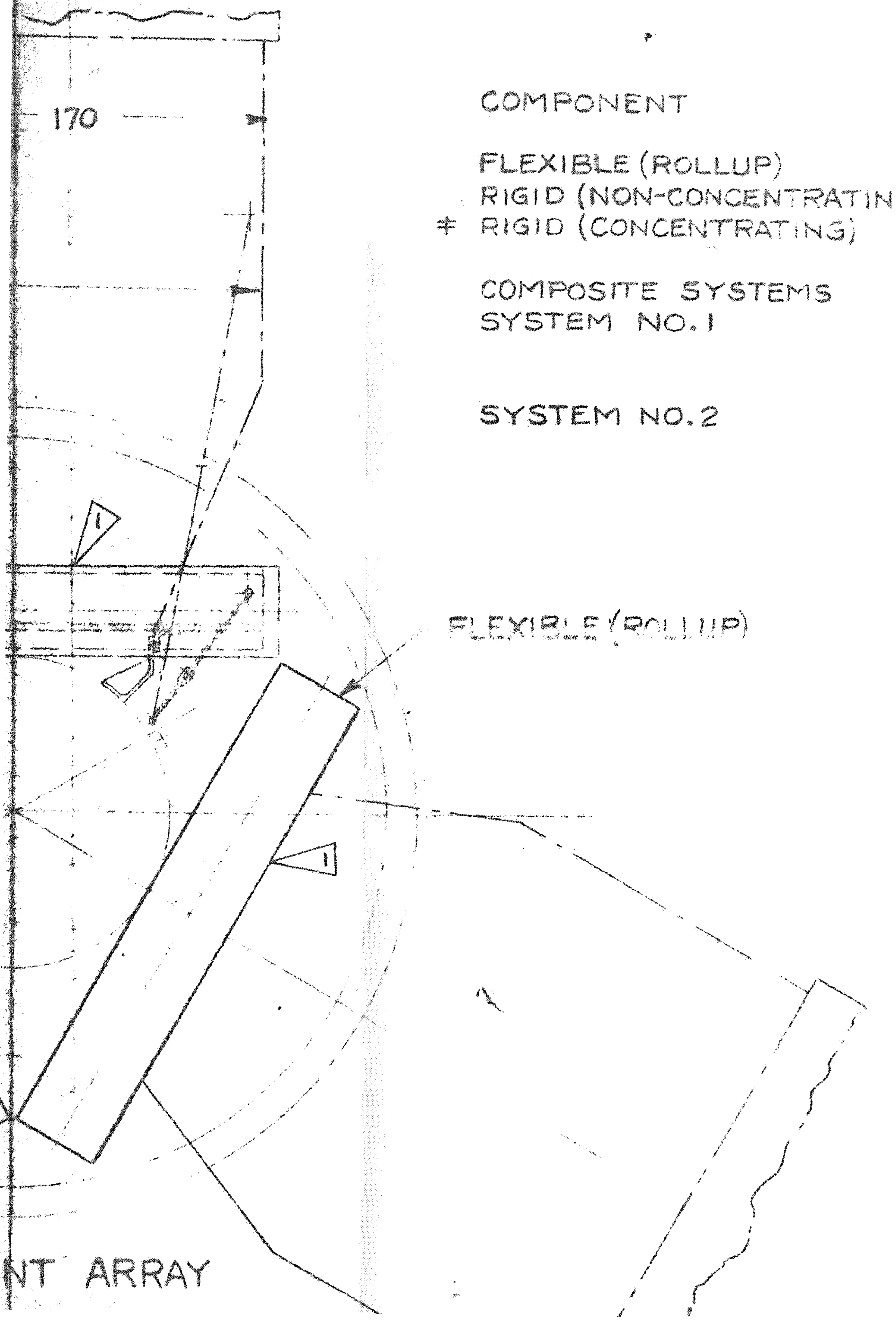

PART 2 of 2

HYBRID SYSTEM PERFORMANCE * (PRELIMINARY ESTIMATE

COMPONENT	UNIT WEIGHT LBS./SQ.FT. **	CELL TEMP. °C **	POWER WATTS/SQ.FT. **	PERFORMANC WATTS/LB.
FLEXIBLE (ROLLUP)	.40	+57/-18	10.0/5.0	25.0/12.5
RIGID (NON-CONCENTRATING)	.85	+63/-13	9.1/4.6	10.7/5.4
# RIGID (CONCENTRATING)	.48	+63/-14	8.1/4.1	16.9/8.4
COMPOSITE SYSTEMS				
SYSTEM NO. 1	.445	—	9.93/4.97	22.3/11.2
SYSTEM NO. 2	.410	—	9.80/4.90	23.9/12.0

SYSTEM NO. 1: 4950 SQ.FT. OF FLEXIBLE + 550 SQ.FT. OF NON-CONCENTRATING RIGID SUBSTRATE WITH SPARS, ACTUATORS, ETC.

SYSTEM NO. 2: 4880 SQ.FT. OF FLEXIBLE + 620 SQ.FT. OF CONCENTRATING RIGID SUBSTRATE WITH SPARS, ACTUATORS, ETC.

* RATED AT 1.0 AU & 1.67AU (1.0AU/1.67AU)

# HIGH EMITTANCE, LOW ABSORBTANCE ANODIC COATING ON BOTH FRONT AND BACK

△1 JETTISON ALL 3 ROLLERS BY PYROTECHNIC DEVICE WITH SPRING SEPARATION.

** Note These numbers represent preliminary estimates only and are not to be used for other than [illegible] configuration purposes

ROLLUP SOLAR ARRAY
S/C-3 CONFIGURATION

FIGURE C. 1-3

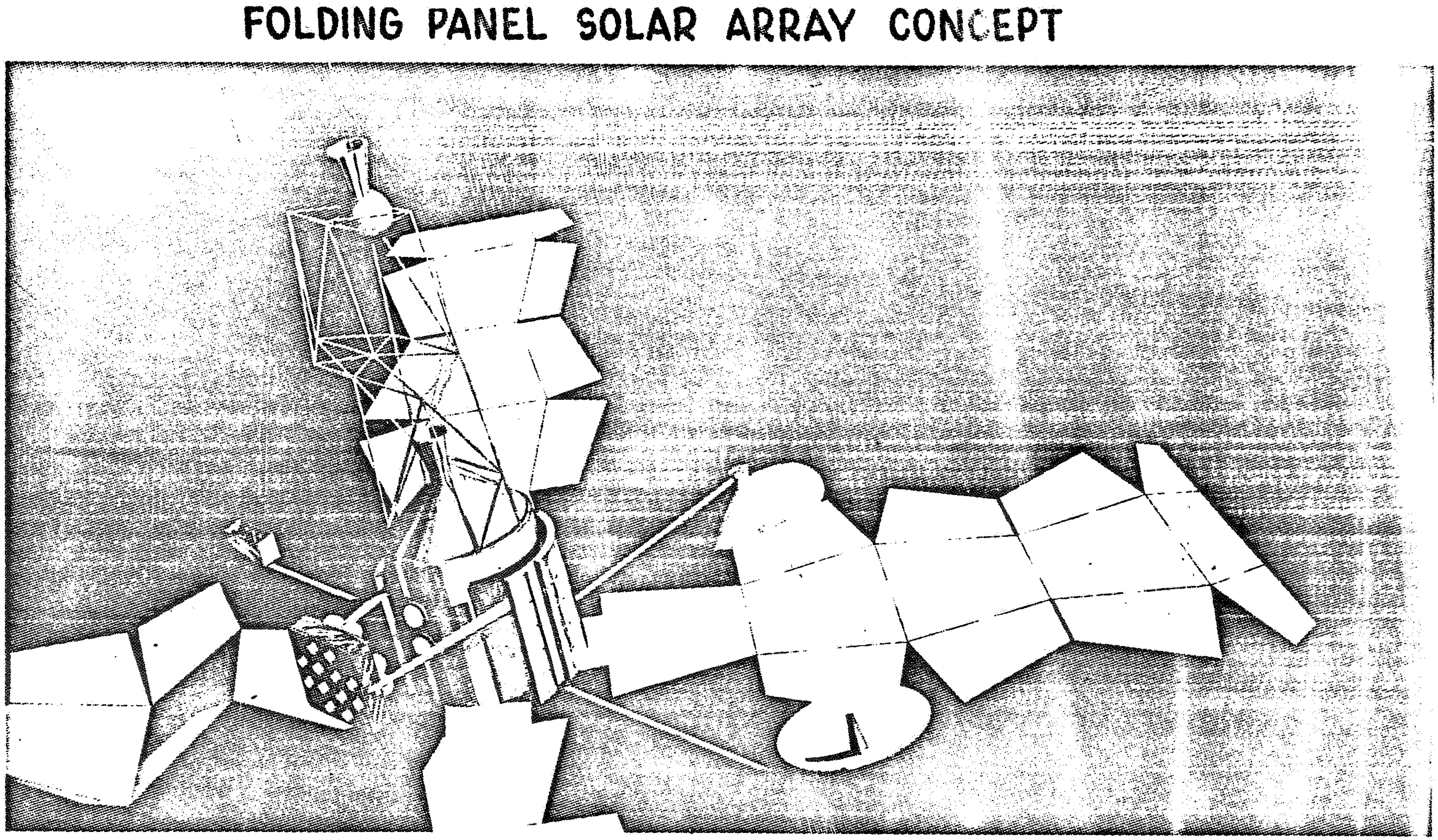
FOLDING PANEL SOLAR ARRAY CONCEPT

Figure C.1-4 FOLDING PANEL SOLAR ARRAY CONCEPT

SOLAR ELECTRIC PROPULSION SPACECRAFT CONCEPTUAL DESIGN

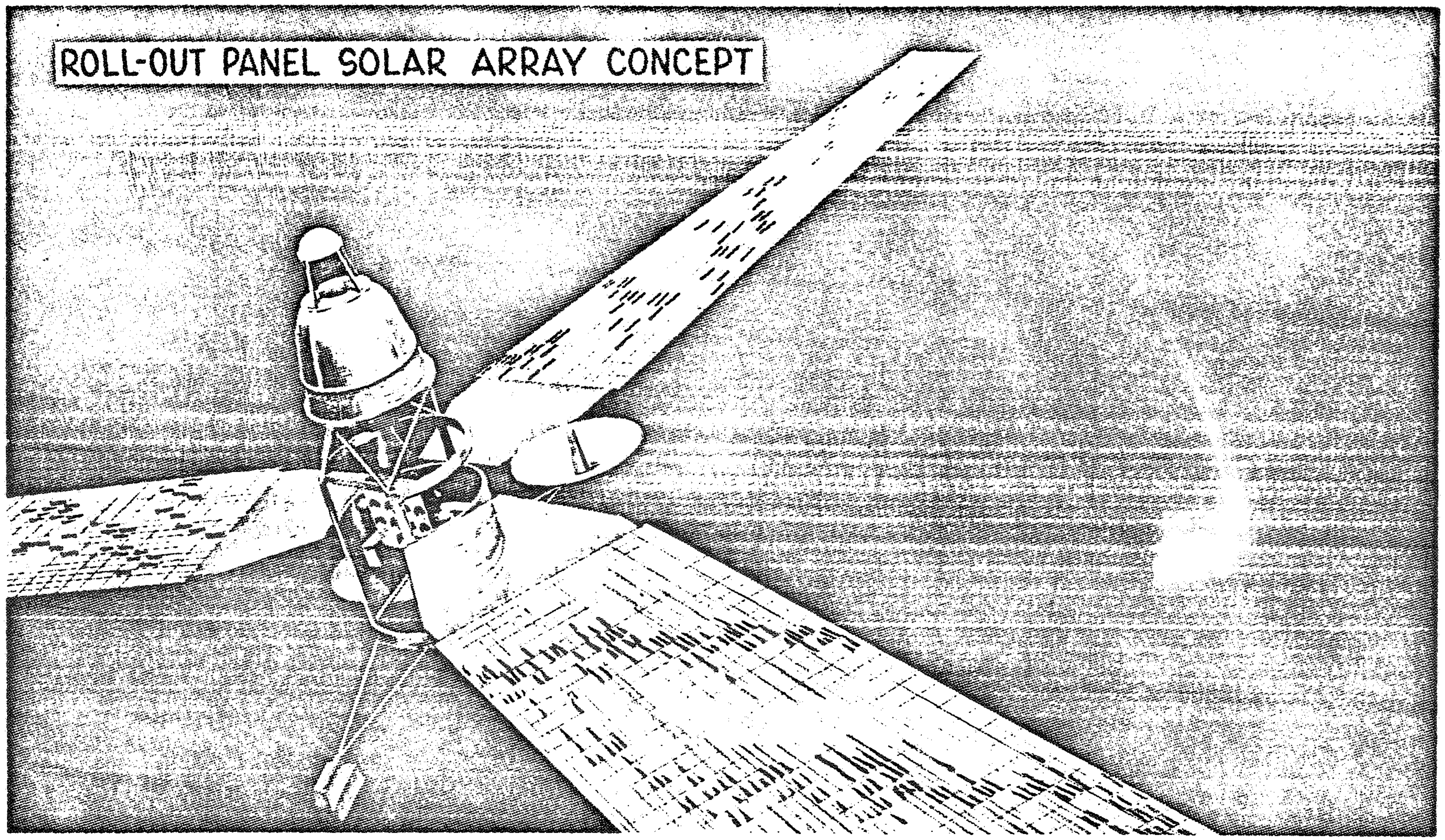
ROLL-OUT PANEL SOLAR ARRAY CONCEPT

Figure C.1-5 ROLL-OUT PANEL SOLAR ARRAY CONCEPT
SOLAR ELECTRIC PROPULSION SPACECRAFT CONCEPTUAL DESIGN

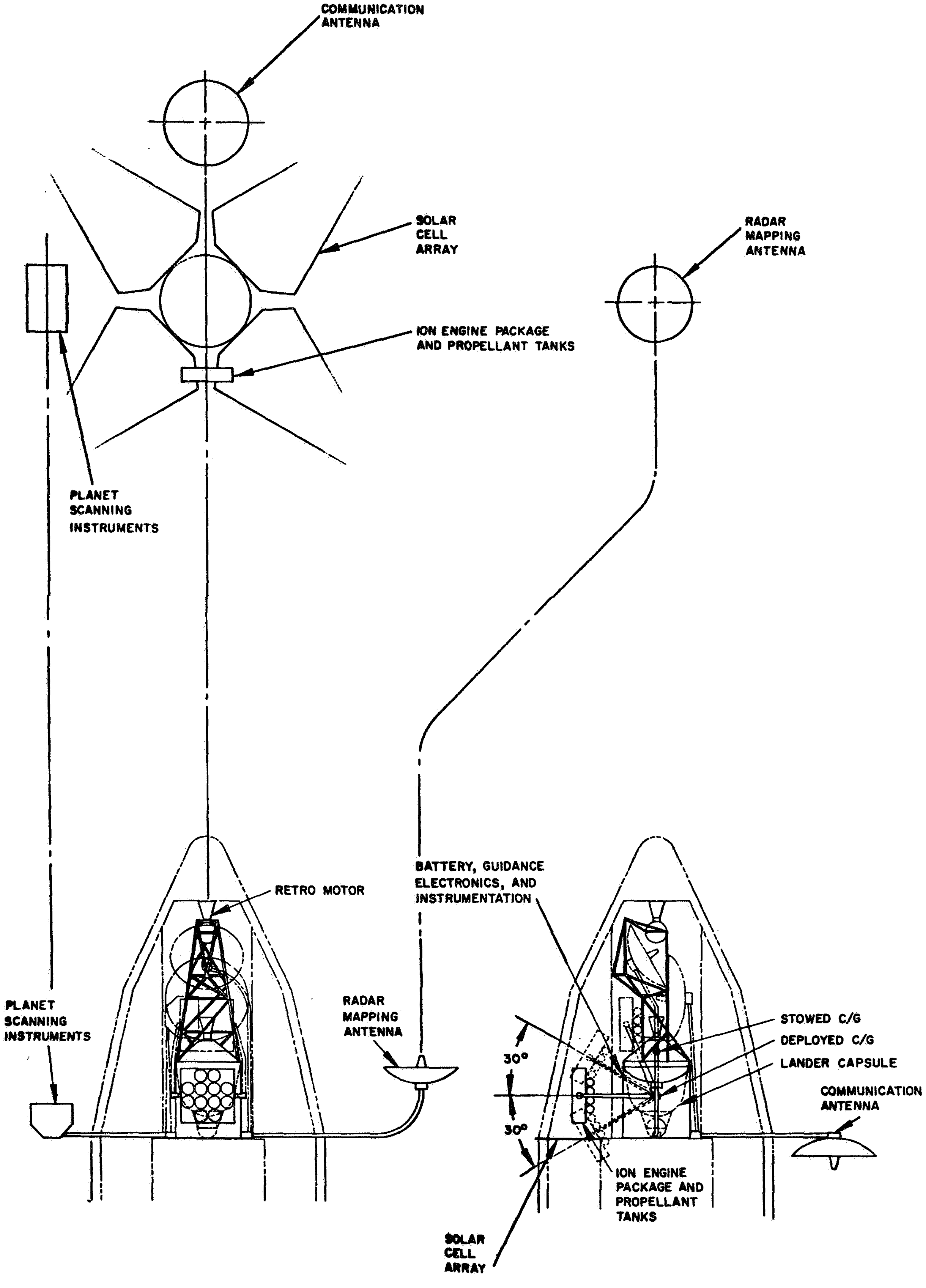
COMMUNICATION ANTENNA
SOLAR CELL ARRAY
RADAR MAPPING ANTENNA
ION ENGINE PACKAGE AND PROPELLANT TANKS
PLANET SCANNING INSTRUMENTS
RETRO MOTOR
BATTERY, GUIDANCE ELECTRONICS, AND INSTRUMENTATION
PLANET SCANNING INSTRUMENTS
RADAR MAPPING ANTENNA
STOWED C/G
DEPLOYED C/G
LANDER CAPSULE
30°
30°
COMMUNICATION ANTENNA
ION ENGINE PACKAGE AND PROPELLANT TANKS
SOLAR CELL ARRAY

Figure C.1-6

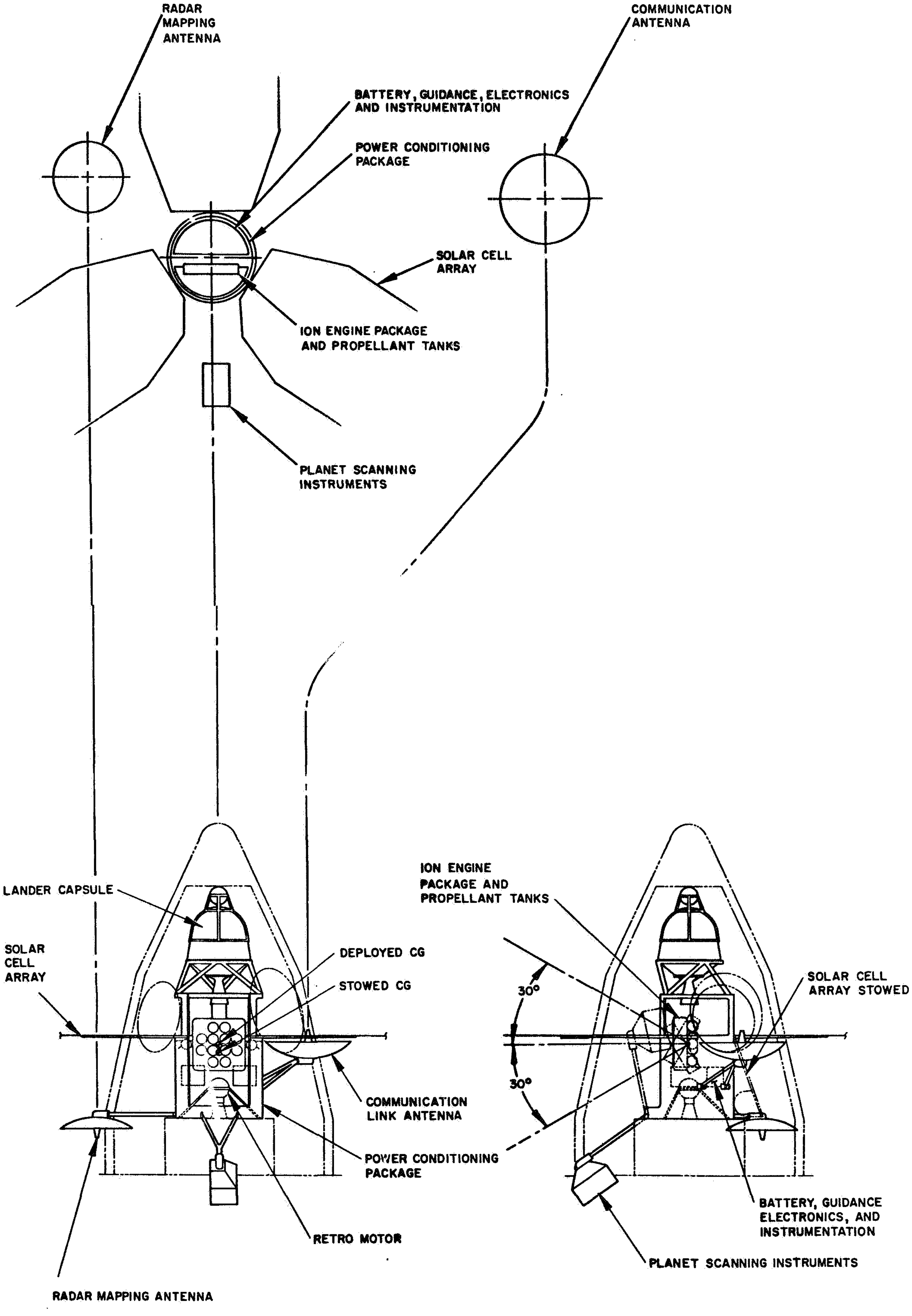
RADAR MAPPING ANTENNA
COMMUNICATION ANTENNA
BATTERY, GUIDANCE, ELECTRONICS AND INSTRUMENTATION
POWER CONDITIONING PACKAGE
SOLAR CELL ARRAY
ION ENGINE PACKAGE AND PROPELLANT TANKS
PLANET SCANNING INSTRUMENTS
LANDER CAPSULE
SOLAR CELL ARRAY
DEPLOYED CG
STOWED CG
ION ENGINE PACKAGE AND PROPELLANT TANKS
30°
30°
SOLAR CELL ARRAY STOWED
COMMUNICATION LINK ANTENNA
POWER CONDITIONING PACKAGE
RETRO MOTOR
BATTERY, GUIDANCE ELECTRONICS, AND INSTRUMENTATION
PLANET SCANNING INSTRUMENTS
RADAR MAPPING ANTENNA

Figure C.1-7

Both conceptual designs are based on the 1971 Mars orbiter mission (with a rendezvous heliocentric transfer trajectory using the electric propulsion system), accommodate a 1700 lb. lander capsule (as per EDP-139 configuration 1) and allow 50 KW of power at 1 a.u. The amount of propellant indicated is based on the use of the Mercury electron bombardment engines and allows for 350 days of continuous operation.

A significant factor in the design of the spacecraft is the provision for orientation of the net thrust vector to pass through the center of gravity of the spacecraft, to avoid the creation of any torque which would cause the spacecraft to deviate from the desired orientation or trajectory. An optimum trajectory for the design mission profile (see Section II A. 1) calls for a thrust vector orientation variation of 60 degrees (with respect to the sun-probe line) during the heliocentric transfer. The orientation of the thrust vector during transit is extremely important when one considers that the solar panels must continuously face the sun. Since, because of their size, the solar panels are body fixed after extension, it has been initially assumed that the entire thrust or array has a gimbaled support to take care of the 60° thrust vector orientation variation. In addition, it appears necessary to include a thrustor array translation capability to accommodate a spacecraft center of gravity shift due to bending of the large span solar panels caused by thermal effects during the heliocentric transfer. Both conceptual designs presented include a gimbaled and translatable thrustor array; while the one (Figure C. 1-4) also requires the thrustor array to be deployed prior to thrusting. It should be noted that the "Folding Modular" solar array (SC-1) has been modified by removal of the interior side panels and adding the equivalent area to the end of the array. This is required to assure non-interference with the ion beams during rotation of the thrustor array through the required 60° angle.

In both configurations the power conditioning modules are mounted to the inside of the 100 inch diameter cylinder, the outside of which serves as a thermal radiator to dissipate the heat generated by the power conditioning equipment. A 90° sector is cut from the cylinder to allow passage of the ion engine exhaust plume in the one case (Figure C. 1-5) and deployment of the entire thrustor array in the other (Figure C. 1-4)

TABLE C-1. Solar-Electric Propelled Spacecraft

WEIGHT BREAKDOWN

	Weight	Pounds
PAYLOAD		2219
o Orbiter	469	
o Lander	1700	
o Data Automation System	50	
TELECOMMUNICATIONS		200
GUIDANCE AND CONTROL		400
ELECTRIC PROPULSION SYSTEM		5116
o Solar Array	2500	
o Power Conditioning	500	
o Thrusters (including controls)	408	
o Propellant	1708	
RETRO-ROCKET		400
STRUCTURE		400
AUXILIARY POWER		60
		8795

Stowage arrangement for both concepts are grossly affected by the large diameter of the two dish antennas, and the "Discoverer" lander capsule. For the one concept (Figure C.1-4), an assymetrical structural truss is required. It is anticipated that accommodation of an "Apollo" shaped capsule having a larger diameter than the "Discoverer" capsule will require gross changes in packaging arrangements.

Since the present spacecraft conceptual designs are based on a "Rendezvous" type mission, the ΔV requirements for the chemical retro system are small (700 to 800 fps), and for solid propellants (assumed for these system designs) result in small diameter rockets. However, for further spacecraft designs which are to be compatible with "Fly-by" missions and possibly storable liquid propellants, the size of the retro-rocket could be a predominate packaging factor.

It should be recognized that the spacecraft designs presented are only "conceptual" in nature, and derived in a comparatively short period of time with the prime purpose of revealing the design problem areas requiring more detailed trade-off studies prior to conducting a detailed preliminary spacecraft design study. These trade-off studies are currently underway.

The following sections define the various subsystems included in the conceptual spacecraft designs presented, indicate the various ground rules established, and discuss the more pertiment trade-offs being evaluated.

2. Scientific Payload

Payload selections for deep space probing and planetary probing fall within two distinct and in may instances completely different categories. These are the selection of experiments and suitable instruments for measurement of the unknowns of interplanetary space and the unknowns of the space around and the surface of a target planet. In the latter case for this study the target planet is Mars.

To adequately design and integrate a complete Spacecraft system, a knowledge and understanding of the scientific payload must be had. There are special mounting assemblies for different experiments depending upon orientation and location requirements.

With respect to the Mars mission currently under consideration there are three subdivisions of the overall payload to consider. First are the spacecraft fixed experiments primarily aimed at interplanetary measurements and some planetary environment measurements. Second are the planet oriented experiments that require a servo driven platform to maintain a direction toward the planet. Third and not considered in detail, there are the experiments related to a lander capsule for direct measurement of the surface and atmospheric characteristics of the planet. Only the first two are reflected in this evaluation of the scientific payload.

A summary of a possible scientific payload and its growth potential for a spacecraft boosted by a Saturn C-IB is shown as Tables I and Table II. The minimum weight considered is 279 pounds and would require a power level of 79 watts (Table I). This payload can be increased to about 469 pounds and a total power requirement of about 155 watts. An exception to this is the possible inclusion of a radar mapping system that can conceivably add a weight of 50 pounds and a power requirement of 1000 watts.

Most of the increase in payload capability is placed in the increased capability of the photographic and telecommunication equipment. From a scientific point of view the increase should go into the camera system. However, the better pictures (this includes an increase in the number of picture elements and gray levels) can only be satisfactorily obtained by use of a good telecommunication system -- high data transmission rate.

TABLE I. MARS ORBITER PAYLOAD (Saturn C-1B)

EXPERIMENT	INSTRUMENT	WEIGHT (lbs)	TOTAL POWER Watts Total	TOTAL POWER (Hrs) Duration	LOCATION	DIMENSIONS or VOLUME	TEMPERATURE RANGE Operating	TEMPERATURE RANGE Non-Operating	REMARKS
o Atmospheres									
Composition	U. V. Spectrometer	22	10		Scan platform	20" x 10" x 9"	-20° to +60 C	-40° to +85° C	Electronics 6" x 10" x 6" at 6 lbs
Aurora and Day Glow, Surface Fluorescence	I. R. Spectrometer	50	15		Scan platform	12" x 12" x 20"	-20° to + 0° C	-150° to +50° C	
	U. V. Photometer	9	5		Scan platform	8" x 4" x 6"	-20° to +60° C	-40° to +80° C	
o Surface Measurements									
Cloud Cover and Surface Features	TV No. 1 High Resol.	125	15		Scan platform	12"^{D} x 30"	-20° to +70° C	-40° to +100° C	20 meter resol. (Includes color
	TV No. 2 Low Resol.	50	15		Scan platform	12"^{D} x 20"	-20° to +70° C	-40° to +100° C	500 meter resol. filters) -Monoscopic-
o Magnetic Field									
Solar and Martian	Metastable Helium Magnetometer	5.0	5		Spacecraft Structure	4"^{D} x 7"	-30° to +100° C	-50° to +100° C	Must be located on end of a boom - length determined by stray magnetic field at solar cell array.
o Interplanetary Measurement									
Solar Wind	Faraday Cup	6.0	12.0		Spacecraft Structure	6"^{D} x 4" Elec. - 2" x 4" x 6"	-20° to +80° C	-55° to +100° C	
Energetic Particles Trapped Radiation, Solar and Cosmic Rays	Geiger-Meuller Tube Array	4.0	1.0		Spacecraft Structure	6" x 8" x 2"	-30° to +50° C	-50° to +65° C	
Cosmic Dust	Micrometeorite Detector	8.0	1.0		Spacecraft Structure		-40° to +100° C	-50° to +100° C	
TOTALS		279	79						The total weights do not include weights of scan platform, boom, and DAS assembly.

TABLE I. MARS ORBITER PAYLOAD (Saturn C-1B) - Continued

SAMPLE RATE	Duration/Orbit (Min.)	Bits per Sec.	Total Bits per Orbit	REMARKS	EXPERIMENTAL COVERAGE												
					Photo-mosaic of surface (lo resol)	Hi resol photos of special areas	Stereo-scopic photos special areas (lo resol)	Atmos-pheric Compo-sition with temp. profile	IR mosaic of surface	Surface structure and compo-sition	Mag-netic field map-ping	Trapped Radiation	Density and Pressure	Surface Winds	Exo-Biological	Micromete-oritic Particles	Radiation Environment
Limb and Terminator	24	2000	2.88×10^6	7.0×10^8 bits for 150 day orbit				P					S				
Morning and Evening Ter	51	2000	6.12×10^6					P	S	S			S		P		
plus Periaspis Pass.	51	500	1.53×10^6					P					S				
1 Picture per min.	15	3×10^5	2.7×10^8	5.0×10^9 bits		P				S				S	P	S	
1 Picture per min.	15	3×10^3	2.7×10^6		P		S			P				S	P		
	Entire transfer time from Earth to Mars plus the orbit time.										P	S					P
			20 - 100	1.3×10^9 bits for 150 day orbit							S						P
											S						P
10 impacts per day		20 bits per impact		1500 impacts for 150 day orbit												P	

TABLE II. ADDITIONAL EXPERIMENTS FOR MARS ORBITER PAYLOAD

EXPERIMENT	INSTRUMENT	WEIGHT (lbs)	TOTAL POWER		LOCATION	DIMENSIONS or VOLUME	TEMPERATURE RANGE		REMARKS
			Watts Total	(Hrs) Duration			Operating	Non-Operating	
o Temperature of Surface Water Vapor	Mars Scanner	20	10		Scan platform	8" x 12" x 16"	-40° to -20°C	150° to $+70^{\circ}$C	
o Atmospheric Composition	Microwave Scanning Spectrometer	30	18		Scan platform		-30° to $+85^{\circ}$C	-50° to $+85^{\circ}$C	
o Thermal Mapping of Surface	IR Radiometer	13	7		Scan platform	8"^{D} x 11"	-30° to $+80^{\circ}$C	-50° to $+85^{\circ}$C	HAC type radiometer (5 channel)
o Particles and Fields Measurement									
Cosmic Ray	Neher Ionization Chamber	2.5	0.5			3" sphere	-30° to $+125^{\circ}$C	-50° to $+125^{\circ}$C	
	Cosmic Ray Spectrum Analyzer	2.0	2.0		Spacecraft Structure	8" x 8" x 12"	-40° to $+50^{\circ}$C	-50° to $+65^{\circ}$C	(Includes solar flare monitoring)
	Cosmic Ray Telescope	3.0	0.5			4"^{D} x 10"	-30° to $+50^{\circ}$C	-50° to $+65^{\circ}$C	
Solar Plasma	Electrostatic-Curred Plate	2.0	0.5		Spacecraft struc	2" x 9" x 6"	-20° to $+80^{\circ}$C	-55° to $+100^{\circ}$C	For use above any magnetic field.
X-Ray	Scintillation Counter	2.0	0.5		Spacecraft struc	3"^{D} x 8"	-30° to $+50^{\circ}$C	-50° to $+65^{\circ}$C	Sun oriented
o Atmospheric Composition	IR Interferometer	26	8		Scan platform	10" x 12" x 12"	-8° to -5°C	-50° to $+60^{\circ}$C	
o Stereoscopic Pictures of Land Formations	TV (low resolution second camera	50	15		Scan platform	12"^{D} x 20"	-20° to $+70^{\circ}$C	-40° to $+100^{\circ}$C	500 meter resolution
o Mars Satellite Photog.	TV Camera (low resolution)	30	10		Separate scan Platform	10"^{D} x 18"	-20° to $+70^{\circ}$C	-40° to $+100^{\circ}$C	Could also be back-up surface TV.
o Atmospheric Composition	RF Occultation Beacon	5.5	1.6		Spacecraft Structure	8" x 8" x 8" w/ 3 ft. antenna	-10° to $+55^{\circ}$C	-50° to $+80^{\circ}$C	
	RF Noise Receiver	4.5	2.0			3" x 3" x 3" with 30 ft. antenna	-10° to $+55^{\circ}$C	-50° to $+80^{\circ}$C	
	TOTALS	190.5	75.6						Total weights do not include weights of scan platform, boom, and DAS assembly.

TABLE II. ADDITIONAL EXPERIMENTS FOR MARS ORBITER PAYLOAD

SAMPLE RATE	Duration/Orbit (Min.)	Bits per Sec.	Total Bits per Orbit	REMARKS	Photo-mosaic of surface (lo resol)	Hi resol photos of special areas	Stereo-scopic photos special areas (lo resol)	Atmos-pheric compo-sition w temp. profile	IR mosaic of surface	Surface Structure and compo-sition	Mag-netic field Map-ping	Trapped Radiation	Density and Pressure	Surface Winds	Exo-Biological	Micromete-oritic Particles	Radiation Environment
	34	3500	7.8×10^6	1 min. calibration				P	P						P		
	51	9	2.75×10^4					P				S	S		S		
	90			Used into the dark side of Mars.	S				P	P							
1 per hour	4 to 48 hours	100 bits per sample	5000	Data rate would increase with sharp increase in particle flux.													P
1 per hour																	P
1 per hour																	P
																	P
1 per 0.5 hour																	P
Continuous	51	1730	5.5×10^6	1 min. calibration - 5 min. at terminators.				P					S				
1 Picture per min.	15	3×10^3	2.7×10^3		S		P			P				S	S		
1-2 per Orbit	15	3×10^3	2.7×10^6	Used only at time of satellite passing.	S												
	2	33		$2000\text{-}10^4$ bits stored				P					P				
2-3 Spectra During Active Period				5000 bits per spectrum				P		P		S					S

The only exobiological experiments that could be madefrom an orbiter are:

- spectral measurement of water vapor lines
- infrared measurements of surface properties
- differentiation between H_20 vapor and D_20 vapor
- high resolution TV or macroscopic life (plant or animal) with color indexing.
- U. V. spectroscopy H and 0 + any UV aurorae

To aid in the spacecraft integration and the communication system design the Tables I and II included size, weight, orientation and data requirements. The data obtained from the various experiments can give use to knowledge about other unknowns than that directly measured. In Tables I and II are indicated the experimental coverage and what overall results can be obtained where P stands for the primary result and closely aligned parameter and S stands for the secondary result derived for a single primary measurement or a group of primary measurements.

As a matter of interest, the scientific payload of the lander capsule is summarized and is shown as Table III. The data rate requirement of the lander capsule should be known in order to develop the on-board (orbiting spacecraft) data processing system for retransmission to Earth. If a direct link communication from the lander to Earth is the only consideration then it is not a part of the system design.

One other scientific payload considered is for a spacecraft launched by an Atlas-Centaur vehicle. In this case, no lander capsule is considered. The payload described in Table IV is a summary of the payload studies reported by JPL (EPD-250). Here again two different payloads have been considered along with the necessary specifications for design implementation and communication system design.

Probably one of the most critical items in the integration of the scientific payload is the placement of the magnetometer. For measurement of the interplanetary magnetic field the ambient stray magnetic field of the spacecraft must be no more than 1 gamma (10^{-5} gauss) at the magnetometer location. The magnetic field of the spacecraft is controlled primarily by

TABLE III. CAPSULE PAYLOAD EXPERIMENTS FOR MARS LANDER (SATURN C 1-B)

EXPERIMENT	WEIGHT	POWER	WATTS HOURS	TOTAL BITS	TEMPERATURE RANGE		REMARKS
					Operating	Non-Operating	
Exobiology	20	21	2980	1×10^8 for 2 weeks	2° to 30°C	0° to +100°C	Bulk of data obtained first day.
Areology	32	23	1100	1×10^8 for 1 month	-40° to +70°C	-30° to 100°C	Bulk of data obtained first day.
Atmospheric	17	13	2950	3.1×10^5	-20° to +70°C	-30° to +100°C	Data taken from first 1/2 hour to duration of mission.
Surface Surveillance	20	20	75	5×10^8 from 2 sensors for 360°	-20° to +40°C	-40° to 100°C	All data can be taken first day.
Soil and Atmosphere Sampling and Processing	10	10	20		-30° to +70°C	-30° to +100°C	
Sounds (Surface and Atmosphere Acoustics)	3	3	1000	5×10^7 for 2 weeks	-20° to +80°C	-30° to +100°C	Continuous data sampling.
Total		90					

TABLE IV. MARS ORBITER PAYLOAD (ATLAS - CENTAUR)

EXPERIMENT	INSTRUMENT	WEIGHT (lbs)	TOTAL POWER Watts Total	TOTAL POWER (Hrs) Duration	LOCATION	DIMENSIONS or VOLUME	TEMPERATURE RANGE Operating	TEMPERATURE RANGE Non-Operating	REMARKS
o Atmospheric Measurement									
Composition	U. V. Spectrometer	23	12		Scan frame	8" x 14" x 20"	-10° to +40°C	-30° to +60°C	
	IR Interferometer	26	8		Scan frame	10" x 12" x 12"	-8° to -5°C	-50° to +60°C	IR Interferometer could be replaced with an IR spectrometer or added to at a weight of 20 lbs and 5 watts.
Density, Thickness, Composition	RF Occultation 2 frequency beacon	5.5	1.6		Spacecraft structure	8" x 8" x 8" with 3' antenna	-10° to +55°C	-50° to +80°C	
Radio Emissions from Atmosphere and Surface	RF Noise Receiver	4.5	2.0		Spacecraft structure	3" x 3" x 3" with 30' antenna	-10° to +55°C	-50° to +80°C	
o Surface Measurement									
Temperature of Surface	Mars Scanner	13.0	9.4		Scan frame	8" x 12" x 16"	-40° to -20°C	-50° to +70°C	
Cloud Cover and Surface Features	TV No. 1 High Resol. TV No. 2 Low Resol.	23.0 16.0	10.0 10.0		Scan frame	Cyl. 12"^{D} x 16	-10° to +55°C -10° to +55°C	-30° to +80°C -30° to +80°C	
o Magnetic Field Measurements - Solar and Martian	Metastable Helium Magnetometer - 3 Component	4.5	5		Spacecraft structure	Cyl. 4"^{D} x 7"	-10° to +55°C	-50° to +80°C	Located on end of boom - length determined by stray magnetic fields.
o Interplanetary Measurements									
Solar Wind	Plasma Probe	10.0	12.0		Spacecraft structure	9" x 9" x 9"	-10° to 55°C	-50° to +80°C	To be correlated with magnetometer measurements.
Energetic Particles (cosmic rays, trapped particles)	Geiger-Meuller tube array	2.5	0.5		Spacecraft structure	6" x 4" x 12"	-10° to +55°C	-30° to +60°C	
Cosmic Dust	Micrometeorite Detector	5.0	0.5		Spacecraft structure	1 plate 10" x 12" x 1.5" 1 plate 8" x 12" x 0.15" elect. 8" x 12" x 1.5"	-10° to +55°C	-50° to +80°C	Plates mounted 90° with each other.
Totals: Payload B		133.0	71.0						
Payload A		68.0	41.0						

TABLE IV. MARS ORBITER PAYLOAD (ATLAS - CENTAUR)

SAMPLE RATE	Duration/Orbit (Min.)	Bits per Sec.	Total Bits per Orbit	REMARKS		Nominal Payload A is the Maximum Payload B minus the Following Experiments.
Limb and Terminator	24	2000	2.4×10^4		Morning terminator is reference point.	o UV Spectrometer
Morning and Evening Terminator plus Peri Apsis Pass	51	1730	5.5×10^6	1 min. calibration: 5 min. at terminators		o IR Interferometer
	2	33		During occultation 2000 - 10^4 bits stored		
2-3 Spectra During Active Period		10 (?)		5000 bits per spectrum		
	31	3500	7.8×10^6	1 min calibration		
	15	8×10^3 to 6.4×10^4	3.0×10^7			
	15	8×10^3 to 6.4×10^4	10^7			o TV No. 2 low resolution
		4				Maximum payload B = 133 lbs. Nominal payload A = 68 lbs.
					Total bits are a function of the transit time from Earth to Mars.	There is a corresponding reduction in weight of scan platform and DAS assembly.
		1			Type I 190 days transit Type II 280 days transit	Payload B 104.5 lbs. Payload A 75.2 lbs
		2				Giving a total of: B = 237.5 lbs. A = 143.2 lbs
20 Bits Per Impact		3				
Payload B			4.57×10^7			180 day mission
Payload A			3.78×10^7			90 day mission

the very large solar panels (5500 square feet); the permanent magnets associated with the TWT for the communication system, the ion engines, and the mapping radar if used as a part of the payload. All of these sources can be controlled to a degree. The permanent magnets can be shielded such that the stray fields are reduced by a factor of 10^3. The solar cells and modules can be wired such that the magnetic fields developed by each module are cancelled and the overall field is weak.

For the purpose of this study thus far, the location of the magnetometer was determined from an estimated magnetic field for the solar panel array. This was done by considering the magnetic moment of each module (a module consists of 5 solar cells each 1 x 2 cm). It is first assumed that each module can be represented by a wire loop (single turn) 5 cm by 0.1 cm.

This gives a look area of 5×10^{-5} meters^2. Using the results of Surveyor solar panel outputs, the current generated in each loop is 2.5×10^{-3} amperes. Now the magnetic moment of a current loop is

$$M = IA$$

where M is the magnetic moment, pole meters
I is the current, in the loop, amperes
A is the loop areas, meter^2

Substituting is the above values the magnetic moment of each module is 1.25×10^{-7} pole meters.

It is further assumed that only 95 percent of the modules cancel each other. Then 5 percent of the total number of modules contribute to the total magnetic moment. In an area of 5500 square feet there are 4.4×10^5 modules. Therefore, the total magnetic moment M is

$$M_T = 1.25 \times 10^{-8} (5 \times 10^{-2}) 4.4 \times 10^5 = 2.75 \times 10^{-3} \text{ pole meters of a dipole}$$

The magnetic field strength of a dipole at a distance d from the center of the pole can be expressed as

$$B = \frac{2M_T}{d^3}$$

Substituting the values from M_T and the field requirement of 10^{-5} gauss the distance d is determined as 8.2 meters or 26.8 feet. If the contribution of the permanent magnetic can be kept to 1 gamma at the same distance, the magnetometer would have to belocated at 10 meters (32.8 feet) to meet the 1 gamma requirement.

If is possible that the stray field requirement may be as low as 0.1 gamma (10^{-6} gauss). The distance would then increase to 21.5 meters.

Further analysis is required before definitization of magnetometer location.

3. Retro Propulsion

Although our current retro-rocket trade-off studies include an evaluation of both solid and space-storable liquid propellant systems, the previous performance comparisons and spacecraft designs are predicated on the use of solid propellant motors with a specific impulse of 315 seconds and a mass fraction of 0.90, which appear reasonable for the 1967 state-of-the-art.

Considerations of the "variable propellant loading" concept - which assumes that a quantity of propellant may be replaced by usable payload mass if the actual launch date injection energy requirement is less than the 30 day launch window requirement - would indicate that liquid retro-propulsion has the advantage in permitting this payload flexibility. It means that propellant must be extracted from or added to the vehicle on the launch pad. If solid propulsion were employed, the substitution would be discrete rather than continuous, and several different sizes of solid motors would have to be available for each launch. Although this factor is not too significant for the "Rendezvous" mission for the first month's effort, consideration of other possible missions, such as those including a "Fly-by" heliocentric transfer trajectory, could make it a significant factor. This factor in addition to specific impulse, mass fractions, volume requirements, thermal control, and reliability, will be evaluated in the current retro-rocket trade-off studies.

4. Thermal Control

One of the major thermal control problems in the design of the vehicle is getting rid of the 5 kilowatts of power that is dissipated in the electrical power conditioning equipment. To keep the temperature of this equipment at 80°F (26.7°C) requires a thermal radiator area of approximately 125 square feet when the vehicle is one astronomical unit from the sun. As the vehicle approaches Mars, the temperature of this equipment will approach -23°F (-30.6°C). This reduction in temperature is due to the reduction in electrical input power to the equipment because the solar intensity is less. This temperature estimate would be lower if solar cell degradation is also accounted for.

By raising the temperature of the thermal radiator to the upper temperature limit of the electrical power conditioning equipment, 158°F (70°C), the area of the thermal radiator can be reduced to approximately 72 square feet. With this smaller thermal radiator the temperature of this equipment near Mars will be approximately 48°F (8.8°C).

For the conceptual spacecraft designs discussed previously in this report, 125 square feet of thermal radiator area was used; although, as indicated above, a substantial reduction may be feasible for later spacecraft designs.

5. Spacecraft Attitude Control

The preliminary selection of a cold gas reaction system for attitude control of a solar electric propulsion vehicle is discussed here. Three axis attitude control must be provided for a period of one year during Earth-Mars transit in the presence of various low level disturbance torques. Two vehicle configurations were assumed for the preliminary sizing estimates. A 5000 square foot solar cell array required a 249 pound attitude control system utilizing cold gas, while a 1000 square foot array required a 221 pound cold gas system. Control moment arms were assumed to 20 feet and 10 feet for the large and small arrays respectively. Cold gas was selected over other mechanizations due to favorable reliability characteristics, and flight proven hardware characteristics. Other systems, including solar vanes, water electrolysis, hot gas, and ion engines, were also considered here as possible alternatives.

Discussion

Attitude control of the solar electric vehicle consists of two basic requirements:

a. manuvers for initial acquisition and subsequent reorientations.

b. maintenance of a sun-referenced attitude in the presence of disturbance torques over the one year transit time.

The attitude behavior can be characterized by a limit cycle with long coasting periods and short control pulses. Ideally the ratio of "on" time to "off" time, i.e., duty cycle should be minimized for minimum fuel consumption and minimum fuel weight. Reduction of control fuel usage is limited by the angular momentum introduced by disturbance torques which must be cancelled by opposing control torque momentum.

Disturbance torques acting on the vehicle fall into two major categories:

a. main thrust vector misalignment from the vehicle center of gravity,

b. low level torques due to external sources such as solar radiation, solar wind, micrometeorites, etc.

Thrust vector misalignment is difficult to predict until more is known about the main ion engine configuration. Hence, study of its control problems will be deferred until later. The external torques can be evaluated with the aid of a few simplifications. Preliminary sizing is accomplished here by evaluating and considering only the external torques.

Inert Cold Gas

A reaction jet system using an inert gas for mass expulsion has been proven to work reliably and effectively in space. This current state-of-the-art device is simple to mechanize and gives favorable confidence levels in its ability to operate over a one year period. Handling and storing of the fuel is also relatively simple. The specific impulse is low and the tankage penalty high due to the high storage pressure used; hence a heavy system results. In addition, very small thrust levels are not available.

Hot Gas

With hot gas systems a better specific impulse can be realized and hence a lower net weight penalty achieved. Reliability could be quentionable for a one year period. Also very low thrust levels and small pulse widths may degrade the realizable specific impulse.

Solar Vanes

For small disturbance torques control forces can be derived from rotatable solar vanes. Very lightweight, large area vanes require extensive mechanical design in view of the unfolding requirements of the solar array itself. Large disturbances require large vanes. The system would, however, be reliable (few moving parts) and there would be no fuel expenditure.

Ion Engines

Ion engines are available on the vehicle. Combining the attitude control function with translational control cannot be fully evaluated until the ion engine configuration is defined. In general, ion engines require a large amount of non-fuel weight for power (solar panels, batteries, etc.) The power drain during thrusting is very large per unit of force. However, fuel weight per unit force is low which suggests advantages for long mission times.

Water Electrolysis

Water electrolysis rockets combine some advantages of hot and cold gas systems. Fuel tankage is lightweight due to the liquid nature of the fuel. Water is easily handled and stored. High specific impulse is obtained for hot gas type operation. Low thrust levels require cold gas type operation (non-firing) with a compromised specified impulse. This type system will be tested by 1967.

Since this mission has a transit time of almost a year, reliability and proven performance must be heavily weighed in tradeoff studies. The cold gas reaction system stands out in this respect. A cold gas system is sized herein and its limit cycle behavior under disturbance torques evaluated.

Vehicle Models

For control system preliminary sizing two vehicle configurations are utilized. Vehicle 'A' contains a 50 kilowatt array while vehicle 'B' is a 10 kilowatt configuration. Table 1 shows the parameters pertinent to control system design.

Table 1. Vehicle Configuration Numbers

Vehicle	A	B
Array Power (kw)	50	10
Moment of Inertia (slug-ft^2)		
Pitch-Yaw	30,000	2,500
Roll	60,000	5,000
Area (ft^2)	5,000	1,000

Disturbance Levels

Torques applied to the spacecraft fall into two major categories:

1. External torques
2. Thrust misalignment torque.

The thrust misalignment will be studied as a separate problem when the ion engine configuration and spacecraft are preliminary designed. External torques are caused by:

1. Electromagnetic radiation pressure
2. Solar wind pressure
3. Micrometeorites
4. Solar flares.

1), 2) and 3) are relatively constant while 4) varies from day to day.* For a 5000 ft^2 array the total torque due to electromagnetic radiation is 3.74×10^{-4} ft-lbs. at the earth. The following assumptions lead to this number:

1) the solar radiation pressure at one A. U. is $p = 9.37 \times 10^{-8}$ lb/ft^2
2) the reflectivity is zero (pure absorber)
3) the total moment arm in one axis is 2 percent of the diameter of a circle of equivalent area.

At Mars the solar pressure is reduced by a factor of 2.25. If the average disturbance is assumed to be the average of the end points then this yields about 2.3×10^{-4} ft-lbs. From Reference (2) the solar wind and average solar flare torque appear to be about the same magnitude as the solar pressure torque. Assuming these add and that an additional margin is required to handle miscellaneous smaller torques (micrometeorites, etc.), a worst case constant disturbance value of 10^{-3} ft-lbs is assumed. This value is used for design purposes for vehicle 'A'. Vehicle 'B' torque is reduced by the ratio of areas (5:1) for a design value of $.2 \times 10^{-5}$ ft-lbs.

6. Preliminary Sizing

Solar Vanes

The area of solar vanes required to cancel the maximum disturbance is now computed. The following assumptions are made based on the edgewise view shown in Figure 1.

1) $20^\circ \pm 20^\circ$ is the nominal travel of the vanes.

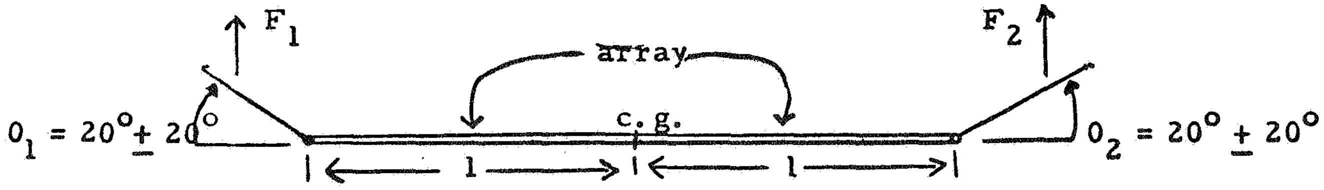

Figure C. 5-1 Solar Vanes in One Channel

---

*The disturbances are discussed in detail in Reference 2.

2) Area of one vane = A_v
3) The vanes have negligible mass
4) Vane reflectance, η equals 1.
5) The control law used required $(\theta_1 - 20^\circ) = -(\theta_2 - 20^\circ)$
6) p_o - solar pressure at 1 a.u. = 9.37×10^{-8} ft-lb/ft^2

The maximum moment is given by equation (1) for $\theta_1 = -\theta_2 = 20^\circ$.

$$M = \ell\ (F_1 - F_2) = \ell\ (1 + \eta)\ p_o\ A_v\ (\cos 0^\circ - \cos 40^\circ) \tag{1}$$

Setting M equal to the maximum disturbance (10^{-3} ft-lbs) and solving equation (1) for A_v yields 142.7 ft^2. This means four panels of approximately 8' x 18' and a separate pitch control system are required for vehicle control. The possibility exists that pitch control could be obtained by adding an additional degree of freedom to the solar vane motion but adds complexity to the system.

Limit Cycle Operation

The system mechanizations previously discussed are all of the 'bang-bang' variety except the solar vanes. Bang-bang operation in steady-state can be characterized by a limit cycle as discussed in Appendix A. Whether a limit cycle is 'hard' or 'soft' depends on the level of the applied disturbance torque. For a fixed set of system parameters the control fuel (proportional to the duty cycle) can be plotted versus disturbance torque as shown in Figure C.5-2. That portion of the curve representing the soft limit cycle is independent of the system parameters (h, τ_1, τ_2, T_c, as defined in Appendix A). In this mode the control torque is operating only to periodically cancel the momentum introduced by the disturbance torque.

The system parameters can be adjusted to control the hard/soft limit cycle break point and its associated duty cycle. The graph illustrates that a reduction of 4 times occurs in duty cycle at the transition point. Parameters should be adjusted such that for a maximum average disturbance soft rather than hard limit cycle operation is achieved. Furthermore, for a fixed disturbance, the minimum fuel usage is obtained in the soft duty cycle, d_{as},

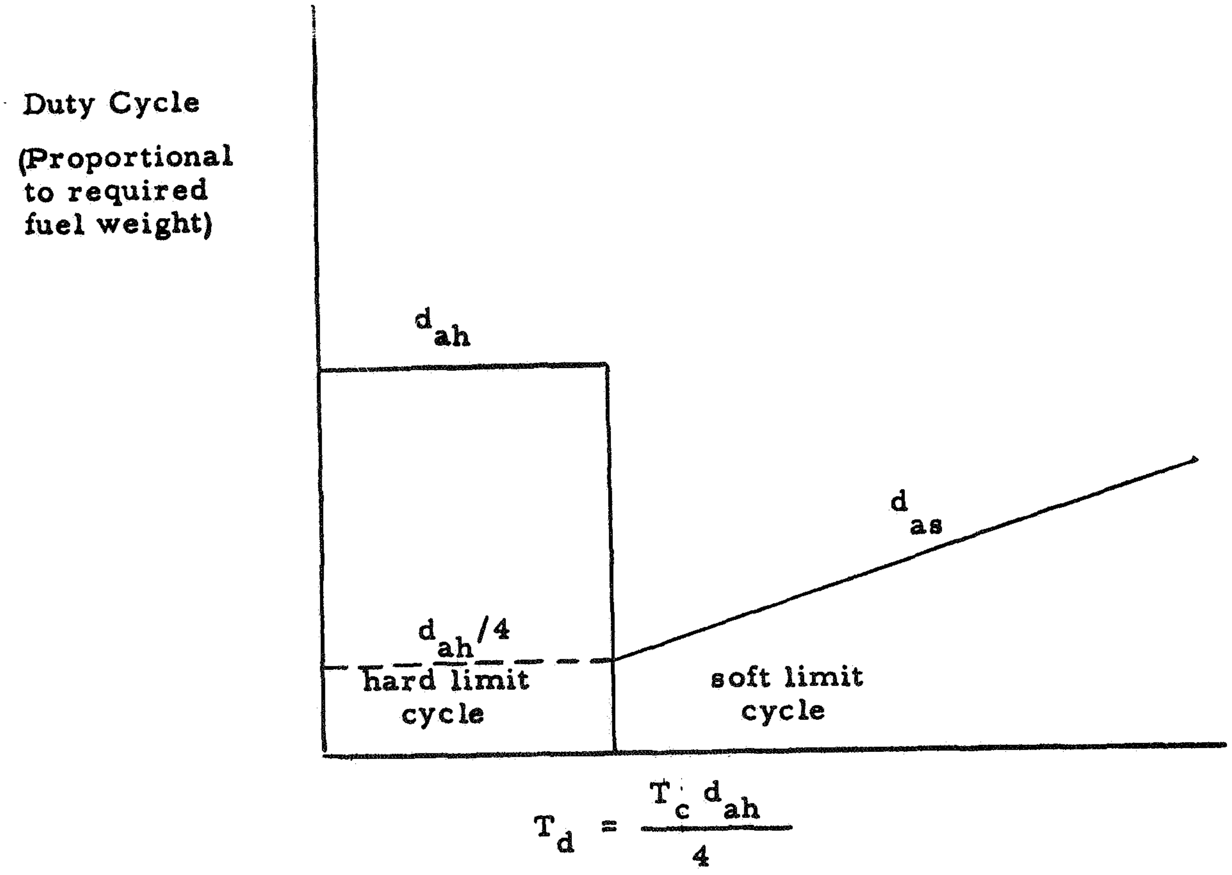

T_d = Disturbance Torque

Figure C.5-2 Disturbance Torque Versus Duty Cycle

since a control system must cancel angular momentum introduced by a disturbance. A hard limit cycle would use a minimum of four times as much fuel for a given disturbance torque. The system must also be designed such that the hard duty cycle (d_{ah}) for zero disturbance is less than or equal to the soft duty cycle (d_{as}) for maximum disturbance. This guarantees that if the disturbance is less than the maximum design level, fuel usage will be equal to or less than that for the maximum. The problem with this design approach is that if d_{ah} is reduced by adjustment of design values, an impractical system may result. That is, capacitor sizes, lead-lag ratios, etc. may be so large that a compromise value of hard duty cycle is the only alternative.

Cold Gas System

The amount of cold gas required for a soft duty cycle can be computed by equation (A-8). An I_{sp} of 50 lb-sec/lb is considered a realistic value for nitrogen. A tankage and plumbing penalty of 150 percent is added for the high pressure system required to handle the fuel. Ten (10) millipounds is considered a lower limit on the thurst level for cold gas valving. Table 2 lists the weights and design values. Design criteria used equated the hard duty cycle under zero disturbance with the soft duty cycle under maximum disturbance.

Table 2. Cold Gas System

	Vehicle	
Design Parameters	**A**	**B**
h, percent	.02	.02
τ_1, sec.	7.25	3.18
τ_2, sec.	.6	.265
F_c, lbs.	.025	.010
θ_d, degree (deadband)	±1.0	±1.0
Weights		
Fuel	95	84
Tankage and Plumbing	142	125
Electronics and Sensors	12	12
Total	249	221

Water Rocket System

Sizing the water electrolysis jet is the same type of procedure used for cold gas. However the lowest limit of force, F_c, which can be used while obtaining an I_{sp} of 350 lb-sec/lb is 0.1 pounds. This thrust leads to unfavorable design values (h, τ_1, τ_2). Hence a compromised hard duty cycle using more fuel is necessary if the system is to operate as a hot gas valve system. Another alternative is to lower the specific impulse by operating in a cold gas (non-igniting) mode. Lower thrust levels are obtainable at an I_{sp} of 150. The system parameters can be chosen to match the nitrogen system of Table 2. Table 3 shows the water rocket system weights.

Table 3. Water Rocket Sizing

	Pounds
Thrust Jets (6 each)	3
Reservoir and Plumbing	15
Electrolysis	
Cell	1
Power Supply (6w)	2
Electronics	6
Pressure Transducer	1
Accumulator	4
Fuel (Water)	40
Miscellaneous	2
Total	74 Pounds

Ion Engines

The ion engine has somewhat different characteristics than a gas thrustor. Long delay times (τ_{d_1} τ_{d_2}) cause different terms to be significant in the expressions of Appendix A. However, duty cycle is of lesser importance because of the high fixed system weight compared to the low fuel weight (high I_{sp}). Sizing of an ion engine is dependent upon a more detailed analysis than is warranted here. However values can be extrapolated from careful evaluation of Reference (3). There is some question as to the reliability of the thrustors and power conditioning unit when operated for the large number of cycles required during transit. Hence three sizing figures are given based on redundancy to achieve reliability. Table 4 illustrates the weight required to mechanize the above described systems.

Table 4. Ion Engine Sizing - Vehicle 'A'

		Lbs.
1)	Single Thrustor	
	Thrustors (8.9 lbs) x 6	53.4
	Electronics	6
	Fuel (4.2 lbs/axis) x 3	12.6
	Tankage (7.8 lbs/axis) x 3	23.4
	Power Conditioning Unit (pcu)	22
	Array Weight (average power + 50 percent)	15
		132.4 lbs
2)	2 Thrustors/station	
	Set of Additional Thrustors	53.4
	50 Percent Weight Redundancy in pcu	11
	Single Thrustor Weight	132.4
	Total	196.8 lbs
3)	3 Thrustors/station	
	2 sets of added thrustors	106.8
	100 Percent Weight Redundancy in pcu	22
	Single Thrustor Weight	132.4
	Total	261.2 lbs

7. Conclusion and Possible Future Work

In view of the life requirement of one year a reliable, proven system is chosen for the preliminary design cycle. Cold gas is reliable although heavy. It is chosen on the basis of confidence that the control task will be accomplished using off-the-shelf hardware. Of the other systems studied the water electrolysis rocket looks most promising due to its lightweight and apparently favorable operating characteristics. Although presently unproven in a space (zero-g) evnironment, by 1967 the water rocket will have been operating in space over an extended period.

At the present time the ion engine also looks promising, particularly from the weight veiw point. This method of control will compare even more favorably for longer mission times such as a 500 day transfer time to Mars, a trip to Jupiter or if planetary spiralling approach or departure is imployed.

Furture investigations are disclosed below:

a. the most outstanding problem requiring detailed investigation is the thrust vector misalignment on the engine cluster. This is potentially a difficult control task which will be studied as soon as more definitive information on the ion engine configuration is available.

b. It has been tentatively established that the engine must be either gimbaled or translated in two dimensions. The next step in the control study is to compare designs based on flexure pivots with those based on translation.

c. It is necessary to rotate the thrust vector through a large angle with respect to the vehicle - sun line, an additional control problem will arise.

d. Cross-coupling effects due to gimbaling of the engine cluster must be considered in connection with pitch control.

Appendix A

Description of Typical Reaction Jet Control System

A typical reaction jet control system for spacecraft attitude control can be represented as shown by the block diagram of Figure C.5-3. While this system is not all inclusive it is representative of most attitude control channels for space applications. Behavior of the system in steady state is characterized by a limit cycle almost entirely within the built-in deadband, θ_d. For small or zero disturbance torques a 'hard' limit cycle occurs as shown in Figure C.5-4. If the disturbance is large enough the system will operate in a 'soft' limit cycle mode as shown by Figure C.5-5.

Figure C.5-3 Block Diagram of Reaction Jet Controller

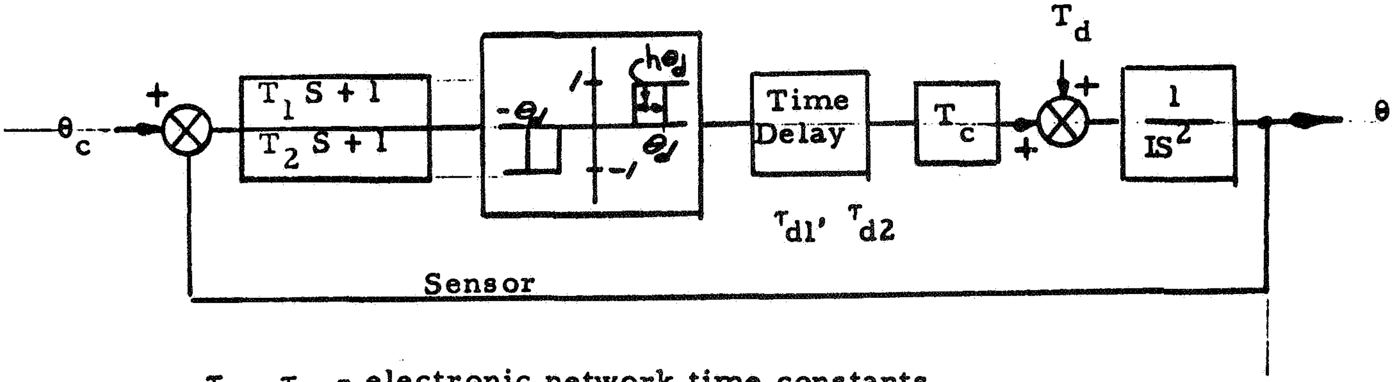
θ_c
+
$\frac{T_1 S + 1}{T_2 S + 1}$
$-\theta_d$
$h\theta_d$
1
-1
θ_d
Time Delay
T_c
T_d
+
+
$\frac{1}{IS^2}$
θ
τ_{d1}, τ_{d2}
Sensor

τ_1, τ_2 - electronic network time constants

h - percent hysteresis

θ_d - deadband

τ_{d1}, τ_{d2} - 'on' time, 'off' time, respectively

T_c - control torque

T_d - disturbance torque

I - moment of inertia

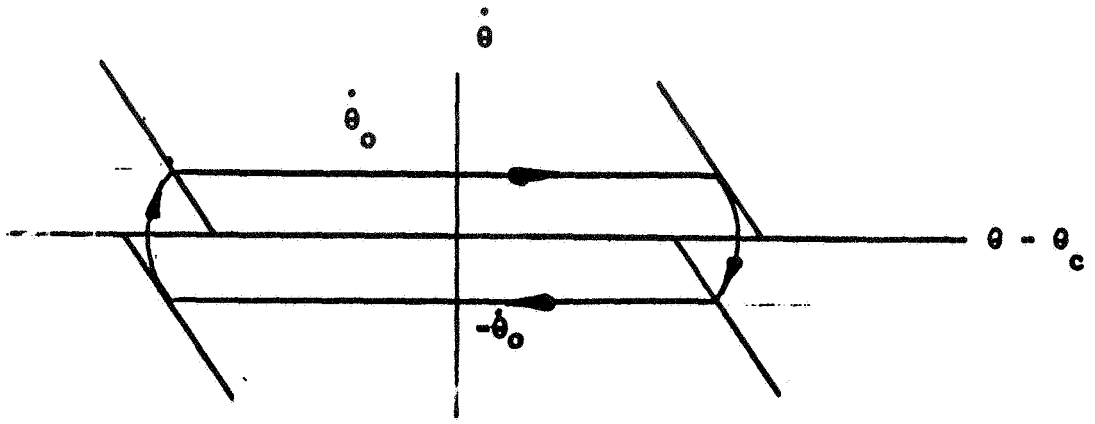
$\dot{\theta}$
$\dot{\theta}_o$
$\theta - \theta_c$
$-\dot{\theta}_o$

Figure C.5-4 Hard Limit Cycle

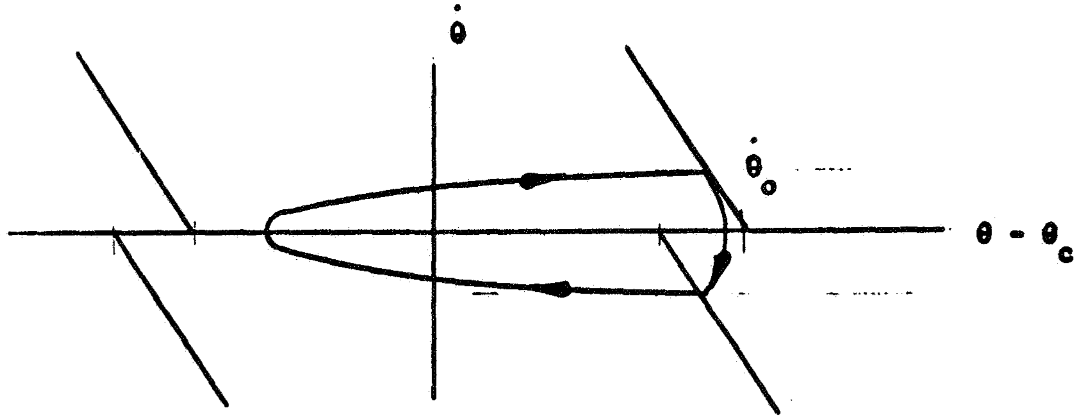
$\dot{\theta}$
$\dot{\theta}_o$
$\theta - \theta_c$

Figure C. 5-5 Soft Limit Cycle

Figure C.5-4 and C. 5-5 - Phase plan diagram of typical 'hard' and 'soft' limit cycles, maximum rate, fuel use, etc. during the limit cycle operation. These are taken from reference (1) and rewritten here.

The quantity $\dot{\theta}_o$ is given by the equation below for a hard or soft limit cycle.

$$\dot{\theta}_o = \frac{h + \lambda_c \tau_{d2} - \lambda^* \tau_{d2}^2/2 + \lambda^* \tau_2 (1 - e^{-t_{01}/\tau_2})}{2\tau - (\tau_{d1} + \tau_{d2})} \qquad (A.2)$$

terms not previously defined are:

$\lambda_c = \frac{T_c}{I}$, command acceleration

$$\lambda^* = \frac{T_c - T_d}{I}, \quad \text{combined acceleration}$$

$$\tau = \left(\tau_1 - \tau_2\right), \text{seconds}$$

$$t_{01} = \text{'on' time}$$

Equation (A-1) can be used to evaluate the 'on'time, t_{01} as given by equation (A-2).

$$t_{01} = \frac{2\dot{\theta}_o}{\lambda^*} \qquad \text{(A-2)}$$

The quantity, t_{01}, also appears in equation (A-1). Hence the two equations must be solved iteratively to obtain an accurate answer. $\dot{\theta}_o$ can also be used to compute the hard duty cycle, d_{ah}, as given by equation (A-3).

$$d_{ah} = \frac{\dot{\theta}_o^2}{\dot{\theta}_o^2 + \theta_d \lambda_c} \qquad \text{(A-3)}$$

If the duty cycle is soft, the simple expression of equation (A-4) can be used.

$$d_{as} = T_d/T_c \qquad \text{(A-4)}$$

The duty cycle is important because of its effect on the amount of control fuel used. The weight of control fuel expended in a time, Δt, is given by equation (A-5).

$$W = \frac{\Delta t \, F_c d}{I_{sp}} \qquad \text{(A-5)}$$

where:

Δt = elapsed time, seconds

F_c = control force, pounds

I_{sp} = fuel specific impulse, lb-sec/lb

d = duty cycle $\frac{\text{'on' time}}{\text{'off' time}}$

The transition point between a hard and soft limit cycle occurs when the coasting portion of the cycle (See Figure C. 5-2) just fails to reach the opposite side before turning back. The disturbance at which this transition point occurs is given by equation (A-6).

$$T_d = \frac{I \dot{\theta}_o^2}{4\theta_d} = \frac{T_c d_{ah}}{4} \text{(for } \dot{0}^2 \ll 0_d \lambda_c\text{)} \qquad \text{(A-6)}$$

Combining equations (A-4) and (A-6) shows that at the hard/soft transition the soft duty cycle is 4 times smaller as given by equation (A-7).

$$d_{as} = d_{ah}/4 \qquad \text{(A-7)}$$

Assuming that a soft duty cycle exists, equation (A-4) can be substituted into Equation (A-5) to compute the fuel expenditure as given by equation (A-8).

$$W = \frac{\Delta t \, T_d}{I_{sp} \, \ell}$$

ℓ = control moment arm, ft.

The interesting conclusion which may be drawn from Equation (A-8) is that the control fuel weight depends only on the elapsed time, Δt, the disturbance torque, the moment arm (torque per unit force), and the fuel figure of merit, I_{sp}.

REFERENCES

1. McElvain, R. J. "A Comparison of Control and Stationkeeping Weights for a 24 hour Synchronous Satellite Mission", HAC IDC 2242/2231, dated 27 Mary 1963.

2. Ange, E. E. "Estimated External Torques on Solar Cell Arrays for Solar Electric Spacecraft on a Mars Mission", HAC IDC 2230.10/110, dated 5 March 1965.

3. McElvain, R. J. "Summary of Ion Engine System Performance Trade-off Analyses", HAC IDC 2242/1562 dated 21 November 1962.

6. Telecommunication System

Summary of Design Mission as a Telecom Task

Mars Rendezvous and then Orbit around Mars	
Range of Launch Dates	March - April 1971
Range of Encounter Dates	January - March 1972
Transit Time	350 days, Solar Electric powered
Probe in Orbit around Mars:	
Altitude above planet surface at peri-apsis	4,000 Km
Apo-apsis	50,000 Km
Period of observation of probe	180 days
Orbit Life	~50 years
DSIF to be available	
Max. available power when in orbit around Mars	1100 Watts
Communication distance	See Figure C-6.1

Antenna

An 8-ft. diameter antenna appears to offer the most favorable tradeoff between desired gain and expected off-axis losses. Antenna performance may be summarized as follows (compare Figure C,6.-2):

Diameter	8-ft. dish
Gain	32.7 db
3-db Beamwidth	3.8°
Off-axis loss at ± 1.4°	1.6 db

Note that for an antenna diameter larger than 8 feet, the narrower beamwidth would required that

$$\text{Pointing Tolerance} < \Sigma\,(\text{Vehicle attitude Error} + \text{Structural Tolerance} + \text{Boresight Error}) = \pm 1.4^{\circ}.$$

Such "fine-control" pointing would place additional dynamic load and stability demands onto the vehicle's attitude control system (unless a planar phased array were used for inertia-less pointing). Furthermore, the high directivity of the antenna would somehow have to be "spoiled" during acquisition, and then re-established after lock is obtained. Finally, increasing the antenna size will rapidly complicate the problem of obtaining sufficient structural rigidity during launch.

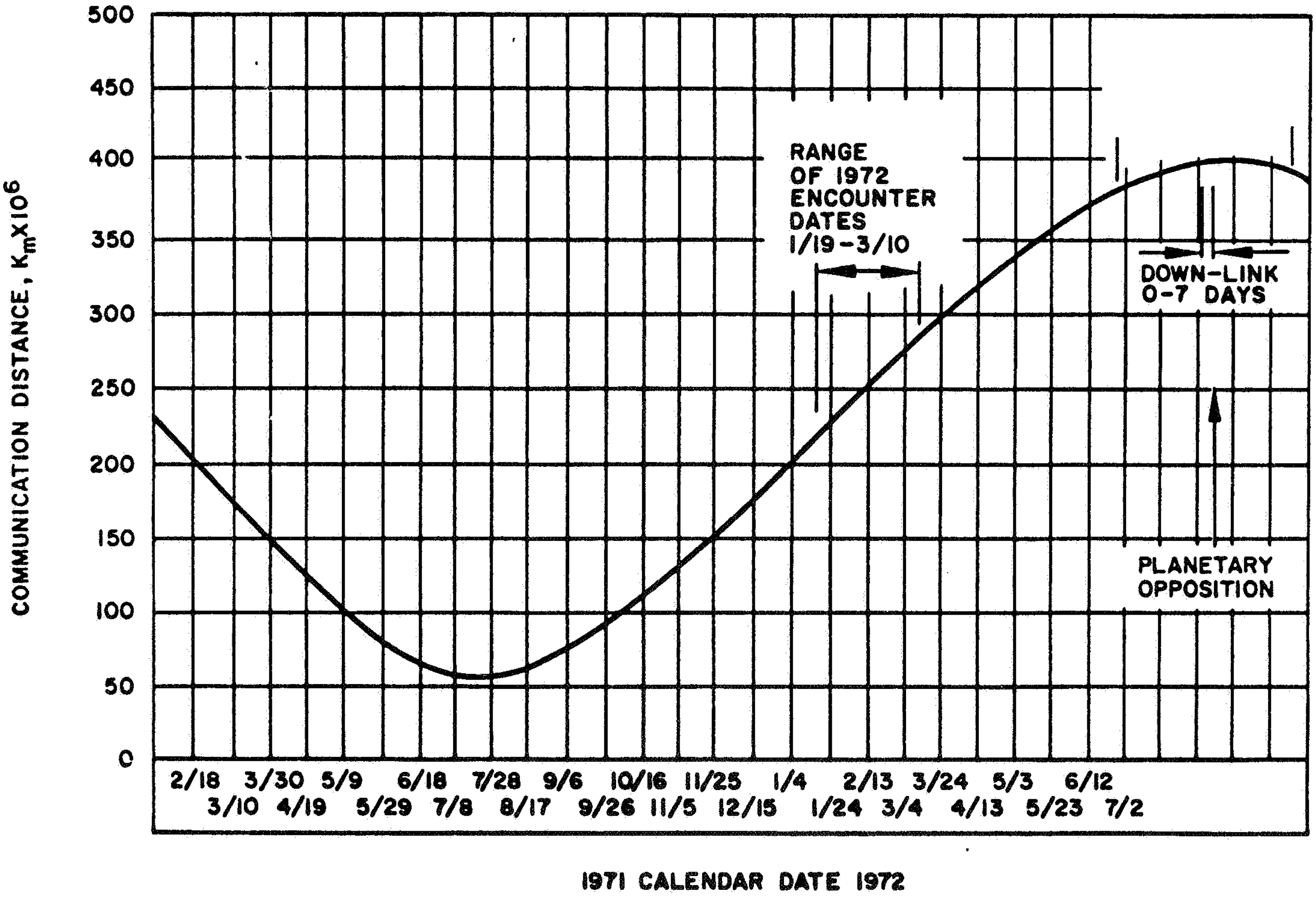

Figure C.6-1

EARTH – MARS COMMUNICATION DISTANCE VERSUS TIME (1971 – 1972)

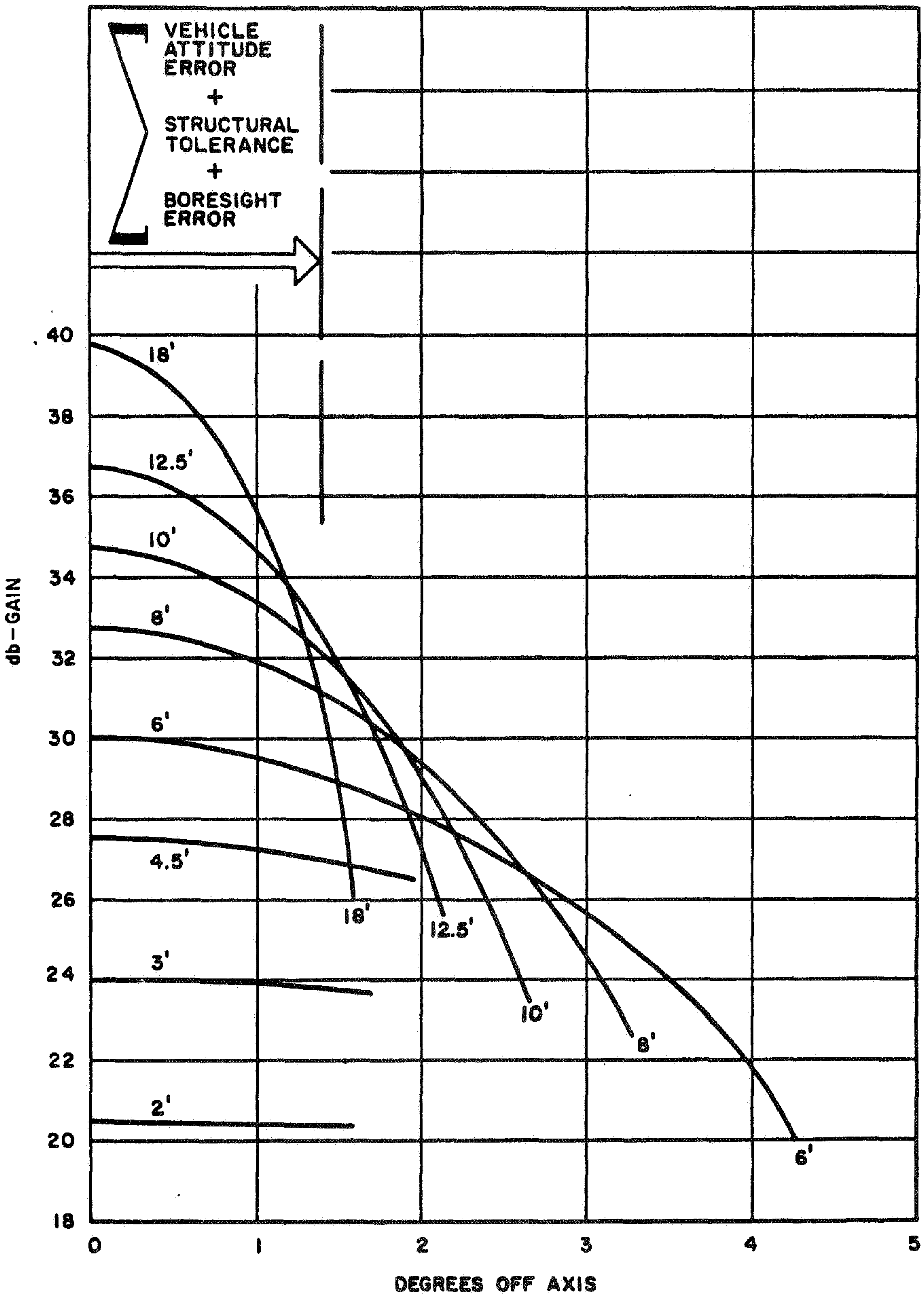

Figure C.6-2

GAIN VERSUS OFF – AXIS POINTING FOR TAPERED CIRCULAR APERTURE

Admittedly, fine-control pointing might achieve a reduction in pointing tolerances by about an order of magnitude. This might then permit increasing the antenna diameter by an order of magnitude, which would increase the antenna gain by two orders of magnitude (20 db). This of course is tantamount to installing an 85-ft. dish on a space vehicle, which is not a practical proposition at this time. On the other hand, the added complexity of fine-control pointing could hardly be justified unless it would yield at least a 10-db increase in antenna gain. But the resulting antenna would then be a 25-ft. diameter aperture, which is still impractical. Thus fine-control pointing seems difficult to justify, and to get by with coarser pointing we should willingly accept an 8-ft. dish. Fortunately this also happens to be a size that will conveniently fit inside the Centaur shroud without resorting to erecting or unfurling antenna configurations. Thus we conclude that the tradeoffs indicating choice of an 8-ft. dish are indeed sharply defined.

No specific antenna mount has been envisioned as yet. It would be attractive, of course, to be able to use a body-fixed antenna for a major portion of the mission. Uncertainty regarding the method of mounting will remain until the trajectories, Mars orbit details, and the corresponding Earth-Track (cone and clock angles) have all been computed.

RF Power Output at 2300 Mc

For a deep space mission departing today, a maximum of 20 watts would be available, using an Apollo-type TWT. A mission departing in 1971, however, could be provided with at least 50 watts of RF power, either by improved performance of a single tube, or by the use of parallel tubes.

Transmitter Efficiency

Present beam efficiency for the Apollo TWT is 35 per cent, including heater power. Power conditioning losses would bring this down to about 30 per cent, and other circuitry for frequency control, drive, and modulation would bring the overall efficiency of the transmitter to 25-27 per cent.

Summary of Telecom Parameters

DOWN LINK

Frequency	2295 Mc
Transmitter Power	50 Watts
Transmitting Antenna	8-ft. dish
Receiving Antenna (at 3 DSIF-sites)	210-ft. dish
Effective Noise Temperature of Receiving System (DSIF)	$55^\circ \pm 10^\circ$K
Max. Bit Rate of Encounter ($280 \cdot 10^6$ Km)	3000 bps
(Transmission time for 500-line TV picture $\approx$ 7 minutes/pix)	
Bit Rate at Maximum Range ($400 \cdot 10^6$ Km)	1400 bps

Quasi-isotropic antenna degrades link by -32. db;
Bit Rate of down link must then be adjusted accordingly.

UP LINK

Frequency	2115 Mc
Transmitter Power (at 3 DSIF-sites)	10 KW
Transmitting Antenna (at 3 DSIF-sites)	85-ft. dish
Receiving Antenna	8-ft. dish or quasi-isotropic antenna
Effective Noise Temperature of Receiver (TDA)	850° K

Max. Bit Rate: Substantially same as for Down Link
(for 8-ft. dish at vehicle, and with 10-KW ground transmitter).

GENERAL

Power Input to Vehicle Telecom ($\eta = 0.27$)	180 Watts
Weight of Vehicle Telecom (incl. Antenna)	200 lbs
Volume of Vehicle Telecom	3500 cubic inches

Telecom Design Areas Requiring Further Investigation

1. Antenna mount detail, as described above.
2. Reappraisal of transmitter power limitations, considering tube capability, reliability, and life, as well as antenna breakdown in vacuum.
3. A specific, recommended configuration to evolve for the transmitter and receiver, along with selected modes of operation.
4. Explore telecom interface aspects of electric propulsion (reflection, absorption, noise power emission) for the transit phase.

7. System Analysis

Primary emphasis during this report period has been on the overall performance comparison between solar electric and chemically propelled vehicles. What has been accomplished from a system analysis viewpoint is the realization of several inter-related design problem areas which are briefly discussed here under separate headings.

Trajectories

Aside from the overall importance of the type of trajectory on performance, an element crucially affecting vehicle design is the apparent necessity to rotate the thrust vector some 60° with respect to the sun line for optimum thrust direction during heliocentric transfer.

Vehicle design has an unusually strong influence on system analysis in the case of a solar electric powered vehicle because of solar panel size, cg uncertainty and movement, thrust direction variation, and long flight times. The 60° thrust vector rotation requirement means the engine must be rotated through that angle with attendant gimballing design problems. A possible way of completely avoiding the problem is to thrust always nearly perpendicular to the sun-probe line. A partial avoidance of the problem is to thrust in only two directions, such as 60° and 120° with respect to the sun-probe line, thereby requiring only two engine gimbal positions instead of continuously rotating the engine. Also, if it were necessary to rotate the thrust line through a small angle, say $\pm 5^{\circ}$, this could be done by rotating the whole vehicle with negligible loss of solar power. Therefore, one of the objectives of trajectory analysis during the next period will be to determine fuel cost of restricting thrust angle variation. This weight penalty will then be compared with the weight and complexity penalty of gimballing the engine cluster.

Another factor to be considered in connection with trajectories is communications intrusion of the earth by the sun. If communication intrusion due to near occultation conditions occurs it lasts for over one month. For the cases of flight times longer than a year effective occultation may occur in the later part of 6 months Mars Orbiting Phase.

Another factor not yet studied is the error introduced by the use of patched conics in the trajectory program. For $C_3 = 0$ the vehicle spends more time(than it does for larger C_3)in the region where both Earth's and Sun's gravity are simultaneously effective. A three body program might result in a considerably different trajectory thrust direction program, and it could affect launch restrictions.

Funding permitting, the fuel cost of out-of-ecliptic corrections will be determined by running the three dimensional trajectory program.

Engine

The number and arrangement of thrustors has an important effect on attitude control design. The larger the number of thrustors, the less effect failure of one will have on thrust mis-alignment. Proper arrangement of a larger number of thrustors could permit direct attitude control by occasionally turning a few strategically placed thrustors on or off, although preliminary indications are that the weight penalty entailed is prohibitive.

Heat

The large radiating area needed to dispose of the heat generated in the power conditioning unit complicates the vehicle design. The feasibility of using some form of heat concentrator such as thermoelectric to raise the temperature of the radiating element should be studied.

Guidance and Instrumentation

Command guidance based on the DSIF is assumed throughout the transfer phase, although no mid-course correction as such is required. The trajectory will be continuously monitored by DSIF tracking. Any deviations from standard, resulting either from change in thrust or other causes, will result in a command to change thrust direction or to start one of the redundant thrustors. The complete failure of a thrustor can also be detected on-board, and the resulting signal would cause a spare thrustor to start. The effects of partial failure of a thrustor would have to be computed from tracking data to determine when another thrustor would be started.

During the terminal phase, however, ($r_{v,♂} < 10^6$ mi) some form of on-board terminal guidance probably will be needed. For example, a landing probe might need precision launching. Even if the DSIF tracking were of sufficient precision to determine the launch when the parent vehicle is on a conic trajectory, it would not necessarily be so in case the thrust of the ion engine changed during the few days preceeding the launch. The dispersion between the vehicle predicted and actual position as obtained from DSIF tracking as a function of thrust variation (and time after thrust variation occurred) determines whether on-board guidance is necessary. In case it is necessary, the addition of a Mars scanner with a minor amount of on-board computing has been shown to be sufficient to provide the desired precision.

Instrumentation can be the same as that of EDP 139 with the possible exception of the Mars scanner mentioned above.

Two unique instrumentation problems are connected with solar electric powered vehicles. Neither may be serious, but are being studied. One concerns the effective aperture of the Canopus tracker. Because Mars will be near its maximum deviation from the plane of the ecliptic for some trajectories, it will be necessary to have a thrust component perpendicular to the palne of the ecliptic during part of the trajectory. Depending on how this component is obtained, the aperture of the Canopus tracker might need to be enlarged. This is a factor in selecting the control method.

The other novel instrument problem is where to mount the Canopus tracker so that (a) it can see Canopus at all times, even after sheding of the solar arrays (b) minimize the inpingement of neutral exhaust particles on the objective lens.

Control

The principal vehicle system problem associated with control is caused by C. G. position, and thrust direction with respect to the C. G.

The distrubance torques due to pressure variation of solar radiation used in the control section of this report to estimate control system weights is equivalent to the thrust line missing the C. G. by less than 1/32 of an inch at all times. Control system weight increases rapidly with larger mis-alignments. The thrust line - C. G. relationship is affected by (1) initial uncertainty of C. G. position, (2) C. G. Shift due to solar panel bending and fuel consumption,

(3) individual thrustor performance. The initial uncertainty of the C. G. position after the solar panels have been extended is estimated to be in doubt by nearly 2 inches. Solar panel bending due to temperature differential across the panel will decrease as distance from the sun increases. The panels bend into parabalas. Current estimates of the tip deflections at 1 a. u. are less than 8 feet. Significant uncertainty will necessarily remain on the estimated because of the difficulty of the calculations, and this may well be greater than one-half the change in bending that occurs due to increasing distance from the sun. Assuming a temperature gradient at Mars of 120° less than an assumed 500° at 1 a. u., linearity between bending and temperature gradient, and that the C. G. of the parabalas is 0. 3 of the length, the panel C. G. moves 1 foot during the trip. Hence, if vehicle C. G. is placed half way between the extremes, the contribution of panel movement to vehicle C. G. shift is 1. 5 inches. To a considerable extent this may be compensated by fuel consumption.

Other smaller C. G. variations during flight will occur (e. g. due to stress relieving of members), but are not being considered now.

Failure of an individual thrustor may cause as much as a 2 inch thrust mis-alignment, depending on number and arrangement of thrustors.

At present then, it is considered that provision must be made in design of the vehicle for at least 3 inches malalignment of thrust line with respect to the C. G. The methods for aligning thrust line with C. G. being evaluated are briefly described in their present order of desirability.

a. Mount the engine cluster on flexure pivots in two planes. The pivot would be light springs so that the engine can be rotated with small electromagnetic actuators. The engine would be caged with respect to the pivots during boost. Rotation would be approximately $\pm 10^{\circ}$, with engine 1. 5 feet off the vehicle C. G. The method is attractive because no moving parts are involved. Objection to this method is the possible cross coupling into roll.

b. Translate the engine $\pm 3^{\circ}$ in two planes. This has moving parts, but eliminates cross coupling.

c. Use auxiliary Cesium ion engines for cross control. These engines can be turned off and on reliably. The objections are several extra kw of solar power, and the fact that for reliability reasons 6 or 8 engines will be necessary.

d. If the weight penalty is not too great and a convenient thrustor arrangement can be found, redundant thrustors can be employed for a coarse control. The only advantage of this method, however, would be reduction in the required angular motion of the engine on its pivots, or equivalent translation.

It should be remembered that cold gas jets or some equivalent form of control will be needed before sun acquisition and during the Mars orbiting phase. Since they are, therefore, already on-board it would seem reasonable to employ them for fine control and limit cycle control during transfer phase.

D. FEASIBILITY HARDWARE

The propulsion system designs under consideration for the Mars SEP Mission require experimental verification of several critical performance objectives. Hughes was assigned the responsibility of confirming the designs of a propulsion system based on mercury bombardment engines. The study program covered in the foregoing sections has established important parameters with regard to the number of system modules required for redundancy and the specific impule to be applied to the propellant. The initial phases of this hardware verification effort have been devoted to comparing the study design recommendations with state-of-the-art hardware and in developing preliminary designs based on these requirements.

1. Ground Rules

The guiding precepts of the hardware verification program are established by mission constraints and by the "state-of-the-art" in Hg Ion Engine equipment. The pertinent mission constraints can be briefly summarized as:

a) Propulsion system specific weight including power conditioning, feed system, controls and ion engine not to exceed 25 lb/kW.

b) Specific impulse,as determined by trajectory studies,to be 3000 to 4000 seconds.

c) Propulsion system mission reliability — 97%.

The specific weight and specific impulse constraints can be verified at early design stages. Initial studies indicate that both objectives can be met by the hardware which will comprise this system. The third constraint, for a mission reliability of 97%, requires extensive life test data as well as system modularization as established by the analytical studies. Life test data taken with a propulsion system which is scaled to an operational system will provide the information required to verify the overall propulsion system reliability target.

The "state-of-the-art" constraint is more subjective. The highly successful mercury bombardment engine system aboard SERT-I is state of the art but cannot be applied to the Mars SEP Mission because the specific weight and specific impulse do not conform to the mission constraints. Larger ion engines, particularly at 20 cm diameter and 50 cm diameter, have been developed and extensively tested at the Lewis Research Center. The decision has been made to incorporate the 20 cm thrustor size in this hardware verification program. This item clearly falls within the state-of-the-art constraint. The power conditioning state-of-the-art (at desirable power to weight ratios) seemed, at the outset, to require that the entire hardware verification program would have to be based on systems in the 4 to 6 kW range. This power level is simply incompatible with the 20 cm ion engine operated at 4000 seconds specific impulse, and a considerable part of the initial design effort was spent in circumventing this obstacle.

2. System Design

Preliminary designs have been completed on a mercury ion engine system module which will conform to the mission constraints and will be entirely satisfactory for verifying the hardware performance and reliability targets. The module will consist of a Lewis Research Center 20 cm mercury bombardment engine design modified by Hughes Research Laboratories, a feed system developed jointly by Hughes Research Laboratories and Jet Propulsion Laboratories, and power conditioning based on unitized inverter designs. These items are discussed separately below.

a. Thrustor Units

The basic LeRC 20 cm engine has been substantially redesigned as part of a company funded project at HRL. Figure D. 2-1 shows the exterior configuration of this engine which employs the basic LeRC optics and stand-off insulator design. The interior design however, consists of concentric shells which guide the propellant to the front of the engine where it is injected into the arc chamber in a generally rearward direction. It is believed that this reverse feed technique will increase the propellant utilization factor. The thrustor is complete and ready to run except for the cathode. Several types of oxide cathodes have been designed and fabricated at HRL and decision as to which device to employ for initial integration tests will be made in the following reporting period. Laboratory type power conditioning

M 3860

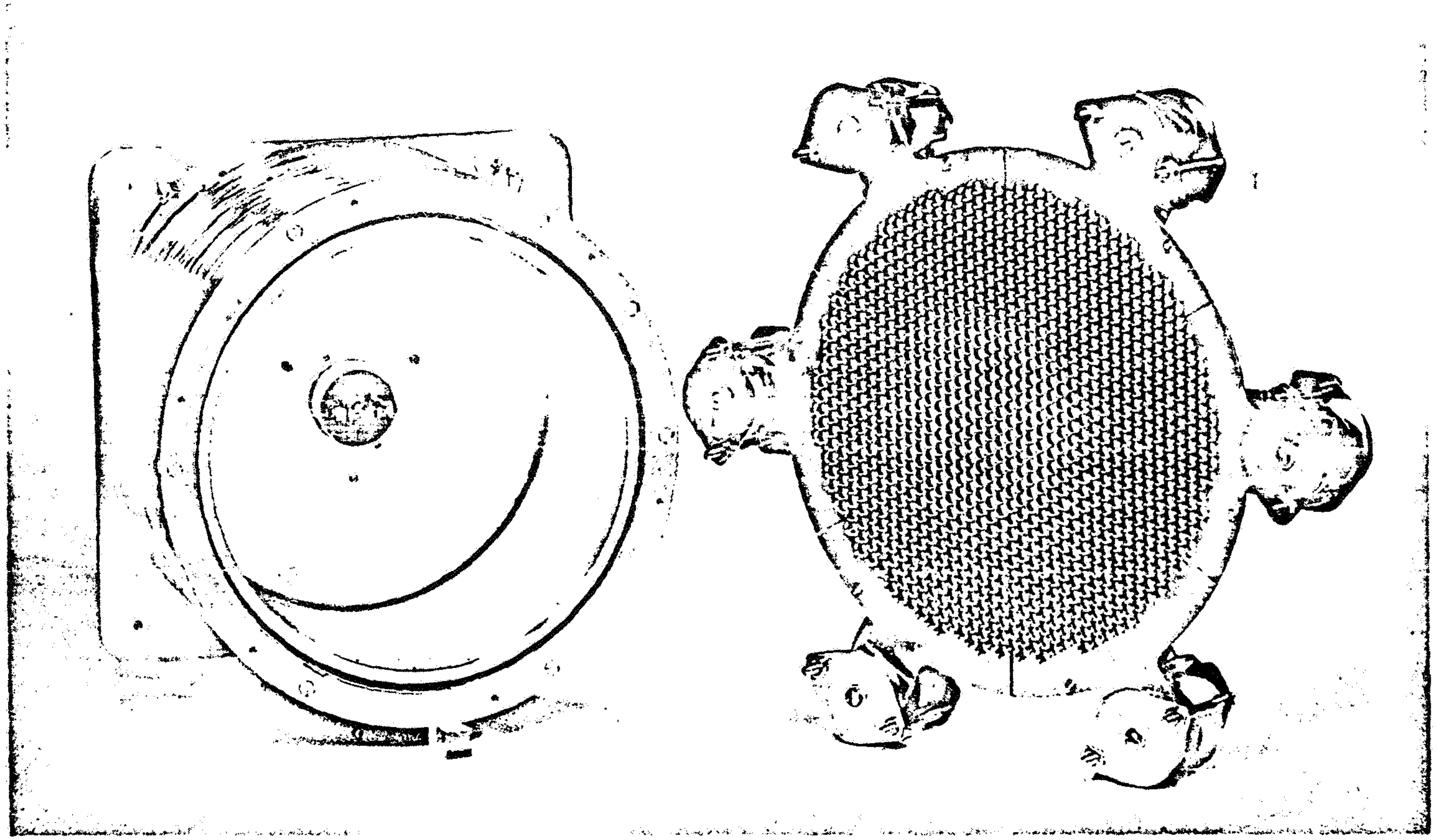

Fig. D.2-1. 20 cm mercury bombardment engine built to HRL designs, using LeRC optics.

equipment to operate the thrustor unit is being completed. Each of the power supplies in this equipment is regulated and controllable by low level input signals. When operated with this power conditioning equipment, the thrustor characteristics will be determined and initial control system development can begin.

b. Feed System

Components of a breadboard feed system have been designed and will be assembled for test in the following reporting period. Figure D. 2-2 shows the basic elements of the feed system which have been undertaken as a joint HRL-JPL project. The mercury propellant tank is a JPL design wherein the propellant is expelled from the poles of a sphere by action of two equatorial diaphragms. The solenoid valve is an HRL design. The vaporizer has been designed and fabricated by JPL. In operation a temperature gradient is established in the vaporizer such that the mercury liquid-vapor interface occurs within the fine pores of the vaporizer. The principal of operation depends on the high impedance of the vaporizer to the gas phase which effectively maintains the interface in equilibrium, as governed by the thermal gradient within the vaporizer and the external flow conditions. A flow meter consisting of a calibrated flow orifice and a capacitive monometer type pressure gauge is being tested in mercury vapor. Initial test results indicate that extremely close temperature control of the flow meter system will be required. Other flow meter principles are being investigated, since the requirement for close temperature control leads to undesirable design constraints.

It is anticipated that a complete integration test of the feed system, 20 cm thrustor and laboratory power conditioning equipment will take place on or before 1 May 1965.

c. Power Conditioning

A modular power conditioning approach employing individual high frequency inverters at approximately 150 W shows promise for application to the system. The basic inverter circuit and a cut-away view of the proposed package configuration is shown in Fig. D. 2-3. Breadboard tests

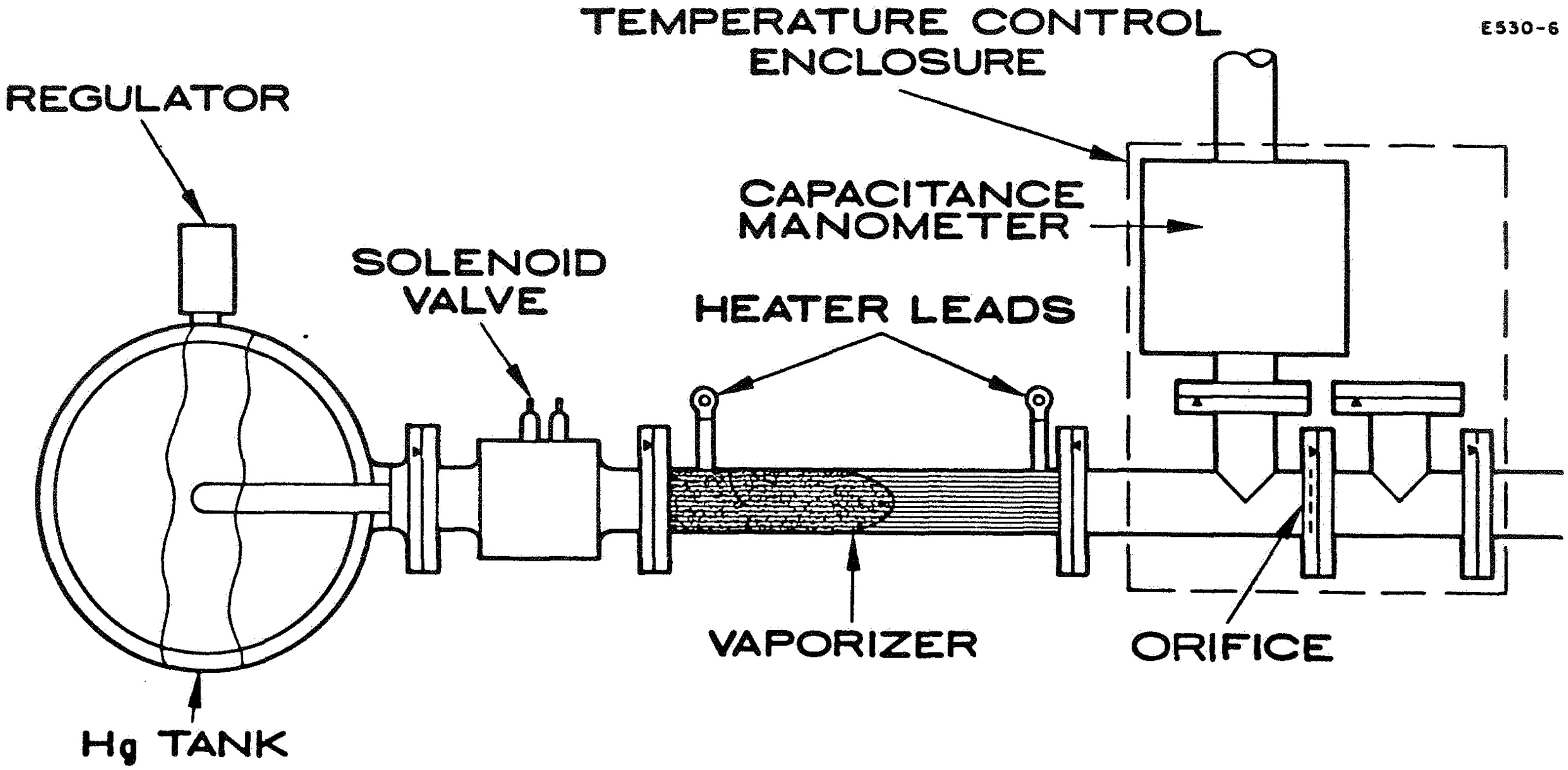
E530-6
TEMPERATURE CONTROL ENCLOSURE
REGULATOR
CAPACITANCE MANOMETER
SOLENOID VALVE
HEATER LEADS
VAPORIZER
ORIFICE
Hg TANK

Fig. D.2-2. Breadboard feed system showing liquid-vapor interface in the vaporizer.

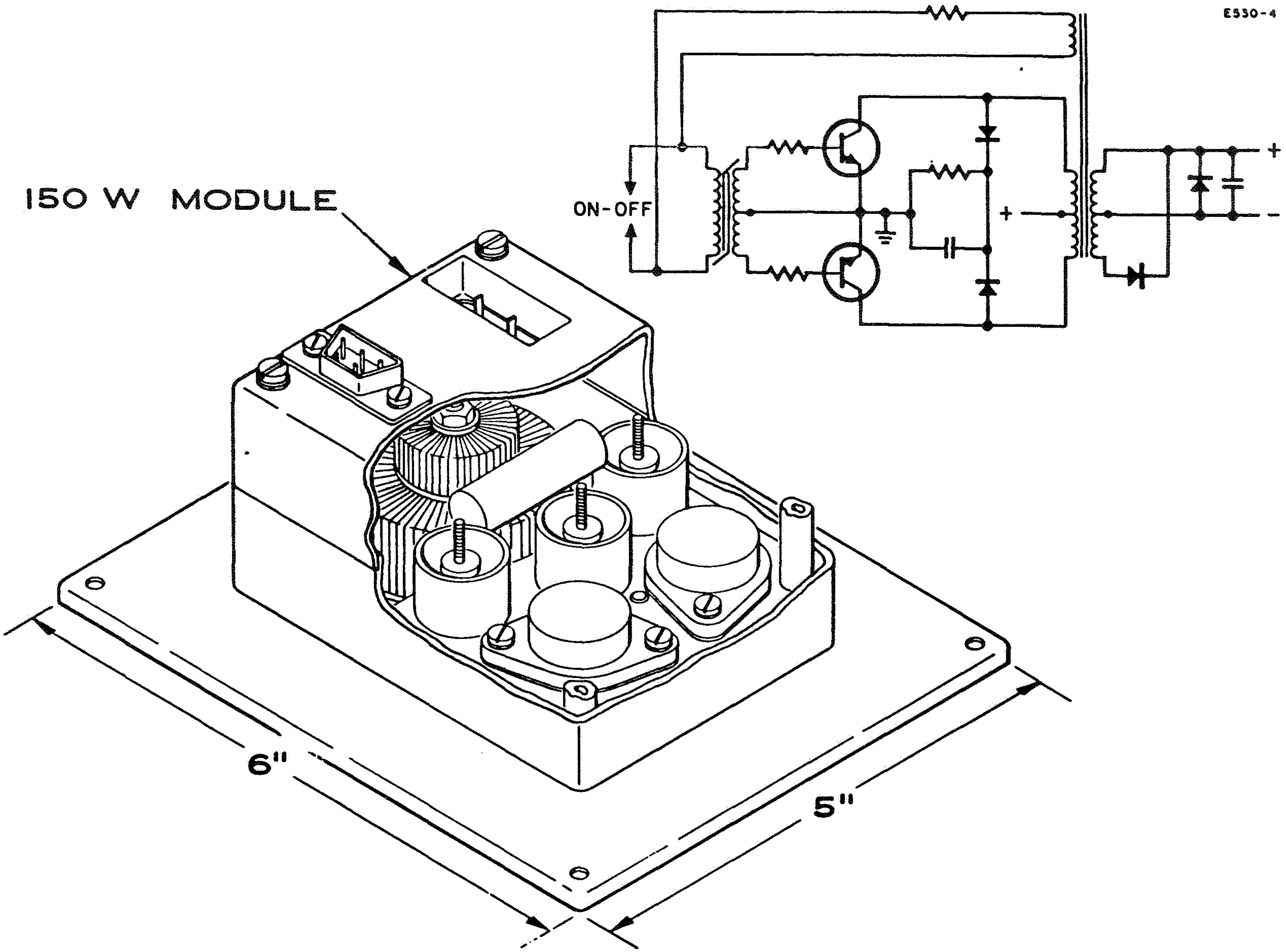
E530-4
150 W MODULE
ON-OFF
+
+
-
6"
5"

Fig. D.2-3. Cut-away view of individual inverter module showing toroidal transformers and rectifiers in high voltage insulating cups.

verifying the behavior of individual circuit modules were conducted with the unit shown in Fig. D. 2-4.

The arrangement of 150 W modules to power a complete 20 cm thrustor system is shown in Fig. D. 2-5. Spare inverters are provided in each of the series strings which comprise the major engine power elements. In the event of failure in any module, the spare unit is activated.

3. Weight and Power Analysis

Electrical and mechanical analysis of the propulsion system module has been completed with the results summarized in Fig. D. 3-1 and Fig. D. 3-2. Propulsion system weights have been established by measurements with existing hardware and it is anticipated that substantial reductions can be achieved in the prototype phase. The system power levels have not as yet been confirmed by experimental measurements but extensive experience with mercury bombardment engines assures a high degree of confidence in the figures as shown.

The consequences of the weight and power analyses are summarized in Fig. D. 3-3. It is significant that an overall power to weight ratio of less than 25 lb/kW has been achieved even under the severe constraints imposed by the relatively small module size, by the 50% redundancy employed throughout the power conditioning system and without any concerted effort to reduce the weights of principal components. It is highly encouraging, at this stage of system development, to be assured that the target specific weight factors can be met. It is anticipated that reduction in the weight of individual components in the prototype designs will result in substantial gains in this figure of merit.

4. Development Schedule

During this reporting period the original development schedule was considerably modified in accordance with the results of the analytical studies. Figure D. 4-1 shows the four main lines of developmental effort which will result in an integrated system module for 500 hour vacuum testing in the fall of 1965. Breadboard integration testing of subsystems will be

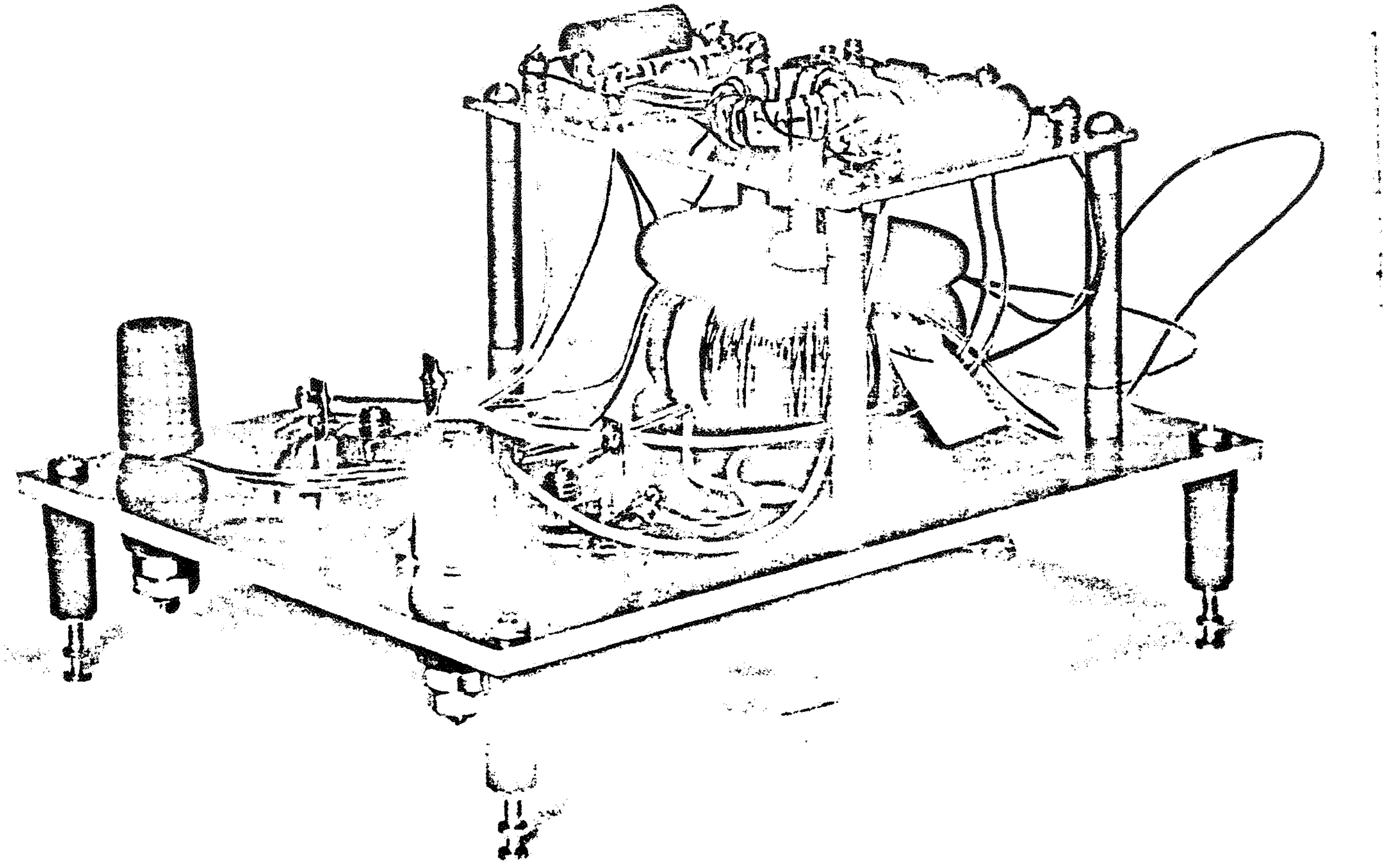

Fig. D. 2-4. Breadboard model of modular inverter unit.

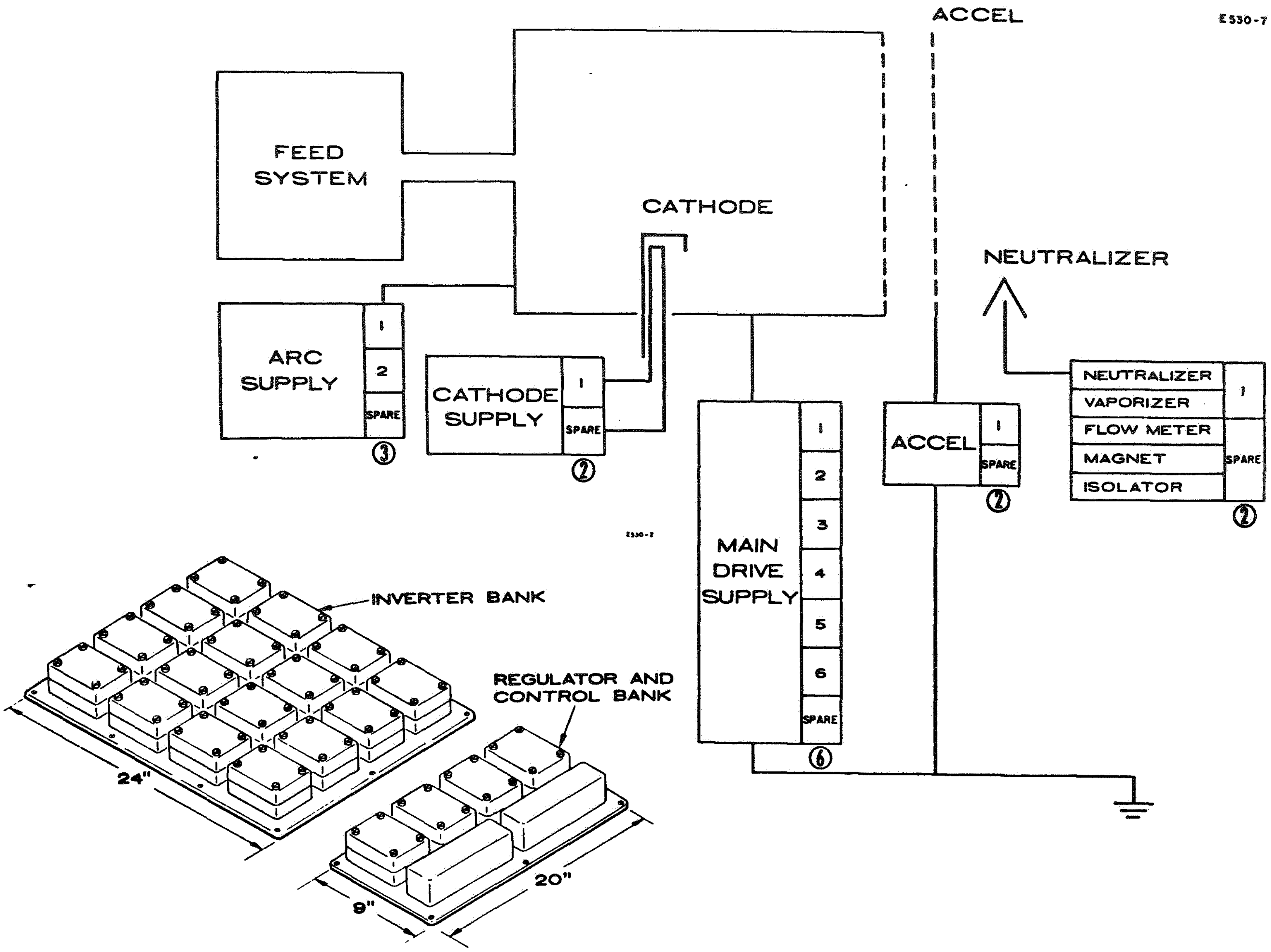
E530-7
ACCEL
FEED SYSTEM
CATHODE
NEUTRALIZER
ARC SUPPLY
1
2
SPARE
③
CATHODE SUPPLY
1
SPARE
②
MAIN DRIVE SUPPLY
1
2
3
4
5
6
SPARE
⑥
ACCEL
1
SPARE
②
NEUTRALIZER
VAPORIZER
FLOW METER
MAGNET
ISOLATOR
1
SPARE
②
E530-2
INVERTER BANK
REGULATOR AND CONTROL BANK
24"
20"
9"

Fig. D. 2-5. Application of modular inverters to Hg ion engine system.

WEIGHT ANALYSIS
Mercury Engine System Module

	Pounds	Pounds
20 CM MERCURY BOMBARDMENT ION ENGINE		10.2
Feed System		
Propellant Tankage (for 100 lb storage)	2.1	
Gas bottle and regulator	1.6	
Valves	1.5	
Vaporizer	0.8	
Isolator	0.8	
Flow meter	1.5	
Plumbing	0.5	
		8.8
Power Conditioning		
150 W modules		
11 operational at 0.81 lb	8.9	
5 spares at 0.81 lb	4.1	
50 W regulators		
5 at 0.4 lb each	2.0	
Instrumentation supplies		
4 at 0.4 lb each	1.6	
Connectors - Harnessing	2.0	
		18.6
Control System		2.4
Structure		1.8
TOTAL SYSTEM WEIGHT		41.8

Fig. D. 3-1.

OPERATING POINTS

20 cm Mercury Bombardment Thrustor

Beam Current	I_B	500 MA
Beam Voltage	V_B	2000 V
Specific Impulse	I_{sp}	4470 sec at 100% prop. 4030 sec at 90%
Accel Voltage	V_A	-2000 V
Accel Current	I_A	7.5 mA
Discharge Voltage	V_{arc}	$\left.\begin{matrix}40\text{ V}\\ 6\text{ A}\end{matrix}\right\}$ or $\left\{\begin{matrix}30\text{ V}\\ 8\text{ A}\end{matrix}\right.$
Discharge Current	I_{arc}	
Cathode Power	P_c	80-100 W
Magnetic Field	B_{screen}	15 Gauss
Magnet Power	P_M	60 W
Neutralizer Power	P_n	15 W

Fig. D.3-2.

WEIGHT/POWER SUMMARY

Mercury Engine System Module

INPUT POWER	1742 W
SYSTEM WEIGHT	41.8 lb
POWER CONDITIONER WEIGHT	
with 5 spare modules	18.6 lb
without spares	14.5 lb
SYSTEM WEIGHT/POWER	24 lb/kW
POWER CONDITIONING WEIGHT/POWER	
with 5 spare modules	10.7 lb/kW
without spares	8.3 lb/kW

Fig. D. 3-3.

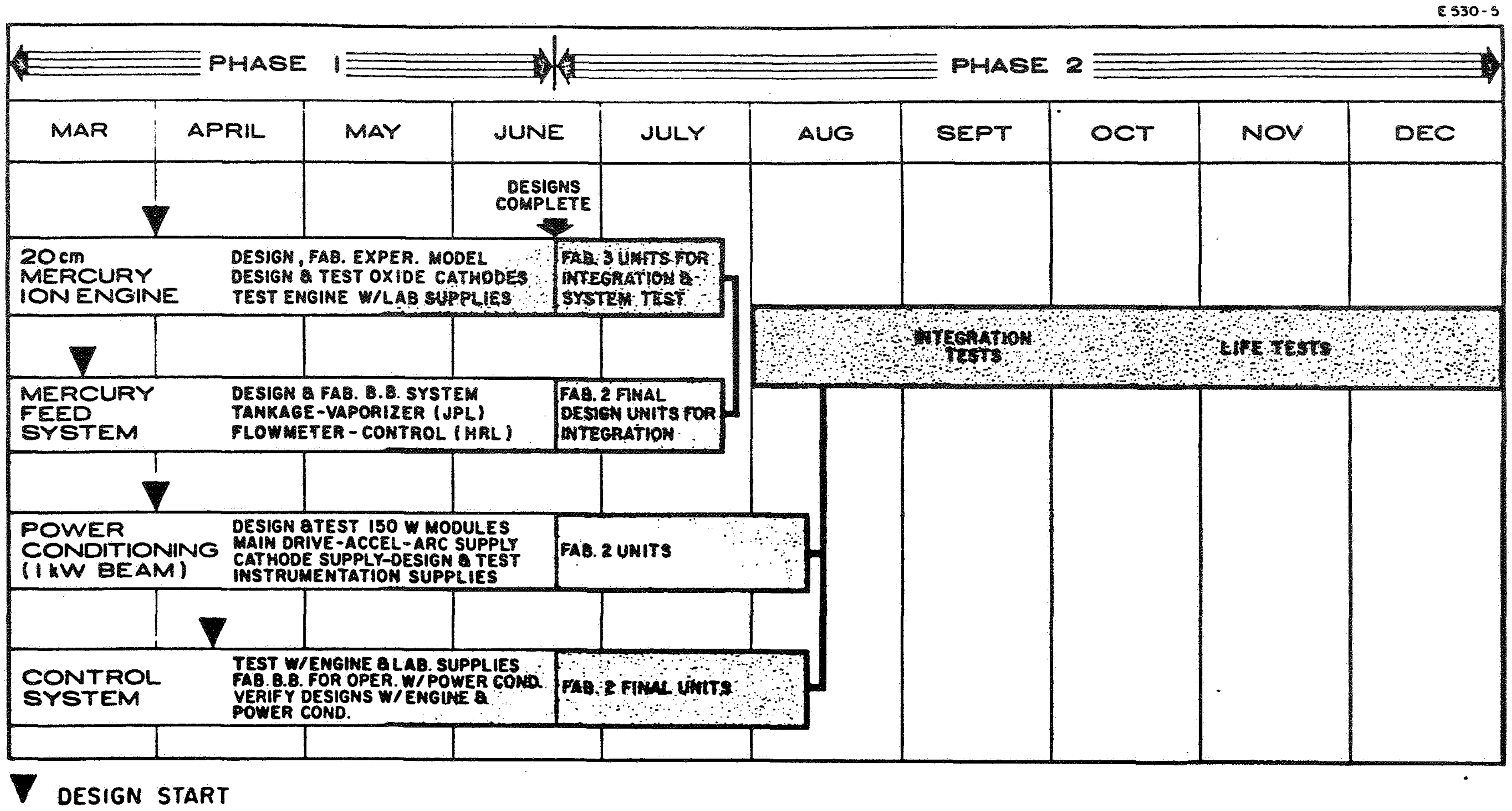

Fig. D. 4-1. Development and test schedule for mercury ion engine system module.

occuring at all early phases in the program, however the schedule shown is based on the final integration of testable components. The June 15 date for completion of designs will be met. Fabrication of items for the Phase II testing must commence on the dates indicated in the shaded portions of the schedule, if the system tests are to be completed by the end of the year.